

**VALVE MORPHOGENESIS**  
**Directing Cardiac Form and Function**

Anne Karine Lagendijk

**Leescommissie:**

Prof. Dr. H.C. Clevers  
Prof. Dr. P. ten Dijke  
Prof. Dr. V.M. Christoffels  
Prof. Dr. R.F. Ketting

---

---

The research described in this thesis was performed at the Hubrecht Institute for Developmental Biology and Stem Cell Research of the Royal Netherlands Academy of Arts and Science (KNAW), within the framework of the Graduate School of Cancer Genomics and Developmental Biology in Utrecht.

Cover: Front, “Viltrikel”, an artistic impression of a zebrafish ventricle at 2 dpf with myocardial Dm-grasp expression in red and *kdr-l:GFP* positive cells of the endocardium in green. Back, an artistic impression of an adult zebrafish.  
(Material: Filt, ironwire. Artist: Janneke Middel)

Financial support by the Dutch Heart Foundation and the J.E. Jurriaanse Stichting for the publication of this thesis is gratefully acknowledged.

Printing of this thesis was financially supported by a personal gift from J. Summerton, Genetools LLC, Philomath, U.S.A.

ISBN: 978-90-393-5690-6

Printed by Digital Printing Partners, Houten

Copyright © 2011 by Anne Karine Lagendijk. All rights reserved. No parts of this book may be reproduced, stored in a retrieval system or transmitted in any form or by any means, without prior permission of the author. The copyright of the publications remains with the publishers.

---

---

# **VALVE MORPHOGENESIS**

## **Directing Cardiac Form and Function**

**Klep morfogenese,  
het sturen van de vorm en de functie van het hart  
(met een samenvatting in het Nederlands)**

### **Proefschrift**

ter verkrijging van de graad van doctor  
aan de Universiteit Utrecht  
op gezag van de rector magnificus, prof. dr. G.J. van der Zwaan,  
ingevolge het besluit van het college voor promoties  
in het openbaar te verdedigen  
op dinsdag 13 december 2011 des middags te 12.45 uur.

door

**Anne Karine Lagendijk**

geboren op 14 december 1980  
te Someren

Promotor: Prof. dr. E. Cuppen

Co-promotor: Dr. J. Bakkers

# CONTENTS

<b>Chapter 1</b>	<b>7</b>
General Introduction	
- The zebrafish heart: from cardiac progenitor cells to a working organ Adapted from: <i>Trends Cardiovasc Med.</i> , 2010 May; <b>20</b> (4):124-8.	
- MicroRNAs: small players of great importance for heart development	
<b>Chapter 2</b>	<b>27</b>
Revealing the details: An improved method for whole mount microRNA <i>in situ</i> hybridizations. <i>Manuscript in preparation</i>	
<b>Chapter 3</b>	<b>39</b>
MicroRNA-23 Restricts Cardiac Valve Formation by inhibiting Has2 and Extracellular Hyaluronic Acid Production <i>Circ Res.</i> , 2011 Sep 2; <b>109</b> (6):649-57.	
<b>Chapter 4</b>	<b>63</b>
Transmembrane protein 2 (Tmem2) is required to regionally restrict atrio- ventricular canal boundary and endocardial cushion development <i>Development</i> , 2011 Oct; <b>138</b> (19):4193-8.	
<b>Chapter 5</b>	<b>81</b>
Zebrafish looping morphogenesis: investigating the influence of contractility, flow and atrio-ventricular canal patterning	
<b>Chapter 6</b>	<b>97</b>
An antisense miR-128 morpholino enhances Bmp signaling independent from miR-128: a story ends with a lesson in morpholino controls	
<b>Chapter 7</b>	<b>113</b>
General Discussion	
<b>Nederlandse samenvatting</b>	<b>122</b>
<b>Dankwoord</b>	<b>126</b>
<b>Curriculum vitea</b>	<b>129</b>
<b>List of publications</b>	<b>130</b>



# GENERAL INTRODUCTION

## **The zebrafish heart: from cardiac progenitor cells to a working organ**

A.K. Lagendijk<sup>1</sup>, K.A. Smith<sup>3</sup> and J. Bakkers<sup>1,2</sup>

Adapted from:

A.K. Lagendijk<sup>1</sup>, K.A. Smith<sup>3</sup> and J. Bakkers<sup>1,2</sup>

Genetics of Congenital Heart Defects: A Candidate Gene Approach

*Trends in Cardiovascular Medicine* 2010 May; **20**:124–128

1. Hubrecht Institute, KNAW & Iniversity Medical Center, Utrecht, The Netherlands.
2. Interuniversity Cardiology, Institute of the Netherlands, Utrecht, The Netherlands
3. Institute for Molecular Bioscience, The University of Queensland, Brisbane, Australia.

## **MicroRNAs: small players of great importance for heart development**

A.K. Lagendijk<sup>1</sup> and J. Bakkers<sup>1,2</sup>

1. Hubrecht Institute, KNAW & Iniversity Medical Center, Utrecht, The Netherlands.
2. Interuniversity Cardiology, Institute of the Netherlands, Utrecht, The Netherlands

# 1

# The zebrafish heart: from cardiac progenitor cells to a working organ

At two days post fertilization (dpf) the zebrafish heart consists of two chambers, one ventricle and one atrium. The outer muscle layer of the heart, the myocardium (Fig. 1A), is lined at the luminal surface by endothelial cells, which form the endocardium (Fig. 1B). The chambers are positioned relative to one another as such that they form an S-shaped structure. A constriction of the heart tube, referred to as the atrio-ventricular canal (AVC), separates the ventricle from the atrium. At the AVC a specialized group of endocardial cells have differentiated to form the superior and inferior endocardial cushions (ECs). These EC cells (Fig. 1C) will later form the cardiac valves. Although full maturation of the valves is not completed at this stage the primordial valves do already function to prevent backflow from the ventricle into the atrium, promoting directional blood circulation.

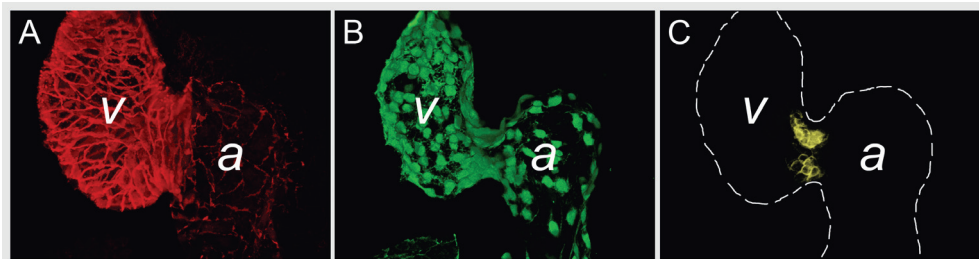


Figure 1: Zebrafish heart tube at 2 dpf

(A) Three dimensional projection of the zebrafish myocardium at 2 dpf (Dm-grasp, red). (B) Three dimensional projection of the endocardium (*Tg(kdr-l:GFP)*, green) lining the myocardium of wild-type zebrafish heart tube shown in A. (C) Dm-grasp-expressing endocardial cushion cells (yellow) located at the AVC. v=ventricle, a=atrium.

The myocardial and endocardial cells that together form this looped heart tube all derive from cardiac precursor cells, which become specified much earlier during zebrafish embryonic development<sup>1</sup>

By fate mapping studies<sup>2-4</sup> both endocardial and myocardial cells have been shown to originate from the marginal zone at the 40% epiboly stage of zebrafish development, before the onset of gastrulation. Myocardial progenitors are already spatially organized at this stage with future ventricle cells positioned closer to the margin and to the dorsal midline compared to atrial myocardial progenitors (Fig. 2A). Endocardial progenitors are not spatially organized at this stage but are positioned intermingled with the other pre-cardiac and other endothelial cells around the margin<sup>4</sup>.

Myocardial specification is manifested by expression of the highly conserved homeobox-containing transcription factor *nkx2.5* starting from the 10 somite stage (14 hours post fertilization (hpf))<sup>5</sup>. At the same time *vegfr4* which is expressed by both endothelial and hematopoietic precursors, can be detected in the anterior lateral plate mesoderm (ALPM)<sup>6</sup>. Time-lapse imaging of *vegfr4:GFP* expressing cells revealed that future endocardial cells migrate and move medially into the cardiac field between the 12 and 14 somite stage (15-16 hpf), preceding the arrival of *nkx2.5* positive myocardial cells (Fig. 2C)<sup>6</sup>. Before migration into the heart field cardiomyocytes have differentiated into a ventricular and atrial population. The most medial cells differentiate first with the onset of



*ventricular myosin heavy chain (vmhc)* expression, followed by the cells located more laterally that start to express *atrial myosin heavy chain (amhc)*<sup>7</sup> (Fig. 2C). Ventricular and atrial identity will be maintained and corresponds to final positioning of these cells in the future chambers of the heart tube.

The two bilateral groups of myocardial cells subsequently move medially and fuse at the anterior and posterior ends. Medial migration of the heart fields requires both intrinsic genetic cues and proper organisation of the extracellular matrix<sup>8-11</sup>. Upon fusion a so-called cardiac disc is formed. The atrial cells form the outer ring surrounding the ventricular cells, whereas the future endocardial cells are located in the center of the disc (Fig. 2D).

Despite the close proximity of endocardial and myocardial cells during medial migration and heart tube formation, these cells do not require one another to form either a disc or later a heart tube. In zebrafish *cloche (clo)* mutants<sup>12</sup>, which lack all endothelial cells, anterior fusion of the two myocardial heart fields is somewhat delayed, nevertheless a cardiac disc is still formed which subsequently transforms into a beating tube<sup>13,14</sup>. *clo* mutant hearts however fail to loop and chamber morphology is altered. The ventricle is severely reduced in size while the atrium is enlarged<sup>14</sup>.

For the cardiac disc to develop into an enclosed linear heart tube, cells of the cardiac disc undergo three main movements. Firstly, the right part of the disc involutes under the cardiac cells positioned in the left half<sup>15,16</sup>. Concomitantly, the whole disc starts to rotate in a clockwise orientation<sup>15,17</sup> and subsequently the premature tube structure elongates telescopically towards the left side of the embryo. This leftward movement of the heart tube is referred to as cardiac “jogging”<sup>18</sup> and is one of the initial asymmetry breaking events in the embryo (Fig. 2E). Cardiac laterality is under the control of left-right signaling pathways and a loss of cardiac asymmetry can cause a wide variety of congenital heart defects<sup>19</sup>.

Cardiac jogging is closely followed by looping of the tubular heart. The leftward positioned tube undergoes an initial rightward bending (D-loop) at the future AVC at around 36 hpf (Fig. 2F). While this rightward D-loop continues the heart moves back to the midline. Concomitantly, outward ballooning of the chambers and constriction of the AVC occurs. These morphological changes finally result in the S-shaped, two-chambered heart at 2 dpf (Fig. 1 A-C and Fig. 2G). While in the linear heart tube the ventricle is positioned proximal of the atrium, in the looped heart the chambers are positioned side by side.

The Bakkers laboratory has performed several forward genetic screens to identify novel players required for cardiac jogging and looping. For this, zebrafish embryos were screened live at 1 dpf and 2 dpf to examine the direction of both cardiac jogging and looping. In Chapter 5 we describe morphogenetic changes of the heart tube during cardiac looping in wild-type zebrafish. In addition, we examined gene expression profiles of five selected looping mutants. Making use of a contractility deficient mutant we could show that looping does not require contraction, though secondary effects on the looping process do occur. For two other looping mutants, we describe a clear expansion of AVC markers simultaneous to incomplete looping. In two remaining looping mutants we detected only minor changes in differentiation of the AVC, implying the existence of thus far unknown factors morphogenesis. Results of this cardiac looping analysis can be found in Chapter 5. When initial bending of the heart tube occurs, endocardial cells at the AVC have been instructed by signals from the overlaying myocardium to differentiate into so-called EC cells<sup>20</sup>. Our group, along with others, have reported that EC specification is accompanied by expression of markers genes like *hyaluronic acid synthase 2 (has2)* and the adhesion



*Figure 2: Stages of cardiac development*

(A) At 5 hpf the blastula (white) covers approximately 50% of the large yolk cell (yellow). At this stage, cardiac progenitor cells are located bilaterally in the lateral marginal zone. Atrial progenitor cells (pink) are located more ventrally than the ventricle progenitor cells (light blue).

(B) During gastrulation, the cardiac progenitor cells move dorsally towards the midline to end up in the anterior later plate mesoderm (ALPM). (B) Cardiogenic differentiation is initiated in the future ventricle myocardial cells by the expression of cardiac myosins (purple) at the 12 somite stage.

(C) During mid- and late-somite stages, the myocardial tissue expands by continuous cardiogenic differentiation into more lateral regions of the ALPM by the cardiogenic differentiation of future atrial myocytes (orange; venous differentiation). (C) Whilst the endocardial cells (light green) have already migrated from the ALPM towards the midline, myocardial cells undergo this migration slightly later.

(D) When the bilateral heart fields fuse at the midline, they form a cardiac disc structure with the endocardial cells situated within the hole at the center. Ventricular myocytes surround the endocardial cells and atrial myocytes are located at the periphery of the disc. Cardiac morphogenesis transforms the cardiac disc into a cardiac tube. The endocardium forms the inner lining of the myocardial tube.

(E) At 28 hpf, the linear heart tube has formed, with the venous pole located at the anterior left and the arterial pole fixed at the mid-line.

(F) Cardiogenic differentiation continues at the arterial pole, and as a result new cardiomyocytes are added to this region (purple gradient). (F) At 36 hpf, cardiac looping has started, with a displacement of the ventricle towards the mid-line, and the constriction at the position of the AVC is first visible.

(G) The heart tube continues to loop and forms an S-shaped loop. Ellipsoid extra-cardiac pro-epicardial cells (brown) are located near the AVC (yellow), from where they start to cover the myocardium with an epicardial layer. The pacemaker cells are positioned at the inflow region of the atrium (dark green).

*Adapted from Bakkars 2011<sup>1</sup>.*

*Figure 3: Model for regulatory interactions during EC development*

(A) During EC induction, Bmp ligands secreted by the myocardium bind Alk2/3 receptors expressed by neighboring endocardial cells, thereby inducing phosphorylation of Smad transcription factors. Bmp signaling activates extracellular HA production by inducing *Has2* expression. Ugdh produces UDP-glucuronic acid, which is then processed by *Has2* into extracellular HA. Subsequently, HA can activate the ErbB2/3 receptor complex, of which *ErbB3* expression is regulated by the transcription factor *Gata4*. HA-ErbB2/3 signaling leads to mesenchymal transformation via activation of Ras and simultaneously triggers positive feedback regulation of HA production via  $\beta$ -catenin and *Has2* activity.

(B) Proliferation of mesenchymal cells requires Bmp signaling. For valve remodeling to take place, Egf signaling is required to inhibit the ongoing Bmp cascade. One of the crucial Egfr ligands during this process is HB-Egf, which is activated after cleavage by Adam17/19.

*Adapted from Legendijk et al. 2010<sup>27</sup>.*

molecule Activated leukocyte cell adhesion molecule a (Alcama/ Dm-grasp) from as early as 30 hpf<sup>20,21</sup>. Differentiated EC cells also undergo cell shape changes resulting in a more cuboidal appearance compared to neighboring cells of the chamber endocardium<sup>20</sup>. In contrast to EC formation in other vertebrates, classical endothelial to mesenchymal transition (EMT) does not seem to occur during zebrafish cushion formation<sup>22</sup>. In mice for instance it has been well established that endocardial cells undergo EMT, move into a swollen cardiac jelly (extracellular matrix between myocardium and endocardium) and proliferate to form a cushion like structure<sup>23,24</sup>. However, in zebrafish endothelial cells have not been detected in the cardiac jelly space<sup>22</sup>. Therefore, cardiac cushions have also been described as an area where endocardial cells locally bulge out because of a thickened cardiac jelly<sup>20,22</sup>.

EC cells within this bulged out area will grow out further and directly form valve leaflets by a process of invagination<sup>22</sup>. Since aberrant EC formation or further valve maturation can cause congenital malformations mostly to valves and septa of the heart, identifying genes

involved in regulating valve formation is of great importance. Even though the process of EC EMT does not occur in zebrafish<sup>22</sup>, EMT related genetic programming of these cells does seem to be conserved both during EC formation and valve maturation<sup>20,25</sup>. Therefore we believe zebrafish can be used as a valuable tool to study the transformation of valve progenitor cells into functional valves. We identified two novel conserved genes (microRNA-23 and *tmem2*) which are both necessary to spatially restrict the process of EC formation. This data will be described in more detail in Chapter 3 (microRNA-23) and Chapter 4 (*tmem2*) of this thesis. Furthermore, by using a candidate gene approach, we have previously identified novel single nucleotide polymorphisms (SNPs) specific to patients diagnosed with AV valve and septum defects<sup>26,27</sup>. Below we discuss how selected candidate genes, in which these polymorphisms were found, functionally interact to regulate EC formation during embryonic development. Many additional genes have been reported to be functionally related to AV valve and/or septa formation making this a highly complex morphogenetic event. For a more complete description we would like to refer to previously published reviews<sup>23,24,28</sup>.

## Identifying genes responsible for congenital valve disease

Congenital malformation of the cardiac valves and septa occur in approximately 6 out of 1000 live births<sup>29-31</sup>. In addition, valve defects such as bicuspid valves, which occur in about 1.5% of the general population, usually remain undetected until later in life<sup>32</sup>. These defects can be severely debilitating to the affected individual and are a leading cause of death from a birth defect<sup>33</sup>. A major underlying determinant for these structural defects has not yet been identified and this deficiency has led to the current dogma that congenital heart malformations are multifactorial diseases. Intrinsic and extrinsic environmental factors have been described, such as maternal smoking or illness, which increase the risk of cardiac malformations<sup>34</sup>. In addition, the use of forward and reverse genetic approaches have identified a number of monogenetic factors responsible for a small but increasing percentage of congenital malformations.

Current conventional approaches for discovering monogenetic factors involved in congenital heart defects (CHDs) include pedigree studies and candidate screens. Classical forward genetic pedigree studies have been highly informative in uncovering novel, unsuspected genetic lesions underlying a heritable disease. Thus far mutations in *GATA4*, *NKX2.5* and *TBX20* have been shown to cause non-syndromic valve and septal defects<sup>35-37</sup>. Unfortunately, this approach relies on large families exhibiting a Mendelian pattern of inheritance for the CHD and such cases are rare (presumably owing to poor survival rates of affected individuals).

In recent years, reverse genetic approaches have been employed to identify SNPs in candidate genes. Candidate genes are typically selected from pre-existing knowledge obtained from basic scientific and clinical studies to uncover putative mutations. This approach has the advantage that genetic variants can be identified relatively rapidly and in small pedigrees or even single individuals. Whilst these candidate approaches have proven useful, the drawback is that these studies are restricted to studying “old friends” - genes previously implicated in the disease, precluding the possibility for discovering novel, unsuspected players.

Array comparative genomic hybridization (aCGH) and next-generation sequencing are relatively new technologies for reverse genetics with promising possibilities for detecting genomic alterations in patients with congenital malformations. Next-generation sequencing, in particular, is set to alter the landscape of personalized diagnostics, through the cataloging of SNPs, deletions, duplications, copy number variations and genomic rearrangements for the entire genome of a single affected individual<sup>38</sup>. Whilst the management of such a volume of data will present its own challenges, the repercussions of such a bulk of information for understanding disease are truly compelling.

Whilst candidate screening, aCGH and next-generation sequencing all remove the requirement for large pedigrees that encumbers that of forward genetics, the major short-coming of these approaches still remains that they are inherently biased, in that any variants discovered within an affected individual or population is classified as potentially disease-causing. The inclusion of bioinformatics tools capable of predicting the damaging effect of a given variant is one measure recruited to overcome this bias. However the most convincing validation of any given variant is demonstrated through functional analysis of the variant product, preferably utilizing *in vivo* models.

## Old friends: signaling pathways involved in cardiac valve development

### ***Bmp signaling and initiation of valve formation***

In the primitive heart tube ECs arise in the AV boundary and the outflow tract (OFT). Chick AVC explant experiments have shown that EC induction requires the presence of AVC myocardium<sup>39,40</sup>. The myocardium secretes growth factors that belong to the Tgf- $\beta$  protein family, which activate the underlying endothelial cells to undergo EMT (Fig. 3A). Bmp ligands secreted by the myocardium are required for valve and septum development<sup>41-44</sup>. Bmp type-I receptors, Alk2 and Alk3, which can each preferentially bind different Bmp ligands<sup>45</sup>, are expressed in the underlying endocardial AVC cells. Both receptors are crucial within the endocardium for the induction of EMT in mouse embryos<sup>46,47</sup>.

A previously identified ALK2 L343P patient mutation is localized within a highly conserved region of the kinase domain, potentially destabilizing this region of the protein<sup>26</sup>. Both *in vitro* and *in vivo* experiments showed that the ALK2 L343P variant functions as a dominant-negative receptor<sup>26</sup>, reducing kinase activity and impairing downstream phosphorylation of Smad proteins. Also, injecting ALK2 L343P RNA into wild-type zebrafish embryos resulted in a loss of EC markers, directly linking this patient mutation to impaired valve development<sup>26</sup>.

### ***The importance of the extracellular matrix: Hyaluronic acid and ERBB2/3 signaling***

Bmp signaling in the AVC can induce *Has2* expression in the endocardium<sup>48</sup>, thereby activating HA-ErbB2/3 signaling<sup>49</sup> (Fig. 3A). *Has2* is an enzyme responsible for the production of hyaluronic acid (HA) by transdifferentiated endothelial cells. HA is released extracellularly into the cardiac jelly, where it functions as a scaffold required for migration of mesenchymal cells. In addition, HA bundles bind water and salt, which leads to swelling of the cardiac jelly resulting in morphologically cushion-like endocardial bulges. HA can also function as a signaling molecule by binding to several receptors<sup>49</sup>. Mice deficient in *Has2* and thus HA production, do not form cushion mesenchyme<sup>50</sup>. In addition, zebrafish *jekyll*/

*ugdh* mutant embryos, deficient for the UDP-glucose dehydrogenase enzyme *Ugdh*, do not form ECs<sup>51</sup>. Interestingly, *Ugdh* converts UDP-glucose into UDP-glucuronic acid, a critical component of HA. Induced phosphorylation of ErbB2 and ErbB3 receptors in *Has2* *-/-* AVC explants can restore mesenchymal transformation and *ErbB3* mutant mice lack cushion mesenchyme, indicating the importance of HA-ErbB2/3 interaction for EC development<sup>52,53</sup>. The transcription factor *Gata4* can regulate ErbB3 transcription in the endocardium<sup>54</sup>. Endocardial-specific deletions of *Gata4* induce hypocellular valve structures<sup>54</sup>, similar to a loss of ErbB3<sup>53</sup>, suggesting a permissive role for *Gata4* in HA-ErbB2/3 signaling in the endocardium<sup>54</sup>.

Activation of the ErbB2/3 receptor by HA results in  $\beta$ -catenin activation<sup>55,56</sup>. Wnt/ $\beta$ -catenin signaling also regulates *Has2* expression in ECs. In zebrafish *apc* mutant embryos, which have constitutively active Wnt/ $\beta$ -catenin signaling, *has2* is ectopically expressed throughout the endocardium, resulting in hyperplastic ECs<sup>57</sup>. Together these data suggest a HA-Wnt/ $\beta$ -catenin positive feedback loop during EMT in the endocardium.

### ***Signaling cascades involved in proliferation and maturation of the endocardial cushions***

Growth of the ECs requires proliferation of both the endothelial and mesenchymal cells (Fig. 3B).

Proliferation of mesenchymal populations of cells is controlled by antagonizing functions of Bmp and Egf signaling. Mice deficient in Heparin-binding epidermal growth factor (HB-Egf) develop malformed, enlarged AV valves while early EC induction and EMT appear to occur normally<sup>58,59</sup>. In addition, a loss of the Egf receptor itself causes similar valve remodeling defects<sup>60</sup>, despite the EgfR binding ligands other than HB-Egf. It has been shown that EgfR signaling is required to inhibit Bmp signaling in the proliferating mesenchymal cells<sup>59,61</sup>. Overactive Bmp signaling in these cells results in excessive proliferation, leading to oversized primordial valves in *Egfr* and *HB-Egf* mutant mice. ProHB-Egf needs processing by metallopeptidases to yield a functional ligand. Both Adam metallopeptidase domain 17 (Adam17), also known as tumor necrosis factor- $\alpha$  converting enzyme (Tace), and 19 (Adam19), also known as meltrin  $\beta$ , can process proHB-Egf<sup>62,63</sup>. Even though Adam17 appears to be primarily responsible for conversion of HB-Egf, Adam19-deficiency also results in thickening of the valves<sup>64,65</sup>. In addition, double mutant *Adam17/19* mouse embryos die *in utero* owing to early myocardial defects, demonstrating the relevance of Adam19 function<sup>62</sup>.

*Vegf* and *Nfat* signaling control outgrowth of the endothelial population of cells in the ECs. Both are restrictively expressed in the EC endothelial cells where they are required to maintain the proliferative state<sup>23</sup>.

Outgrowth of the proliferating cushions leads to fusion of separate cushion areas. These fused structures are referred to as valve primordia. For the primordial valves to become stable endothelial mature valves, mesenchymal cells must return back to the endothelial state<sup>38</sup> by regaining intercellular connections. Primordial valves will finally elongate and remodel into a stratified structure organized in parallel to the direction of blood flow<sup>28</sup>. The blood first meets an elastin rich layer, which makes the valve flexible to open. On the opposite end of the valve a high amount of collagen fibers has been deposited making the valve more rigid and fall back into place once blood pressure is lost. In between these two

layers the ECM is more sponge like. Therefore, this layer is believed to capture and divide the pressure of blood throughout the opening valve. Although some genes have been linked to valve remodeling, very little is known about the genetic mechanisms regulating this process. Interestingly, mature valves seem to share genetic programming with other tissues, which need to handle biomechanical forces, like cartilage and bone<sup>66</sup>. Mature zebrafish valves appear to undergo remodeling into a similar stratified structure as that described for mouse and chick<sup>25,67</sup>.

# MicroRNAs: small players of great importance for heart development

Initially microRNAs (miRNAs), a class of small (22 nucleotides) non-coding RNA molecules, were recognized in worms and the fruit fly to function as regulators of developmental processes. To date, thousands of miRNAs have been identified in many other organisms. Emerging fields of miRNA research have proven miRNAs are extremely versatile and function also to regulate various diseases processes, like tumor metastasis and cardiac hypertrophy.

## Biosynthesis of functional miRNA molecules: from transcription to mRNA targeting

MiRNAs are transcribed as long primary transcripts (pri-miRNAs) (Fig. 4). The vast majority of pri-miRNAs are subsequently subjected to canonical Drosha/DGCR8-mediated processing, leaving a hairpin like precursor miRNAs (pre-miRNAs) (Fig. 4). Interestingly, several classes of small RNAs have been proven to not require processing by Drosha, the miRtrons, tRNAZ, and small nucleolar RNA (snoRNAs) (reviewed in 68 and 69). Drosha cleavage can be specifically regulated for individual miRNAs, for example miR-21 Drosha processing is enhanced by a complex of Smad proteins and the RNA helicase DDX5 (p68)<sup>70,71</sup>. Pre-miRNAs are exported from the nucleus into the cytosol by Exportin-5, which forms a complex with Ran-GTP (Fig. 4)<sup>72</sup>. In the cytosol pre-miRNA hairpins encounter another crucial processing enzyme, Dicer. Dicer, a member of the RNase III family of endonucleases, was shown to cut double stranded RNA targets<sup>73</sup>. When meeting Dicer, the pre-miRNA hairpin loop and the base of the pre-miRNA hairpin will be removed, leaving short double stranded RNA molecules that constitute mature miRNAs (Fig. 4). Two additional proteins have been shown to enhance Dicer function, TRBP (Tar RNA binding protein) and PACT (protein activator of PKR)<sup>73,74</sup>. Recently, four exceptional mature miRNAs were proven to be still expressed in zebrafish *dicer* null embryos, suggesting Dicer-independent processing<sup>75</sup>. One of these miRNAs, miR-451, was shown both in zebrafish and mouse models to be alternatively cleaved by Argonaute-2 (Ago-2)<sup>75,76</sup>.

Dicer-processed miRNA duplexes consist of a guide and a passenger strand, the guide strand will be loaded into the RNA-Induced Silencing Complex (RISC). Once loaded in RISC, mature miRNAs guide the complex to recognition sequences present mainly in 3'UTRs of messenger RNAs (mRNAs)<sup>77</sup>. In plants miRNA:mRNA binding sites are fully complementary. In animals however the interaction between miRNAs and their targets occurs via partial Watson-Crick base pairing. The first 8 nucleotides of the mature miRNA sequence, the so-called "seed" sequence, mainly dictates mRNA target recognition in animals<sup>77,78</sup>. Once a target is bound, an Argonaute family member that is also situated within RISC, can cleave the targeted mRNA<sup>79</sup>. However, cleavage requires a high degree of miRNA:mRNA complementarity which is rare for animals. Both translational repression and mRNA destabilization have been proposed as miRNAs modes of action when binding a partial complementary mRNA target<sup>80</sup>. High throughput mRNA and protein expression profiling revealed that miRNA induced changes at the protein level were reflected by fluctuations in mRNA expression<sup>81,82</sup>. These data implied that mRNA destabilization might represent the major mechanism of miRNA action in animals since translational repression would not result in major changes



in mRNA expression. Guo and colleagues subsequently used ribosome profiling to confirm that destabilization of mRNAs, by de-adenylation and de-capping, is indeed the main mechanism for both ectopic and endogenous miRNAs to mediate mRNA degradation in animals (Fig. 4)<sup>83</sup>. Since miRNA seed sequences are so short, computational prediction of mRNA targets has been extremely challenging. Thus far most miRNA:mRNA interactions have been established by combining target predictions with experimental target validation. Target prediction is mostly based on the presence of evolutionarily conserved target recognition sequences<sup>77</sup>. Experimental proof mostly comes from miRNA silencing assays where artificially cloned 3'UTR sequences prevent translation of a linked reporter gene, like GFP or luciferase. However, tools to show *in vivo* interaction are emerging, like Argonaute pull-down techniques<sup>84</sup>.

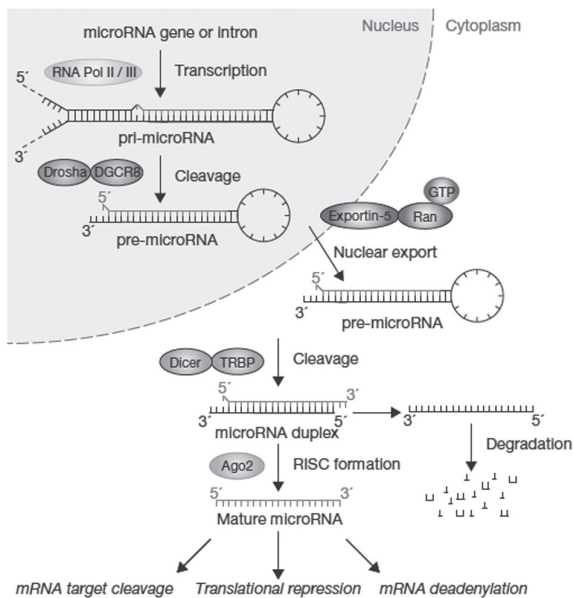


**Figure 4: Canonical microRNA biogenesis**  
 Canonical maturation starts by the production of the primary miRNA transcript (pri-miRNA) by RNA polymerase II or III and cleavage of the pri-miRNA by the microprocessor complex Drosha–DGCR8 in the nucleus. The resulting precursor hairpin, the pre-miRNA, is exported from the nucleus by Exportin-5–Ran-GTP. In the cytoplasm, the RNase Dicer, in complex with the double-stranded RNA-binding protein TRBP, cleaves the pre-miRNA hairpin to its mature form. The functional strand of the mature miRNA is loaded together with Argonaute (Ago2) proteins into the RNA-induced silencing complex (RISC), where it guides RISC to silence target mRNAs through mRNA cleavage, translational repression or deadenylation, whereas the passenger strand (black) is degraded. For divergent roads of miRNA processing we refer to the main text. Adapted from Winter et al. 2009<sup>68</sup>.

## Loss of miRNA function during myocardial development and cardiogenic diseases

MiRNA function during organogenesis has been studied mainly by generating conditional *Dicer* knockout models, since a full loss of *Dicer* results in a failure to maintain the stem cell population during early mouse development<sup>85</sup>. Zhou and colleagues described a *Tie2* induced deletion of *Dicer* from hematopoietic cells and endothelial cells<sup>86</sup>. However, potential endocardial defects were not reported for these mice and additional reports on miRNA function during endocardial development from other systems are limited. *Dicer* has also been depleted in myocardial cells using cardiomyocyte specific promoter regions of *Nkx2.5*<sup>87,88</sup> and *α-Mhc*<sup>89</sup>. Two different regulatory sequences of *Nkx2.5* have been investigated. Due to differences in timing and range of expression in the two *Nkx2.5*-Cre constructs, one promoter sequence is active from E8.5<sup>87</sup>, while the second construct results in a later onset of Cre expression<sup>88</sup>. Both studies show that losing miRNA function in the

myocardium causes cardiac failure, which leads to premature lethality of the embryos from E11.5 onwards<sup>87,88</sup>. Histological analysis of the failing hearts revealed poorly developed ventricular walls, due to trabeculation defects<sup>87</sup>. *Dicer* null embryos however did express most markers of initial cardiac differentiation and patterning, such as *Tbx5*, *Hand1*, *Hand2*, and *Mlc2v*<sup>87</sup>. Analysis of *Dicer* loss of function phenotypes using the later-expressed *Nkx2.5* promoter-driven Cre revealed prominent outflow tract (OFT) defects, like double-outlet right ventricle (DORV) that causes a mixture of oxygenated and de-oxygenated blood<sup>88</sup>. Candidate gene RNA expression profiling by *in situ* hybridization revealed *Pitx2c* and *Sema3c* to be differentially expressed in these *Dicer* null hearts. Interestingly, both genes are known to be required for OFT development<sup>90,91</sup>. Loss of myocardial *Dicer* under the control of a  $\alpha$ -*Mhc*-Cre, which has a later onset than the previously described *Nkx2.5* promoter regions, did not cause lethality *in utero*<sup>89</sup>. Instead, *Dicer* null embryos were indistinguishable from littermates at birth, yet died shortly after. These *Dicer* knockout mice exhibited several features of dilated cardiomyopathy (DCM) and heart failure.

Thus far miR-133 and miR-1 family members, transcribed as bicistronic clusters from the genome, are some of the most intensively studied myocardial miRNAs during embryology<sup>87,92-95</sup>. The miR-133 family consists of three members; miR-133a-1, miR-133a-2, and miR-133b transcribed together with miR-1-2, miR-1-1, and miR-206, respectively. The miR-1-2/miR-133a-1 and miR-1-1/ miR-133a-2 genes are expressed specifically in cardiac and skeletal muscle, whereas the miR-206/miR-133b gene is expressed only in skeletal muscle<sup>96,97</sup>.

Approximately half of miR-133a double knockout mice die *in utero*, mostly due to ventricular septum defects (VSDs)<sup>92</sup>. MiR-133a target gene analyses reveal miR-133a is required to promote cardiac proliferation and inhibit the smooth muscle gene program<sup>92</sup>. Therefore, loss of miR-133a function is suggested to be responsible for cardiac hypoplasticity and fibrosis. Depletion of miR-1-2 from cardiomyocytes also causes embryonic lethality due to VSDs. Furthermore, analysis of miR-1-2 mutant pups that survived to birth revealed myocardial dysfunction and cardiac conduction abnormalities<sup>87</sup>.

However, not all miRNAs that are expressed in myocardial cells during embryonic development appear to be required for cardiac development. Recently, mouse mutants for miR-208a, miR-208b and miR-499 (together referred to as MyomiRs) were shown to be indistinguishable from their littermates up to adulthood<sup>98,99</sup>. Upon myocardial infarction however these MyomiRs were proven to be essential components of a regulatory circuit promoting the slow muscle gene program<sup>98,99</sup>. MiR-208 knockout mice therefore were protected from this pathological response to cardiac stress<sup>98</sup>. On the contrary, *in vivo* knockdown of miR-133 could instantly induce a hypertrophic response in healthy animals, suggesting a protective potential of miR-133<sup>100</sup>. However, this effect was not recapitulated in double knockout mice for both miR-133a-1 and miR-133a-2<sup>92</sup>. Several other miRNAs have also been implicated in playing a role in cardiac disease by regulating mechanisms upon cardiac stress<sup>101,102</sup>. Since some miRNAs have been reported to exert a switch in the hypertrophic response, miRNAs have become a major interest as disease modifiers and therapeutic targets. In addition, miRNA levels can be modulated *in vivo* by using oligonucleotide inhibitors (antimiRs) and miRNA mimics for temporal knockdown and overexpression respectively. However, the contradictory results described previously obtained by using miR-133 modifiers on the one hand and miR-133 knockout models on the other, underline the necessity of cautious implementation of pharmacological approaches to study *in vivo* miRNA function.

## Zebrafish as a model to study miRNAs required for cardiac development

Since zebrafish embryos rely solely on yolk nutrition for the first few days of development, the zebrafish model forms a valuable tool for studying the cardiovascular system. While *Dicer* null mice are not viable<sup>85</sup>, zebrafish embryos lacking maternal and zygotic (MZ)*Dicer* protein do survive for a few days, although they are heavily truncated<sup>103</sup>. MiR-430 family members have been shown previously to be essential during maternal to zygotic transition by clearing maternally provided transcripts<sup>104</sup>. Injecting MZ*dicer* mutant embryos with miR-430 oligonucleotides therefore could restore gastrulation movements and rescue the morphological defects observed in tissues such as the brain. Cardiomyocytes were shown to be specified in *dicer* deficient embryos<sup>103</sup>, yet cardiac disc formation via fusion of the two bilateral cardiac field is impaired (A.K. Lagendijk and J. Bakkers, personal communication). MiR-430 injection was sufficient to restore fusion of the cardiac fields (A.K. Lagendijk and J. Bakkers, personal communication). Despite the early rescue of cardiac disc formation, miR-430 injection is not sufficient to regulate correct morphogenesis of the heart tube, suggesting a requirement for additional miRNAs<sup>103</sup>.

Temporal miRNA knockdown studies in zebrafish have identified a handful of miRNAs that regulate cardiac development. MiR-143 was reported to target *adducin3* RNA, coding for an F-actin capping protein, in the ventricular myocardium. Repression of miR-143 function caused ventricular collapse since abrogated F-actin remodeling disrupted cardiomyocyte growth and elongation<sup>105</sup>. An additional study provided two other miR-143 target genes; *retinaldehyde dehydrogenase 2 (raldh2/aldh1a2)* and *retinoid x receptor alpha b (rxrab)*, both players in retinoic acid (RA) signaling<sup>106</sup>. Interestingly, myocardial and endocardial expression of miR-143 was shown to be dependent on cardiac contractility. Therefore, a loss of contractility induced expression of RA signaling components. The miR-143:RA interaction was suggested to be specific to the endocardium, resulting in secondary non-cell autonomous myocardial defects<sup>106</sup>. Previously, however miR-143 expression was reported to be specific to myocardial cells<sup>105</sup>. Also, loss of RA signaling has been shown to cause an increase in both atrial and ventricular myocytes<sup>107,108</sup>. However, Deacon and co-workers reported that the amount of cardiomyocytes was unaffected upon a loss of miR-143 function<sup>106</sup>. Myocardial miR-138 function has also been implicated in regulation of RA signaling. MiR-138 specifically repressed 3' UTR target sequences of the RA synthesis enzyme *aldehyde dehydrogenase-1a2 (aldh1a2)* and the RA target gene *versican (cspg2)*<sup>109</sup>. Repression of RA signaling by miR-138 in the ventricle prevents expression of AVC genes thereby maintaining spatial differentiation of the myocardium.

MiR-126 is one of the most abundant miRNAs showing conserved expression in embryonic endothelial cells. Morpholino knockdown of miR-126 expression in zebrafish revealed the requirement of miR-126 for maintenance of endothelial integrity<sup>110</sup>. MiR-126 was shown, also by studies in miR-126 deficient mice, to repress negative regulators of Vegf signaling<sup>110-112</sup>. Recently, miR-126 has also been suggested to promote Vegf signaling in maturing cardiac valves thereby assuring valve elongation<sup>113</sup>.

The Slit2/3-encoded miR-218 family members have been described to control the migration of the cardiac fields to the midline in zebrafish<sup>114</sup>. MiR-218 was shown to modulate gene dosage of one of its targets, *robo1*, in the endocardium. Additional *in vitro* experiments implicated *robo1* can promote phosphorylation of the Vegfr2 in response to Vegf ligand binding. Interestingly, Vegf signaling was shown to also be required for migration of the

cardiac fields<sup>114</sup>. Since both gain and loss of *robo1* function was shown to induce failure of cardiac disc formation, fine-tuning *robo1* expression levels by miR-218 was suggested to be of importance during the process of cardiac fusion.

In Chapter 3 we describe a novel miRNA, miR-23, required to maintain proper patterning of the ECs. During this study we experienced difficulties in generating compelling miR-23 *in situ* hybridization data. Therefore, we developed an optimized *in situ* hybridization protocol, described in Chapter 2. This method greatly enhanced specificity detecting miR-23 and other miRNAs. In Chapter 4 we also describe another gene, *tmem2*, required to restrict the population of cells differentiating into ECs. Loss of *tmem2* also results in a failure of the heart tube to loop. A more detailed description of the looping process in zebrafish and characterization of a group of five looping mutants can be found in Chapter 5. Together, this thesis provides novel insights in EC formation and the cardiac looping process.

## REFERENCES

1. J. Bakkers, Zebrafish as a model to study cardiac development and human cardiac disease. *Cardiovasc Res* **91**, 279 (Jul 15, 2011).
2. D. Y. Stainier, R. K. Lee, M. C. Fishman, Cardiovascular development in the zebrafish. I. Myocardial fate map and heart tube formation. *Development* **119**, 31 (Sep,1993).
3. R. K. Lee, D. Y. Stainier, B. M. Weinstein, M. C. Fishman, Cardiovascular development in the zebrafish. II. Endocardial progenitors are sequestered within the heart field. *Development* **120**, 3361 (Dec,1994).
4. B. R. Keegan, D. Meyer, D. Yelon, Organization of cardiac chamber progenitors in the zebrafish blastula. *Development* **131**, 3081 (Jul, 2004).
5. J. N. Chen, M. C. Fishman, Zebrafish tinman homolog demarcates the heart field and initiates myocardial differentiation. *Development* **122**, 3809 (Dec, 1996).
6. J. Bussmann, J. Bakkers, S. Schulte-Merker, Early endocardial morphogenesis requires Scl/Tal1. *PLoS Genet* **3**, e140 (Aug, 2007).
7. E. Berdougou, H. Coleman, D. H. Lee, D. Y. Stainier, D. Yelon, Mutation of weak atrium/atrial myosin heavy chain disrupts atrial function and influences ventricular morphogenesis in zebrafish. *Development* **130**, 6121 (Dec, 2003)
8. Z. V. Garavito-Aguilar, H. E. Riley, D. Yelon, Hand2 ensures an appropriate environment for cardiac fusion by limiting Fibronectin function. *Development* **137**, 3215 (Oct, 2010).
9. N. Osborne et al., The spinster homolog, two of hearts, is required for sphingosine 1-phosphate signaling in zebrafish. *Curr Biol* **18**, 1882 (Dec 9, 2008).
10. L. A. Trinh, D. Y. Stainier, Fibronectin regulates epithelial organization during myocardial migration in zebrafish. *Dev Cell* **6**, 371 (Mar, 2004).
11. D. Y. Stainier et al., Mutations affecting the formation and function of the cardiovascular system in the zebrafish embryo. *Development* **123**, 285 (Dec, 1996).
12. T. Horsthuis et al., Gene expression profiling of the forming atrioventricular node using a novel tbx3-based node-specific transgenic reporter. *Circ Res* **105**, 61 (Jul 2, 2009).
13. N. G. Holtzman, J. J. Schoenebeck, H. J. Tsai, D. Yelon, Endocardium is necessary for cardiomyocyte movement during heart tube assembly. *Development* **134**, 2379 (Jun, 2007).
14. D. Y. Stainier, B. M. Weinstein, H. W. Detrich, 3rd, L. I. Zon, M. C. Fishman, Cloche, an early acting zebrafish gene, is required by both the endothelial and hematopoietic lineages. *Development* **121**, 3141 (Oct, 1995).
15. K. A. Smith et al., Rotation and asymmetric development of the zebrafish heart requires directed migration of cardiac progenitor cells. *Dev Cell* **14**, 287 (Feb, 2008).
16. S. Rohr, C. Otten, S. Abdelilah-Seyfried, Asymmetric involution of the myocardial field drives heart tube formation in zebrafish. *Circ Res* **102**, e12 (Feb 1, 2008).

17. K. Baker, N. G. Holtzman, R. D. Burdine, Direct and indirect roles for Nodal signaling in two axis conversions during asymmetric morphogenesis of the zebrafish heart. *Proc Natl Acad Sci U S A* **105**, 13924 (Sep 16, 2008).
18. J. N. Chen et al., Left-right pattern of cardiac BMP4 may drive asymmetry of the heart in zebrafish. *Development* **124**, 4373 (Nov, 1997).
19. J. Bakkers, M. C. Verhoeven, S. Abdelilah-Seyfried, Shaping the zebrafish heart: from left-right axis specification to epithelial tissue morphogenesis. *Dev Biol* **330**, 213 (Jun 15, 2009).
20. D. Beis et al., Genetic and cellular analyses of zebrafish atrioventricular cushion and valve development. *Development* **132**, 4193 (Sep, 2005).
21. A. K. Lagendijk, M. J. Goumans, S. B. Burkhard, J. Bakkers, MicroRNA-23 Restricts Cardiac Valve Formation by Inhibiting Has2 and Extracellular Hyaluronic Acid Production. *Circ Res* **109**, 649 (Sep 2, 2011).
22. P. J. Scherz, J. Huisken, P. Sahai-Hernandez, D. Y. Stainier, High-speed imaging of developing heart valves reveals interplay of morphogenesis and function. *Development* **135**, 1179 (Mar, 2008).
23. E. J. Armstrong, J. Bischoff, Heart valve development: endothelial cell signaling and differentiation. *Circ Res* **95**, 459 (Sep 3, 2004).
24. A. D. Person, S. E. Klewer, R. B. Runyan, Cell biology of cardiac cushion development. *Int Rev Cytol* **243**, 287 (2005).
25. R. T. Martin, T. Bartman, Analysis of heart valve development in larval zebrafish. *Dev Dyn* **238**, 1796 (Jul, 2009).
26. K. A. Smith et al., Dominant-negative ALK2 allele associates with congenital heart defects. *Circulation* **119**, 3062 (Jun 23, 2009).
27. A. K. Lagendijk, K. A. Smith, J. Bakkers, Genetics of congenital heart defects: a candidate gene approach. *Trends Cardiovasc Med* **20**, 124 (May, 2010).
28. M. D. Combs, K. E. Yutzey, Heart valve development: regulatory networks in development and disease. *Circ Res* **105**, 408 (Aug 28, 2009).
29. P. J. Gruber, J. A. Epstein, Development gone awry: congenital heart disease. *Circ Res* **94**, 273 (Feb 20, 2004).
30. J. I. Hoffman, S. Kaplan, The incidence of congenital heart disease. *J Am Coll Cardiol* **39**, 1890 (Jun 19, 2002).
31. L. D. Botto, A. Correa, J. D. Erickson, Racial and temporal variations in the prevalence of heart defects. *Pediatrics* **107**, E32 (Mar, 2001).
32. C. Ward, Clinical significance of the bicuspid aortic valve. *Heart* **83**, 81 (Jan, 2000).
33. D. Lloyd-Jones et al., Heart disease and stroke statistics--2010 update: a report from the American Heart Association. *Circulation* **121**, e46 (Feb 23, 2009).
34. K. J. Jenkins et al., Noninherited risk factors and congenital cardiovascular defects: current knowledge: a scientific statement from the American Heart Association Council on Cardiovascular Disease in the Young: endorsed by the American Academy of Pediatrics. *Circulation* **115**, 2995 (Jun 12, 2007).
35. V. Garg et al., GATA4 mutations cause human congenital heart defects and reveal an interaction with TBX5. *Nature* **424**, 443 (Jul 24, 2003).
36. J. J. Schott et al., Congenital heart disease caused by mutations in the transcription factor NKX2-5. *Science* **281**, 108 (Jul 3, 1998).
37. E. P. Kirk et al., Mutations in cardiac T-box factor gene TBX20 are associated with diverse cardiac pathologies, including defects of septation and valvulogenesis and cardiomyopathy. *Am J Hum Genet* **81**, 280 (Aug, 2007).
38. M. L. Metzker, Sequencing technologies - the next generation. *Nat Rev Genet* **11**, 31 (Jan, 2009).
39. C. H. Mjaatvedt, R. C. Lepera, R. R. Markwald, Myocardial specificity for initiating endothelial-mesenchymal cell transition in embryonic chick heart correlates with a particulate distribution of fibronectin. *Dev Biol* **119**, 59 (Jan, 1987).
40. R. B. Runyan, R. R. Markwald, Invasion of mesenchyme into three-dimensional collagen gels: a regional and temporal analysis of interaction in embryonic heart tissue. *Dev Biol* **95**, 108 (Jan, 1983).
41. R. Y. Kim, E. J. Robertson, M. J. Solloway, Bmp6 and Bmp7 are required for cushion formation and septation in the developing mouse heart. *Dev Biol* **235**, 449 (Jul 15, 2001).
42. W. Liu et al., Bmp4 signaling is required for outflow tract septation and branchial-arch artery remodeling. *Proc Natl Acad Sci U S A* **101**, 4489 (Mar 30, 2004).
43. L. Ma, M. F. Lu, R. J. Schwartz, J. F. Martin, Bmp2 is essential for cardiac cushion epithelial-mesenchymal transition and myocardial patterning. *Development* **132**, 5601 (Dec, 2005).
44. J. Rivera-Feliciano, C. J. Tabin, Bmp2 instructs cardiac progenitors to form the heart-valve-inducing field. *Dev Biol* **295**, 580 (Jul 15, 2006).
45. M. de Caestecker, The transforming growth factor-beta superfamily of receptors. *Cytokine Growth Factor Rev* **15**, 1 (Feb, 2004).
46. L. Song, R. Fassler, Y. Mishina, K. Jiao, H. S. Baldwin, Essential functions of Alk3 during AV cushion morphogenesis in mouse embryonic hearts. *Dev Biol* **301**, 276 (Jan 1, 2007).
47. J. Wang et al., Atrioventricular cushion transformation is mediated by ALK2 in the developing mouse heart. *Dev Biol* **286**, 299 (Oct 1, 2005).
48. M. Shirai, K. Imanaka-Yoshida, M. D. Schneider, R.

- J. Schwartz, T. Morisaki, T-box 2, a mediator of Bmp-Smad signaling, induced hyaluronan synthase 2 and Tgfbeta2 expression and endocardial cushion formation. *Proc Natl Acad Sci U S A* **106**, 18604 (Nov 3, 2009).
49. J. A. Schroeder, L. F. Jackson, D. C. Lee, T. D. Camenisch, Form and function of developing heart valves: coordination by extracellular matrix and growth factor signaling. *J Mol Med* **81**, 392 (Jul, 2003).
  50. T. D. Camenisch et al., Disruption of hyaluronan synthase-2 abrogates normal cardiac morphogenesis and hyaluronan-mediated transformation of epithelium to mesenchyme. *J Clin Invest* **106**, 349 (Aug, 2000).
  51. E. C. Walsh, D. Y. Stainier, UDP-glucose dehydrogenase required for cardiac valve formation in zebrafish. *Science* **293**, 1670 (Aug 31, 2001).
  52. T. D. Camenisch, J. A. Schroeder, J. Bradley, S. E. Klewer, J. A. McDonald, Heart-valve mesenchyme formation is dependent on hyaluronan-augmented activation of ErbB2-ErbB3 receptors. *Nat Med* **8**, 850 (Aug, 2002).
  53. S. L. Erickson et al., ErbB3 is required for normal cerebellar and cardiac development: a comparison with ErbB2- and heregulin-deficient mice. *Development* **124**, 4999 (Dec, 1997).
  54. J. Rivera-Feliciano et al., Development of heart valves requires Gata4 expression in endothelial-derived cells. *Development* **133**, 3607 (Sep, 2006).
  55. L. Y. Bourguignon, K. Peyrollier, E. Gilad, A. Brightman, Hyaluronan-CD44 interaction with neural Wiskott-Aldrich syndrome protein (N-WASP) promotes actin polymerization and ErbB2 activation leading to beta-catenin nuclear translocation, transcriptional up-regulation, and cell migration in ovarian tumor cells. *J Biol Chem* **282**, 1265 (Jan 12, 2007).
  56. L. Y. Bourguignon, W. Xia, G. Wong, Hyaluronan-mediated CD44 interaction with p300 and SIRT1 regulates beta-catenin signaling and NFkappaB-specific transcription activity leading to MDR1 and Bcl-xL gene expression and chemoresistance in breast tumor cells. *J Biol Chem* **284**, 2657 (Jan 30, 2009).
  57. A. F. Hurlstone et al., The Wnt/beta-catenin pathway regulates cardiac valve formation. *Nature* **425**, 633 (Oct 9, 2003).
  58. R. Iwamoto et al., Heparin-binding EGF-like growth factor and ErbB signaling is essential for heart function. *Proc Natl Acad Sci U S A* **100**, 3221 (Mar 18, 2003).
  59. L. F. Jackson et al., Defective valvulogenesis in HB-EGF and TACE-null mice is associated with aberrant BMP signaling. *Embo J* **22**, 2704 (Jun 2, 2003).
  60. B. Chen et al., Mice mutant for Egfr and Shp2 have defective cardiac semilunar valvulogenesis. *Nat Genet* **24**, 296 (Mar, 2000).
  61. R. S. Lo, D. Wotton, J. Massague, Epidermal growth factor signaling via Ras controls the Smad transcriptional co-repressor TGIF. *Embo J* **20**, 128 (Jan 15, 2001).
  62. K. Horiuchi, H. M. Zhou, K. Kelly, K. Manova, C. P. Blobel, Evaluation of the contributions of ADAMs 9, 12, 15, 17, and 19 to heart development and ectodomain shedding of neuregulins beta1 and beta2. *Dev Biol* **283**, 459 (Jul 15, 2005).
  63. S. W. Sunnarborg et al., Tumor necrosis factor-alpha converting enzyme (TACE) regulates epidermal growth factor receptor ligand availability. *J Biol Chem* **277**, 12838 (Apr 12, 2002).
  64. K. Kurohara et al., Essential roles of Meltrin beta (ADAM19) in heart development. *Dev Biol* **267**, 14 (Mar 1, 2004).
  65. H. M. Zhou et al., Essential role for ADAM19 in cardiovascular morphogenesis. *Mol Cell Biol* **24**, 96 (Jan, 2004).
  66. J. Lincoln, A. W. Lange, K. E. Yutzey, Hearts and bones: shared regulatory mechanisms in heart valve, cartilage, tendon, and bone development. *Dev Biol* **294**, 292 (Jun 15, 2006).
  67. N. Hu, D. Sedmera, H. J. Yost, E. B. Clark, Structure and function of the developing zebrafish heart. *Anat Rec* **260**, 148 (Oct 1, 2000).
  68. J. Winter, S. Jung, S. Keller, R. I. Gregory, S. Dieberichs, Many roads to maturity: microRNA biogenesis pathways and their regulation. *Nat Cell Biol* **11**, 228 (Mar, 2009).
  69. R. W. Carthew, E. J. Sontheimer, Origins and Mechanisms of miRNAs and siRNAs. *Cell* **136**, 642 (Feb 20, 2009).
  70. B. N. Davis, A. C. Hilyard, G. Lagna, A. Hata, SMAD proteins control DROSHA-mediated microRNA maturation. *Nature* **454**, 56 (Jul 3, 2008).
  71. B. N. Davis, A. C. Hilyard, P. H. Nguyen, G. Lagna, A. Hata, Smad proteins bind a conserved RNA sequence to promote microRNA maturation by Drosha. *Mol Cell* **39**, 373 (Aug 13, 2010).
  72. R. Yi, Y. Qin, I. G. Macara, B. R. Cullen, Exportin-5 mediates the nuclear export of pre-microRNAs and short hairpin RNAs. *Genes Dev* **17**, 3011 (Dec 15, 2003).
  73. E. Bernstein, A. A. Caudy, S. M. Hammond, G. J. Hannon, Role for a bidentate ribonuclease in the initiation step of RNA interference. *Nature* **409**, 363 (Jan 18, 2001).
  74. A. D. Haase et al., TRBP, a regulator of cellular PKR and HIV-1 virus expression, interacts with Dicer and functions in RNA silencing. *EMBO Rep* **6**, 961 (Oct, 2005).
  75. Y. Lee et al., The role of PACT in the RNA silencing pathway. *Embo J* **25**, 522 (Feb 8, 2006).
  76. D. Cifuentes et al., A novel miRNA processing pathway independent of Dicer requires Argonaute2

- catalytic activity. *Science* **328**, 1694 (Jun 25, 2010).
77. S. Cheloufi, C. O. Dos Santos, M. M. Chong, G. J. Hannon, A dicer-independent miRNA biogenesis pathway that requires Ago catalysis. *Nature* **465**, 584 (Jun 3, 2010).
  78. D. P. Bartel, MicroRNAs: target recognition and regulatory functions. *Cell* **136**, 215 (Jan 23, 2009).
  79. D. P. Bartel, MicroRNAs: genomics, biogenesis, mechanism, and function. *Cell* **116**, 281 (Jan 23, 2004).
  80. C. Ender, G. Meister, Argonaute proteins at a glance. *J Cell Sci* **123**, 1819 (Jun 1, 2010).
  81. E. Huntzinger, E. Izaurralde, Gene silencing by microRNAs: contributions of translational repression and mRNA decay. *Nat Rev Genet* **12**, 99 (Feb, 2011).
  82. D. Baek et al., The impact of microRNAs on protein output. *Nature* **455**, 64 (Sep 4, 2008).
  83. M. Selbach et al., Widespread changes in protein synthesis induced by microRNAs. *Nature* **455**, 58 (Sep 4, 2008).
  84. H. Guo, N. T. Ingolia, J. S. Weissman, D. P. Bartel, Mammalian microRNAs predominantly act to decrease target mRNA levels. *Nature* **466**, 835 (Aug 12, 2010).
  85. Y. Andachi, A novel biochemical method to identify target genes of individual microRNAs: identification of a new *Caenorhabditis elegans* let-7 target. *RNA* **14**, 2440 (Nov, 2008).
  86. E. Bernstein et al., Dicer is essential for mouse development. *Nat Genet* **35**, 215 (Nov, 2003).
  87. L. Zhou et al., Tie2<sup>cre</sup>-induced inactivation of the miRNA-processing enzyme Dicer disrupts invariant NKT cell development. *Proc Natl Acad Sci U S A* **106**, 10266 (Jun 23, 2009).
  88. Y. Zhao et al., Dysregulation of cardiogenesis, cardiac conduction, and cell cycle in mice lacking miRNA-1-2. *Cell* **129**, 303 (Apr 20, 2007).
  89. A. Saxena, C. J. Tabin, miRNA-processing enzyme Dicer is necessary for cardiac outflow tract alignment and chamber septation. *Proc Natl Acad Sci U S A* **107**, 87 (Jan 5, 2010).
  90. J. F. Chen et al., Targeted deletion of Dicer in the heart leads to dilated cardiomyopathy and heart failure. *Proc Natl Acad Sci U S A* **105**, 2111 (Feb 12, 2008).
  91. C. Liu et al., Pitx2c patterns anterior myocardium and aortic arch vessels and is required for local cell movement into atrioventricular cushions. *Development* **129**, 5081 (Nov, 2002).
  92. Q. Jia et al., Smad signaling in the neural crest regulates cardiac outflow tract remodeling through cell autonomous and non-cell autonomous effects. *Dev Biol* **311**, 172 (Nov 1, 2007).
  93. N. Liu et al., microRNA-133a regulates cardiomyocyte proliferation and suppresses smooth muscle gene expression in the heart. *Genes Dev* **22**, 3242 (Dec 1, 2008).
  94. Y. Zhao, E. Samal, D. Srivastava, Serum response factor regulates a muscle-specific microRNA that targets Hand2 during cardiogenesis. *Nature* **436**, 214 (Jul 14, 2005).
  95. C. Xu et al., The muscle-specific microRNAs miR-1 and miR-133 produce opposing effects on apoptosis by targeting HSP60, HSP70 and caspase-9 in cardiomyocytes. *J Cell Sci* **120**, 3045 (Sep 1, 2007).
  96. L. Qian et al., Tinman/Nkx2-5 acts via miR-1 and upstream of Cdc42 to regulate heart function across species. *J Cell Biol* **193**, 1181 (Jun 27, 2011).
  97. E. van Rooij et al., Dysregulation of microRNAs after myocardial infarction reveals a role of miR-29 in cardiac fibrosis. *Proc Natl Acad Sci U S A* **105**, 13027 (Sep 2, 2008).
  98. J. J. McCarthy, MicroRNA-206: the skeletal muscle specific myomiR. *Biochim Biophys Acta* **1779**, 682 (Nov, 2008).
  99. E. van Rooij et al., Control of stress-dependent cardiac growth and gene expression by a microRNA. *Science* **316**, 575 (Apr 27, 2007).
  100. E. van Rooij et al., A family of microRNAs encoded by myosin genes governs myosin expression and muscle performance. *Dev Cell* **17**, 662 (Nov, 2009).
  101. A. Care et al., MicroRNA-133 controls cardiac hypertrophy. *Nat Med* **13**, 613 (May, 2007).
  102. E. M. Small, R. J. Frost, E. N. Olson, MicroRNAs add a new dimension to cardiovascular disease. *Circulation* **121**, 1022 (Mar 2, 2010).
  103. E. M. Small, E. N. Olson, Pervasive roles of microRNAs in cardiovascular biology. *Nature* **469**, 336 (Jan 20, 2011).
  104. A. J. Giraldez et al., MicroRNAs regulate brain morphogenesis in zebrafish. *Science* **308**, 833 (May 6, 2005).
  105. A. J. Giraldez et al., Zebrafish MiR-430 promotes deadenylation and clearance of maternal mRNAs. *Science* **312**, 75 (Apr 7, 2006).
  106. D. C. Deacon et al., The miR-143-adducin3 pathway is essential for cardiac chamber morphogenesis. *Development* **137**, 1887 (Jun, 2010).
  107. K. Y. Miyasaka et al., Heartbeat regulates cardiac genesis by suppressing retinoic acid signaling via expression of miR-143. *Mech Dev* **128**, 18 (Jan-Feb, 2011).
  108. J. S. Waxman, B. R. Keegan, R. W. Roberts, K. D. Poss, D. Yelon, Hoxb5b acts downstream of retinoic acid signaling in the forelimb field to restrict heart field potential in zebrafish. *Dev Cell* **15**, 923 (Dec, 2008).
  109. B. R. Keegan, J. L. Feldman, G. Begemann, P. W. Ingham, D. Yelon, Retinoic acid signaling restricts the cardiac progenitor pool. *Science* **307**, 247 (Jan 14, 2005).
  110. S. U. Morton et al., microRNA-138 modulates cardiac patterning during embryonic development.

- Proc Natl Acad Sci U S A* **105**, 17830 (Nov 18, 2008).
111. J. E. Fish et al., miR-126 regulates angiogenic signaling and vascular integrity. *Dev Cell* **15**, 272 (Aug, 2008).
  112. F. Kuhnert et al., Attribution of vascular phenotypes of the murine *Egfl7* locus to the microRNA miR-126. *Development* **135**, 3989 (Dec, 2008).
  113. S. Wang et al., The endothelial-specific microRNA miR-126 governs vascular integrity and angiogenesis. *Dev Cell* **15**, 261 (Aug, 2008).
  114. K. Stankunas, G. K. Ma, F. J. Kuhnert, C. J. Kuo, C. P. Chang, VEGF signaling has distinct spatiotemporal roles during heart valve development. *Dev Biol* **347**, 325 (Nov 15, 2010).
  115. J. E. Fish et al., A Slit/miR-218/Robo regulatory loop is required during heart tube formation in zebrafish. *Development* **138**, 1409 (Apr, 2011).







# REVEALING THE DETAILS: AN IMPROVED METHOD FOR WHOLE MOUNT IN SITU HYBRIDIZATIONS

A.K. Lagendijk<sup>1</sup>, J.D Moulton<sup>3</sup> and J. Bakkers<sup>1,2</sup>

*Manuscript in preperation*

1. Hubrecht Institute, KNAW & Iniversity Medical Center, Utrecht, The Netherlands.
2. Interuniversity Cardiology, Institute of the Netherlands, Utrecht, The Netherlands
3. GeneTools, Philomatch, Oregon, United Stated of America

2

## ABSTRACT

Non-coding microRNA (miRNA) molecules modulate the amount of messenger RNAs that will continue to translate into protein. Spatial expression data for miRNAs is of great importance to provide information on where each miRNA can interact with potential mRNA targets. Although current miRNA *in situ* hybridization protocols work well for high abundance miRNAs, technical problems are encountered when detecting low-abundance miRNAs. Particularly, non-specific background staining can perturb analysis of genuine miRNA expression. Here, we describe two new methodologies that can be added to the miRNA *in situ* toolbox. Firstly, we show that whole mount 1-ethyl-3-(3-dimethyl-aminopropyl) carbodiimide fixation is a powerful tool to enhance specificity of miRNA *in situ* signals in zebrafish embryo and adult tissues. Secondly, we successfully have used Morpholino based miRNA *in situ* probes for whole mount miRNA detection. The combination of both methods will allow the use of a single antisense Morpholino oligomer for both miRNA knockdown as well as miRNA whole mount *in situ* hybridization experiments.

## INTRODUCTION

Since the discovery of the first regulating small RNAs (later classified as microRNAs), *lin-4* and *let-7*, in the nematode *Caenorhabditis elegans*<sup>1,2</sup>, on-going high throughput cloning approaches have led to the discovery of hundreds of miRNAs. MicroRNAs (miRNAs) inhibit protein expression by binding mainly to 3'UTR sequences of messenger RNA molecules (reviewed in Bartel et al.<sup>3</sup>). Functional studies thus far have implicated miRNAs to function in various processes during embryonic development and disease (reviewed in Hagen et al.<sup>4</sup>). Since miRNAs do not translate into protein, identification of miRNA expression by *in situ* hybridization has been proven to be a valuable tool to indicate in which cell types individual miRNAs are present. Wienholds and colleagues performed the first high throughput miRNA *in situ* hybridization screen using locked nucleic acid (LNA) modified DNA probes on zebrafish embryos<sup>5</sup>. They revealed expression patterns for 115 conserved miRNAs, most of which having striking temporal and spatial specificity<sup>5</sup>. This LNA *in situ* hybridization method was described in more detail in 2006, nicely presenting a minimal length for LNA probes and providing optimised hybridization times and temperatures<sup>6</sup>. To date, LNA probes complementary to mature miRNA sequences remain the most commonly used oligos for miRNA detection from various species<sup>7-9</sup>, both for *in situ* hybridization and as probes on microarray platforms. Nevertheless, alternatives to using LNA based probes have been published<sup>10</sup>.

We found that by using the Kloosterman *in situ* hybridization protocol in our laboratory we could reproduce miRNA expression profiles comparable to what had been reported previously<sup>5,10</sup>. However, for detecting low levels of expression, at earlier developmental stages or for low abundant miRNAs, the Kloosterman protocol did not provide full satisfaction.

An interesting observation regarding miRNA *in situ* specificity was made by Pena and co-workers in 2009<sup>11</sup>. They showed that by fixing mouse paraffin sections with 1-ethyl-3-(3-dimethyl-aminopropyl) carbodiimide (EDC) the *in situ* signal intensity was greatly improved. When fixing sections traditionally in formaldehyde, miRNAs tend to be fixed inefficiently and therefore they diffuse from the tissue during high temperature *in situ* washes. EDC however, prevents miRNA diffusion by crosslinking miRNA 5'ends with amino groups in the protein matrix<sup>11</sup>. Thereby, EDC fixation prevents diffusion of miRNAs that were insufficiently fixed using formaldehyde. Diffusion can decrease target RNA concentration below the detection limit, especially for miRNAs of low-abundance. Reproducibility of this EDC fixation method however has been debated by others<sup>12</sup>.

We have applied EDC fixation on zebrafish (*Danio rerio*) embryos and adult zebrafish tissues prior to whole mount miRNA *in situ* staining using LNA probes. Our results demonstrate that EDC fixation increased intensity of miRNA *in situ* signals also for whole mount *in situ* hybridizations. In addition, we introduce carboxyfluorescein(CF)-labelled Morpholino oligomers (MOs) as effective miRNA *in situ* probes with detection specificity comparable to LNA probes.

# MATERIAL AND METHODS

## Tissue preparation

Zebrafish embryos were staged live and subsequently fixed in 4% paraformaldehyde (PFA) overnight at 4°C. Next, embryos were washed twice in PBS containing 0.01% Tween-20 (PBS-T) to remove residual PFA and subsequently dehydrated through a series of methanol (MeOH) washes (25% MeOH, 50% MeOH, 75% MeOH) in PBS-T. Embryos were stored in 100% MeOH at -20°C.

Zebrafish adult hearts and fins were fixed in 4% PFA for minimally 36 hours up to 1 week at 4°C. PFA fixed tissues were dehydrated by applying the previously described series of MeOH washes and finally stored at -20°C in 100% MeOH.

## EDC fixation

PFA fixed embryos and adult tissues were washed twice in PBS-T and subsequently washed three times in 1-methylimidazole buffer (1-mib). Next, embryos and adult tissues were fixed again at 4°C in 0.16M EDC in 1-mib (pH 8.0). Embryos were fixed in EDC overnight, adult tissues were fixed for minimally 36 hours. Finally, PFA+EDC fixed embryos and tissues were dehydrated through a series of MeOH washes and stored in 100% MeOH at -20°C.

## MicroRNA *in situ* hybridization

Whole mount *in situ* hybridizations on zebrafish embryos and tissues were performed as described previously<sup>6</sup> with the following adjustments:

Proteinase K (10 µg/ml in PBS-T) treatments used for embryos fixed at 1 dpf, 2 dpf, 3 dpf and 4 dpf were 15 minutes (min), 30 min, 45 min and 60 min respectively at 37°C. Adult tissues were treated in proteinase K for 90 min at 37°C. After proteinase K treatment embryos were fixed for 10min and adult tissues for 20 min in 4% PFA. To improve blocking we used 1 mg/ml tRNAs during pre-hybridization and overnight hybridization with probes.

For LNA probes (Exiqon) pre-hybridization, probe hybridization and post hybridization washes were performed at 23°C below the company provided melting temperatures ( $T_m$ ). For MO based probes (Gene Tools) pre-hybridization, probe hybridization and post hybridization washes were performed at 50-55°C below company provided melting temperatures ( $T_m$ ). A 10 µM stock of the double Digoxigenin labelled (3' and 5') miR-23a LNA probe was ordered (Exiqon) and diluted in hybridization buffer as a working stock. Other LNA oligonucleotides were diluted to a 10 µM stock and subsequently labelled with digoxigenin-11-ddUTP (Roche) Digoxigenin (Roche) at the 3' end using a terminal transferase kit (Roche). A 1 mM stock of CF-labelled MO probes was diluted 1:50000 in hybridization buffer as a working dilution. All LNA and MO probe working dilutions were re-used up to 10 times. To improve specificity of digoxigenin and fluorescein antibodies (Roche), these were pre-incubated for at least one hour in blocking buffer (2% sheep serum and 20 mg/ml BSA in PBS-T) containing fragments of zebrafish embryonic tissue collected at various stages. Sodium azide (0.02%) was added to the resulting supernatant to prevent moulding. The final antibody solutions were diluted 50 times in blocking buffer for overnight antibody incubation steps. To terminate staining reactions embryos and tissues were washed three times in PBS-T. All stained samples were subsequently fixed in 4% PFA at 4°C overnight. After fixation, samples were washed again three times in PBS-T followed by two subsequent

washes in 100% MeOH to remove diffused staining. All samples were finally transferred into Murray's solution (benzylbenzoate:benzylalcohol 2:1) and stored for at least one night at 4°C before imaging. LNA and MO probe sequences,  $T_m$  values and hybridization temperatures are listed in Table 1.

## Morpholino injections

MiR-23a MO (Gene Tools) was diluted and injected as described previously<sup>13</sup>. MiR-206-1 and miR-206-2 MOs (Gene Tools) used for injection were designed to overlap either the Drosha or the Dicer cleavage site respectively. MiR-206 precursor MO sequences:

miR-206-1 drosha MO 5'-gacaaattcccctgaaccacac-3'

miR-206-2 dicer MO 5'-tccatagattaattctgaatggg-3'.

For injection, miR-206 MOs were diluted to 0.2 mmol/l, of which 1 nl was injected at the one cell stage.

probe	sequence (5' – 3')	$T_m$ (°C)	hyb. temp (°C)
LNA miR-23a	tggaatccctggcaatgtgat	80	57
LNA miR-21	caacaccagtctgataagcta	72	49
LNA miR-138	gattcacaacaccagct	73	50
MO miR-124	tgccattaccgcgtgccttaa	98.9	45
MO miR-21	gccaacaccagtctgataagcta	89	34
MO-miR-206	ccacacctccttacattcca	91.3	37

Table 1: List of probes used for this study

Sequences of probes used are listed together with company predicted melting temperatures of the sequences and the temperatures used for hybridization during the *in situ* procedure. The LNA  $T_m$  prediction tool is accessible at [www.exiqon.com](http://www.exiqon.com). The MO predicted  $T_m$  values were provided by Genetools.

## RESULTS AND DISCUSSION

### Whole mount EDC fixation improves specificity and reveals sparse miRNAs

To optimise the current miRNA *in situ* protocol we investigated whether addition of EDC fixation<sup>11</sup>, would improve whole mount miRNA expression signals. We fixed a clutch of wild-type zebrafish embryos at 3 days post fertilization (3 dpf) in 4% paraformaldehyde (PFA) overnight. Embryos were subsequently divided in two groups. One group was washed to 100% methanol (MeOH) and stored at -20°C. The second group was washed three times in 1-methylimidazole buffer and fixed again overnight in EDC at 4°C. Afterwards, EDC fixed embryos were also dehydrated and stored in MeOH. We performed *in situ* hybridizations on both batches of embryos using a double digoxigenin (DIG) labelled (3'end and 5'end) LNA based probe for miR-23a, a miRNA we had previously found in our laboratory was difficult to detect specifically<sup>13</sup>. When developing miR-23a *in situ* stainings we observed

that in embryos solely fixed in 4% PFA, non-specific background staining became apparent alongside miR-23a specific staining (Fig. 1A-C). In contrast, the PFA+EDC fixed embryos remained mostly blank while robust restrictive miR-23a expression was detected in specific cell populations without the non-specific background staining as observed with only PFA fixation, like the endocardial cushions in the heart (Fig. 1D-F, black arrowheads). Since in PFA fixed embryos the increasing background staining perturbed visibility of miR-23a specific staining, the reaction had to be stopped after 5-8 hours. The PFA+EDC fixed embryos could be stained for much longer (up to 5 days) without manifestation of background staining in

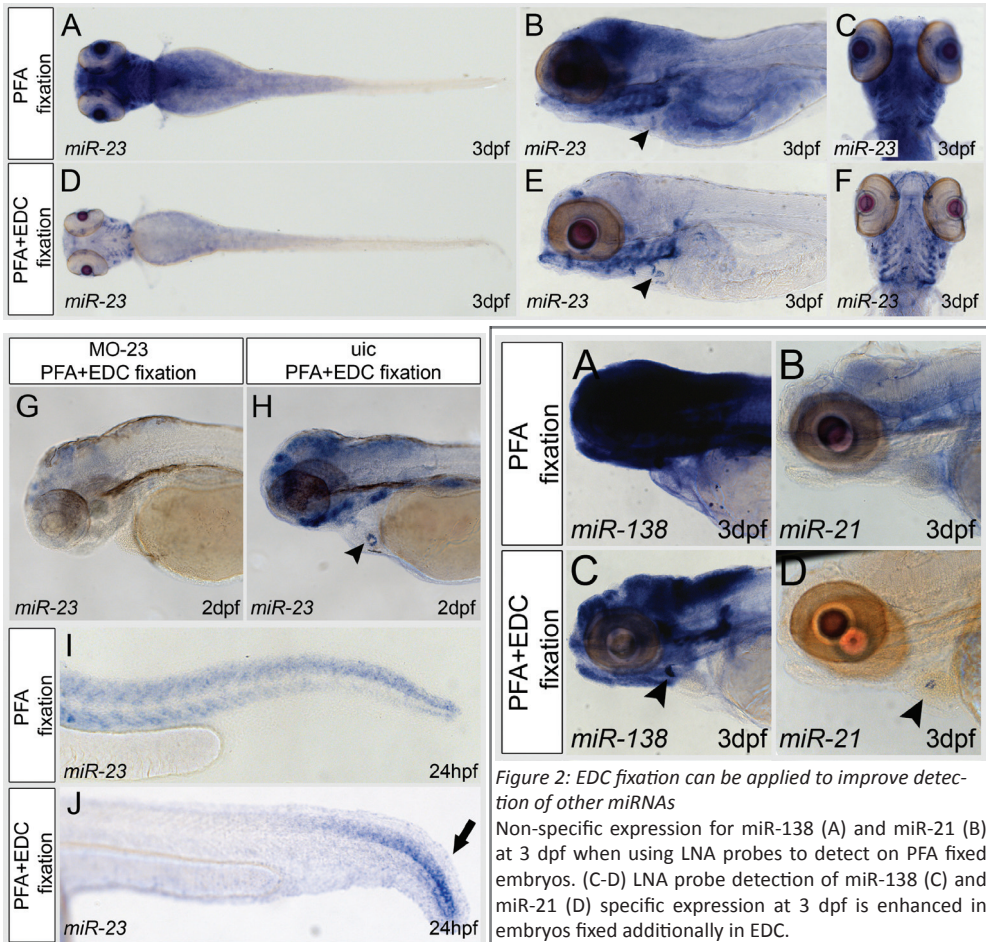


**Figure 1: EDC fixation enhances miRNA in situ hybridization specificity**

(A-C) miR-23a expression at 3 dpf on PFA fixed embryos, dorsal views shown in A and C, lateral view in B. (D-F) More restricted miR-23a expression at 3 dpf upon PFA+EDC fixation, dorsal views shown in D and F, lateral view in E. Black arrowheads in B and D indicate miR-23a expression in the endocardial cushions of the heart. (G-H) Wild-type miR-23a expression at 2 dpf (H) is lost upon miR-23a MO injection (G). Black arrowhead in H indicates the endocardial cushion cells at 2 dpf. By applying EDC fixation we could detect restricted miR-23a expression at 24 hpf specifically in the tip of the tail (black arrow in J) while PFA fixation resulted in non-specific diffuse staining throughout the embryonic tail (I).

**Figure 2: EDC fixation can be applied to improve detection of other miRNAs**  
 Non-specific expression for miR-138 (A) and miR-21 (B) at 3 dpf when using LNA probes to detect on PFA fixed embryos. (C-D) LNA probe detection of miR-138 (C) and miR-21 (D) specific expression at 3 dpf is enhanced in embryos fixed additionally in EDC.



other parts of the embryo (A.K.L. and J.B. personal communication). To exemplify that the observed miR-23a expression was indeed specific we performed miR-23a *in situ* analysis on non-injected embryos at 2 dpf versus embryos that had been previously injected with a miR-23a MO. MiRNA MOs have been reported to specifically bind to miRNA precursors and thereby inhibit further processing and suppress mature miRNA expression<sup>14</sup>. As expected we did not detect any signal for miR-23a in MO injected embryos (Fig. 1G). In non-injected siblings miR-23a could be detected again in a spatially overlapping pattern compared to what we had observed previously at 3 dpf (Fig. 1H, black arrowhead).

For most miRNAs expression levels increase slowly during development<sup>5</sup>, and so it can be challenging to pinpoint the onset of miRNA expression using the Kloosterman method<sup>6</sup>. Therefore we applied PFA+EDC fixation to a series of embryonic stages to investigate whether we could improve detection of specific expression at earlier stages. We again performed miR-23a *in situ* hybridizations using a double DIG labelled (3'end and 5'end) LNA probe on embryos fixed at 24 hours post fertilization (hpf) up to 3 dpf. We found that upon PFA+EDC treatment we could detect miR-23a specifically as early as 24 hpf in the tip of the tail while in PFA fixed siblings no miR-23a specific staining was detected (Fig. 1I and J).

Next, we examined whether EDC fixation could be used to improve signal intensity for other miRNAs. We performed *in situ* analysis on embryos fixed at 3 dpf and probed for miR-138 and miR-21 using 3'end DIG-labelled LNA probes. Again we observed that embryos fixed in 4% PFA developed intense background staining mostly in the head region (Fig. 2A and B). In PFA+EDC fixed embryos however we could clearly distinguish miR-138 and miR-21 specific expression in respectively the developing bulbus arteriosus/ outflow tract (black arrowhead in Fig. 2C) and the endocardial cushions of the heart (black arrowhead in Fig. 2D). Taken together, these results demonstrate a robust improvement to both efficiency and specificity of miRNA *in situ* staining when embryos were fixed in EDC. In addition, the time window of miRNA detection was extended since using this procedure revealed low-abundance miRNA expression at earlier in development.

## EDC fixation reveals miRNA expression on whole mount zebrafish adult tissues

In addition to whole mount *in situ* hybridizations on zebrafish embryos, which are relatively small in size, we investigated whether EDC fixation would improve detection of miRNA expression in larger tissues. Currently, *in situ* hybridizations on larger tissues are mostly performed on paraffin embedded sections<sup>7,11,15</sup>. However, tissue sectioning can induce damage to overall tissue morphology. Therefore, whole mount *in situ* hybridizations might offer a more realistic histological image. We dissected adult zebrafish hearts and fins and again performed miR-23a *in situ* analysis using an LNA based double DIG labelled probe. While we did not observe any specific staining when hearts were fixed only in PFA (data not shown), we did observe restricted miR-23a expression at the venous pole of the heart (black arrowhead in Fig. 3A) and in coronary arteries (white arrows in Fig. 3B) of PFA+EDC fixed adult hearts. In addition, we observed specific miR-23a expression in bone element of adult fins when fixed in PFA+EDC (black arrows in Fig. 3C). To control for probe specificity and endogenous peroxidase activity in these adult tissues we also added a “no probe” control, hearts hybridized without addition of a LNA probe. As expected we did not detect any specific staining in unprobed hearts (Fig. 3D).

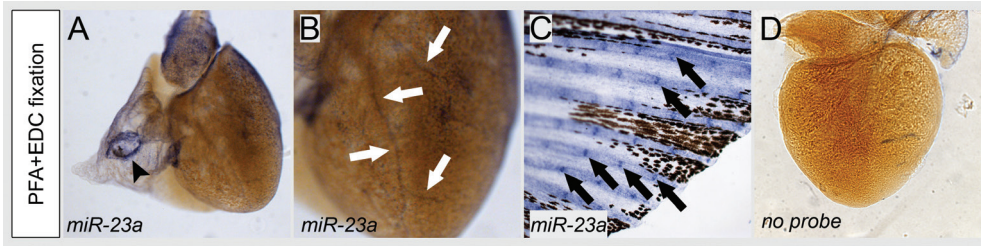


Figure 3: EDC fixation reveals miRNA expression in whole mount adult tissues

(A-B) MiR-23a expression in a zebrafish adult heart. Black arrowhead in A indicates a ring of miR-23a expression surrounding the atrial inflow site (n=6/6). White arrows in B indicate miR-23a expression in coronary arteries overlaying the ventricle myocardium. (C) MiR-23a expression in a zebrafish adult caudal fin (n=4/4). Black arrows in C indicate miR-23a expression in segments of the bones/ cartilage in the fin rays. (D) No expression in negative control heart processed without addition of a miRNA probe (n=4/4).

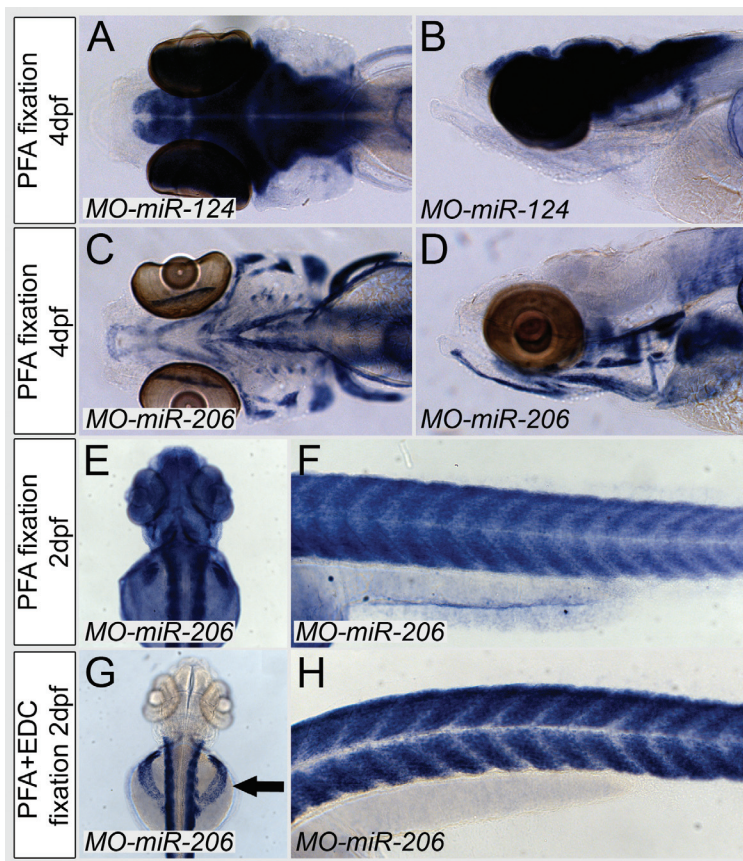


Figure 4: Morpholino probes can detect miRNA expression in embryos

MiR-124 specific expression (A; dorsal view, B; lateral view) in the developing brain at 4 dpf using a CF-labeled MO miR-124 probe. (C-D) MiR-206 specific expression (C; dorsal view, D; lateral view) in the skeletal muscle cells at 4 dpf using a CF-labeled MO miR-206 probe. (E-F) Diffuse miR-206 staining (E; dorsal view, F; lateral view) at 2 dpf in PFA fixed embryos, detected by a CF-labeled MO miR-206 probe. (G-H) Signal specificity is enhanced for CF-labeled MO detection of miR-206 at 2 dpf in EDC fixed embryos (G; dorsal view, H; lateral view). Black arrow in G indicated miR-206 expression not detectable in embryos only fixed in PFA (E).

Due to the regenerative capacity of zebrafish adult fins and hearts, these tissues are often used for gene expression analysis. Whole mount miRNA *in situ* hybridizations with EDC fixation on adult tissues offers a novel tool for this field of research

## Morpholino oligomers can probe miRNA expression with efficacy similar to LNA

Thus far LNA modified probes are most often used for miRNA *in situ* detection. However Morpholino oligomers (MOs) have also been shown to bind miRNAs with high affinity and thereby efficiently knockdown miRNA expression in zebrafish embryos<sup>14</sup>. LNA oligonucleotides were shown to exert toxic effects on zebrafish embryonic development when used as a knockdown reagent<sup>14</sup>. We hypothesized that MOs could also function to probe miRNAs for *in situ* hybridization analysis knowing their potential to stably bind to miRNAs *in vivo*. We used CF-labelled MOs as miRNA probes, complementary to the mature miRNA sequences of miR-124 and miR-206. For this, we first fixed embryos at 2 dpf and 4 dpf in 4% PFA only. We detected specific expression for both miRNAs, which were most prominent at 4 dpf (Fig. 4A-D). The spatial expression was indistinguishable from previously published miR-124 and miR-206 expression patterns detected by LNA probes<sup>5,6</sup>. Though we could detect miR-124 and miR-206 specifically at 4 dpf, background staining was still apparent at mostly at 2 dpf (Fig. 4E and F). We were able to increase specificity however by applying additional EDC treatments. Interestingly, we observed miR-206 expression in cells that did not stain when using PFA fixation only (Fig. 4E with 4G, black arrow).

Since for many miRNAs several genomic copies have been identified, which share the same mature miRNA sequence, mature (guide) strand probes are not able to distinguish between the expressions of the various miRNA copy variants. We used knockdown MOs to target the hairpin for knockdown MOs to target the hairpin for each of the two miR-206 copies that reside in the zebrafish genome. We subsequently performed *in situ* hybridization analysis using the miR-206 probe complementary to the miR-206 mature sequence at 24 hpf. We observed clear miR-206 expression in non-injected control embryos (Fig. 5, left). When embryos were injected either with a miR-206-1 or a miR-206-2 MO, expression was still detected in the same cells but less intense (Fig. 5, middle and right). These results suggest that mature miRNA expression derived from the two copies of miR-206 reside in the same cells and therefore these two copies complement each other's function.

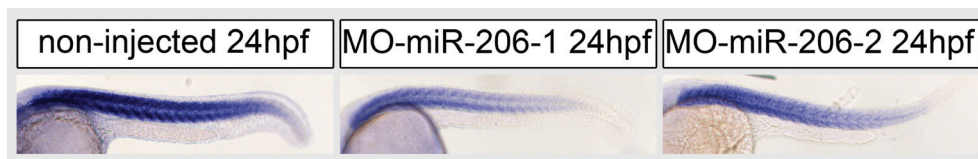


Figure 5: MiR-206 precursor knockdown results in decreased mature miR-206 expression

(Left) Mature miR-206 expression detected by a CF-labeled MO probe in skeletal muscle cells of non-injected control embryo (n=6/6). (Middle) Lowered mature miR-206 expression detected by a CF-labeled MO probe in skeletal muscle cells of embryo injected with miR-206-1 MO (n=7/7). (Right) Lowered mature miR-206 expression detected by a CF-labeled MO probe in skeletal muscle cells of embryo injected with miR-206-2 MO (n=6/6).

# CONCLUSIONS

With this study we have demonstrated that EDC fixation significantly enhances miRNA detection in whole mount zebrafish embryos and zebrafish adult tissues compared to conventional PFA fixation only. In addition, we introduced MO probes as a novel tool for miRNA *in situ* detection. MiRNA expression data retrieved using morpholino probes were as competent as previous expression data published for LNA probes<sup>5,6</sup>.

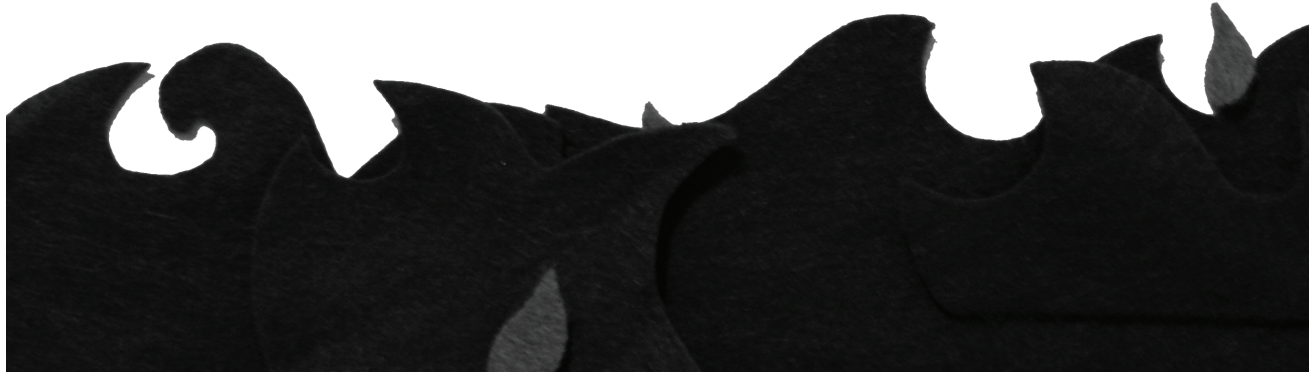
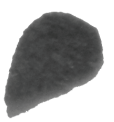
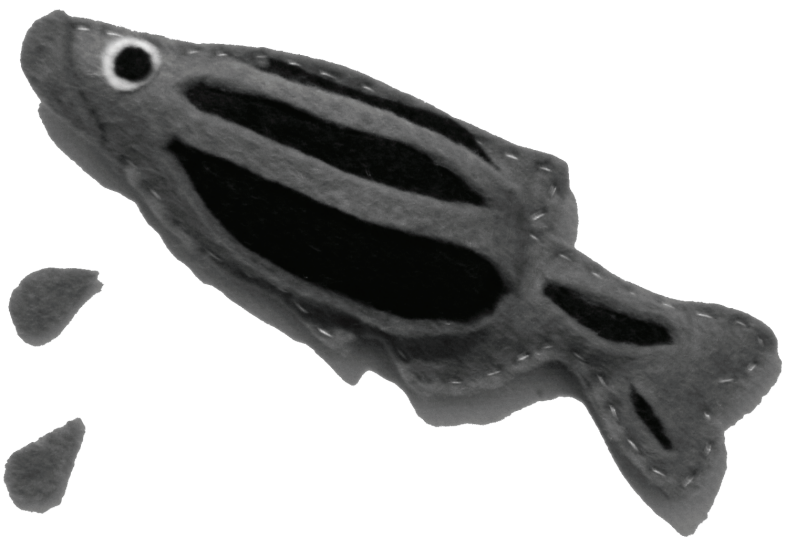
Spatial miRNA expression analysis reveals important clues on miRNA function, since mRNA targets should be present in the same cells. Although miRNA *in situ* protocols have been described showing robust miRNA expression, reproducibility can still be challenging. Especially low abundant miRNAs can be difficult to detect. Due to technical difficulties conflicting results describing miRNA expression have been published. MiR-143 for instance was reported to be expressed exclusively in the ventricular myocardium by Deacon and colleagues<sup>16</sup>. A later study however suggests miR-143 is also expressed in endocardial cells, which was supplemented with the identification of endocardial mRNA target genes<sup>17</sup>. To resolve such issues, we believe high quality *in situ* data with increased specificity are a necessity for miRNA research and EDC fixation can contribute to improved miRNA detection. To our knowledge the adult miRNA expression data presented in this study represent the first whole mount miRNA expression data on zebrafish tissues of this size. For spatial expression profiling, for instance during a regenerative response, this method can be a valuable new tool.

Currently LNA oligonucleotides are mainly used for miRNA expression analysis while MOs are commonly applied as miRNA knockdown reagent. The introduction of an additional application for MOs as miRNA probes opens up the possibility to use a single oligonucleotide for both purposes. Indeed we demonstrated that MO based probes are as efficient as LNA based probes to detect miRNA expression patterns using whole mount *in situ*. As shown for miR-138 previously, spatial expression can differ between miRNA copies<sup>15</sup>. Others and we showed that MOs can be used to knockdown individual miRNA copies<sup>6</sup>. For future studies, MO can be used to investigate tissue specific function of differentially expressed miRNA copies. A single MO can be used to knockdown and detect expression from of a specific hairpin precursor, while another MO with a different sequence can subsequently be used detect expression from another miRNA copy. Therefore MO based probes are a useful addition to the growing toolbox to investigate miRNA functions.

# REFERENCES

1. R. C. Lee, R. L. Feinbaum, V. Ambros, The *C. elegans* heterochronic gene *lin-4* encodes small RNAs with antisense complementarity to *lin-14*. *Cell* **75**, 843 (Dec 3, 1993).
2. B. J. Reinhart et al., The 21-nucleotide *let-7* RNA regulates developmental timing in *Caenorhabditis elegans*. *Nature* **403**, 901 (Feb 24, 2000).
3. D. P. Bartel, MicroRNAs: target recognition and regulatory functions. *Cell* **136**, 215 (Jan 23, 2009).
4. J. W. Hagen, E. C. Lai, microRNA control of cell-cell signaling during development and disease. *Cell Cycle* **7**, 2327 (Aug, 2008).

5. E. Wienholds et al., MicroRNA expression in zebrafish embryonic development. *Science* **309**, 310 (Jul 8, 2005).
6. W. P. Kloosterman, E. Wienholds, E. de Bruijn, S. Kauppinen, R. H. Plasterk, In situ detection of miRNAs in animal embryos using LNA-modified oligonucleotide probes. *Nat Methods* **3**, 27 (Jan, 2006).
7. G. Obernosterer, J. Martinez, M. Alenius, Locked nucleic acid-based in situ detection of microRNAs in mouse tissue sections. *Nat Protoc* **2**, 1508 (2007).
8. D. K. Darnell et al., MicroRNA expression during chick embryo development. *Dev Dyn* **235**, 3156 (Nov, 2006).
9. B. Ason et al., Differences in vertebrate microRNA expression. *Proc Natl Acad Sci U S A* **103**, 14385 (Sep 26, 2006).
10. M. J. Soe, T. Moller, M. Dufva, K. Holmstrom, A Sensitive Alternative for MicroRNA In Situ Hybridizations Using Probes of 2'-O-Methyl RNA + LNA. *J Histochem Cytochem* **59**, 661 (Jul, 2011).
11. J. T. Pena et al., miRNA in situ hybridization in formaldehyde and EDC-fixed tissues. *Nat Methods* **6**, 139 (Feb, 2009).
12. J. Lu, A. Tsourkas, Imaging individual microRNAs in single mammalian cells in situ. *Nucleic Acids Res* **37**, e100 (Aug, 2009).
13. A. K. Lagendijk, M. J. Goumans, S. B. Burkhard, J. Bakkers, MicroRNA-23 Restricts Cardiac Valve Formation by Inhibiting Has2 and Extracellular Hyaluronic Acid Production. *Circ Res*, **109**, 649-657.
14. W. P. Kloosterman, A. K. Lagendijk, R. F. Ketting, J. D. Moulton, R. H. Plasterk, Targeted inhibition of miRNA maturation with morpholinos reveals a role for miR-375 in pancreatic islet development. *PLoS Biol* **5**, e203 (Aug, 2007).
15. G. Obernosterer, P. J. Leuschner, M. Alenius, J. Martinez, Post-transcriptional regulation of microRNA expression. *RNA* **12**, 1161 (Jul, 2006).
16. D. C. Deacon et al., The miR-143-adducin3 pathway is essential for cardiac chamber morphogenesis. *Development* **137**, 1887 (Jun, 2010).
17. K. Y. Miyasaka et al., Heartbeat regulates cardiogenesis by suppressing retinoic acid signaling via expression of miR-143. *Mech Dev* **128**, 18 (Jan-Feb, 2011).



# MICRORNA-23 RESTRICTS CARDIAC VALVE FORMATION BY INHIBITING HAS2 AND EXTRACELLULAR HYALURONIC ACID PRODUCTION

A.K. Legendijk<sup>1</sup>, M.J. Goumans<sup>3</sup>, S.B. Burkhard<sup>1</sup> and J. Bakkers<sup>1,2</sup>  
*Circulation Research* 2011 Sep 2;109(6):649-57

1. Hubrecht Institute, KNAW & Iniversity Medical Center, Utrecht, The Netherlands.
2. Interuniversity Cardiology, Institute of the Netherlands, Utrecht, The Netherlands
3. Department of Molecular Cell Biology and Centre for Biomedical Genetics, Leiden University Medical Center, Leiden, The Netherlands

3

## ABSTRACT

Rationale: Since their discovery almost 20 years ago, microRNAs have been shown to perform essential roles during tissue development and disease. Although roles for microRNAs in the myocardium during embryo development and cardiac disease have been demonstrated, very little is known about their role in the endocardium or during cardiac valve formation.

Objective: To study the role of microRNAs in cardiac valve formation.

Methods and Results: We show that zebrafish *dicer* mutant embryos, lacking mature miRNAs, form excessive endocardial cushions. By screening miRNAs expressed in the heart, we found that miR-23 is both necessary and sufficient for restricting the number of endocardial cells that differentiate into endocardial cushion cells. In addition, in mouse endothelial cells, miR-23 inhibited a transforming growth factor- $\beta$ -induced endothelial-to-mesenchymal transition. By *in silico* screening of expression data with predicted miR-23 target sites combined with *in vivo* testing, we identified *hyaluronic acid synthase 2 (has2)*, *inhibitor of  $\beta$ -catenin and TCF-4 (icat/ctnnbip1)* and *transmembrane protein 2 (tmem2)* as novel direct targets of miR-23. Finally, we demonstrate that the upregulation of Has2, an extracellular remodeling enzyme required for endocardial cushion and valve formation, is responsible for the excessive endocardial cushion cell differentiation in *dicer* mutants.

Conclusions: MiR-23 in the embryonic heart is required to restrict endocardial cushion formation by inhibiting *has2* expression and extracellular hyaluronic acid production.



## INTRODUCTION

The development of valve structures occurs in distinguishable phases, which are highly conserved<sup>1</sup>. The first event during valve development is the induction of endocardial cushions (ECs) within the atrioventricular (AV) canal (AVC) and outflow tract of the primitive heart tube. It has been well established that Bone morphogenetic protein (Bmp), a member of the TGF- $\beta$  superfamily, is the major myocardial signal that initiates EC formation from human to zebrafish<sup>2-5</sup>. Compromised Bmp signaling results in downregulation of multiple pathways including TGF- $\beta$ , Has2 (Hyaluronic acid synthase 2), and Notch1, as well as the transcription factors Snail1 and Twist<sup>1,2,4</sup>. The importance of regulating *Has2* expression in the endocardium has been exemplified by the observation that in *Has2* deficient mice the cardiac jelly does not expand and ECs fail to form<sup>6</sup>. Has2 is responsible for the production of hyaluronic acid (HA), one of the ECM components of cardiac jelly<sup>6</sup>. HA production leads to expansion of the extracellular space because it binds salt and water and induces PI3K and ErbB signaling (reviewed by B. Toole<sup>7</sup>). Despite differences in the cellular processes that precede valve formation the molecular signals regulating valve formation (eg, Notch, NFAT, ErbB, and TGF- $\beta$  signaling) have been conserved between amniotes and zebrafish<sup>8-11</sup>.

MiRNAs are a class of 21- to 25-nucleotide single-stranded noncoding RNAs transcribed from DNA but not translated into protein. Instead, miRNAs interact with messenger RNAs in the cytosol and regulate their final output at the protein level<sup>12</sup>. Dicer, an RNase III endonuclease, processes hairpinlike pre-miRNAs into double-stranded miRNA molecules. MiRNA function during organogenesis has been studied mainly by generating conditional *Dicer* knockout mouse models because conventional *Dicer* mutant mice are embryonic lethal<sup>13</sup>. Conditional depletion of Dicer from the endocardium has been previously performed, using the *Tie2-Cre* line (which excises *Dicer* from all hematopoietic and endothelial cells); however, the status of the endocardium in these animals was not reported<sup>13</sup>. We report excessive EC formation in *dicer* null mutants accompanied by a strong increase in cardiac jelly. We found that the loss of miR-23 was responsible for the observed endocardial defects in *dicer* knockout embryos by regulating *has2* expression and HA production. Together, our data suggest the existence of a negative miR-23-Has2 feedback mechanism to control EC size in the AVC.

## MATERIAL AND METHODS

### Fish lines

Fish were kept under standard conditions. The *dicer* allele used in this study is *dicer*<sup>Hu896</sup><sup>14</sup>. To generate transgenic MZ*dicer* lines, we performed *dicer* mutant germ cell transplantations into *Tg(kdr-l:GFP)* embryos as previously described<sup>15</sup>.

### Immunohistochemistry

Immunohistochemistry was carried out as previously described<sup>16</sup>. Mouse anti-GFP (Santa Cruz Biotechnology) and mouse anti-zn8 (Dm-grasp, DSHB) were applied 1:200. F-actin was

stained with phalloidin-TRITC (Sigma; 1:100). Dm-grasp staining was quantified by manual counting using Volocity software (Improvision). The ratio of Dm-grasp-positive endocardial cells was calculated by the number of Dm-grasp-positive endocardial cells divided by the total number of GFP-positive endocardial cells per heart. We used myocardial Dm-grasp staining as a reference outline of the heart. Statistical significance was determined by a *t*-test (Microsoft Excel). Results are expressed as mean±SEM. ImageJ software was applied to remove myocardial Dm-grasp expression for 3D reconstructions shown in Figures 1, 2, 4, and 7.

### ***In situ* hybridization**

*In situ* hybridization was carried out as previously described<sup>17</sup>. Embryos were cleared in methanol and mounted in benzylbenzoate/benzylalcohol (2:1) before pictures were taken. MiRNA *in situ* hybridizations were performed as described by Kloosterman et al<sup>18</sup>. Modifications to this protocol were as follows. Overnight fixing in 4% PFA was followed by an additional overnight fixation in 1-ethyl-3-(3-dimethylaminopropyl) carbodiimide (EDC) to prevent diffusion of the signal<sup>19</sup>. We used an LNA-modified miR-23a probe (1:500 Exiqon), sequence 5'-tggaatccctggcaatgat-3', DIG modified on both ends.

### **Morpholino and RNA injections**

Morpholino oligonucleotides (MOs; Gene Tools) were dissolved in water to 5 mmol/L (miR-23a MO) and 1 mmol/L (*p53* MO and *has2* MO). For injection, MOs were diluted to concentrations between 0.2 mmol/L and 1 mmol/L, of which 1 nL was injected at the one cell stage. In a dose-response experiment, the most optimal concentration for the miR-23 MO was determined as 0.5 mmol/L. Capped zebrafish *has2* RNA was prepared with the SP6 Message Machine kit (Ambion) and injected at 50 ng/ μL. MiRNA mimics for miR-430, miR-23, and miR-27 were all injected at 200 ng/ μL. Morpholino and miRNA mimic sequences are provided in the Online Supplement Materials and Methods at <http://circres.ahajournals.org>.

### **Quantitative reverse transcriptase-PCRs**

Total RNA from mouse embryonic endothelial cells (MEECs) was isolated using TRIzol Reagent (Invitrogen). cDNA was transcribed using Superscript III reverse transcriptase (Invitrogen). Reverse transcriptase (RT)-PCRs were performed using RedTaq polymerase (Sigma). Sequences of qRT-PCR primers and detailed protocol are provided in the Online Supplement Materials and Methods. Results are expressed as mean fold change±SEM. Statistical significance was determined by a *t*-test (Microsoft Excel).

### **HA staining**

Staining was performed on paraffin sections as described previously<sup>20</sup>. Serum-free medium of HEK293 cells expressing a neurocan-alkaline phosphatase fusion protein was a generous gift from Uwe Rauch, University of Lund.

### **GFP silencing assays**

We use a full-length *tmem2* 3'-UTR (full length 3'-UTR for *has2* and *icat* prevented stable GFP expression). In addition, a 111 bp, 165 bp, and 348 bp PCR fragment from the zebrafish

*has2* 3'-UTR, *tmem2* 3'-UTR, and *icat* 3'-UTR, respectively, was amplified, each containing the predicted miR-23 target sites. Primer sequences used and cloning strategy are provided in the Online Supplement Materials and Methods.

## Cell culture

MEECs were cultured as previously described<sup>21</sup>. MEECs were transfected with 50  $\mu$ mol/L miR-23 mimics duplex oligos (IDT), using oligofectin, following the manufacturer's protocol (Invitrogen), resulting in approximately 95% transfection efficiency. To induce epithelial-to-mesenchymal transition (EMT), MEECs were stimulated with 1 ng/mL TGF- $\beta$  for 2 days.

## Western blot analysis

MEECs were lysed in sample buffer containing 10% SDS, 20% glycerol, 0,1% bromophenol blue, 5% -mercapto-ethanol, and Tris HCl, pH 6.8. Homogenates were size-fractionated on 10% PAGE gels and transferred to Hybond PVDF membranes. Membranes were incubated with the anti- $\alpha$ -smooth muscle actin (SMA) (1:2000; Sigma) and anti-Pecam-1 (1:1000; Santa Cruz) followed by incubation with a horseradish peroxidase–labeled secondary antibody.

# RESULTS AND DISCUSSION

## Cardiac jelly and ECs of *dicer* mutants are structurally altered

To study miRNA function during heart development, we generated wild-type females carrying a homozygous *dicer* mutant germline by germ cell transplantation<sup>15</sup>. Embryos derived from such females (lacking all maternal and zygotic Dicer [MZ*dicer*]), were injected with miR-430 to clear the embryo from maternal mRNA transcripts and thereby rescue early gastrulation defects<sup>15</sup>. At 3 days after fertilization (dpf), pericardial edema was evident in MZ*dicer*+430 mutant embryos (Supplemental Fig. I). However, ventricular and atrial chamber differentiation occurred normally, and both chambers maintained contractile capabilities (Supplemental Fig. I). The size of the heart and cardiac looping, however, were impaired in MZ*dicer*+430 mutant embryos (Supplemental Fig. I). We consistently observed lumen narrowing in both the atrium and the ventricle accompanied by increased space between the endocardium and myocardium, where the cardiac jelly resides (Supplemental Fig. I). Because the extracellular glycosaminoglycan HA is a major component of the cardiac jelly, we analyzed HA levels in the heart tissue. We detected excessive deposition of HA between the endocardium and the myocardium, indicating an excessive production of cardiac jelly components in MZ*dicer* mutants (n=18/18 Fig. 1B) compared with wild-type embryos (Fig. 1A).

## Ectopic expression of EC markers in MZ*dicer* embryos

We analyzed patterning of myocardial AVC differentiation in MZ*dicer*+430 mutant embryos. *nppa* (*natriuretic peptide precursor type A*) is expressed in ventricular and atrial working myocardial cells, whereas *bmp4* (*bone morphogenetic protein 4*) shows a reciprocal expression pattern, restricted to the AVC myocardium. Spatial expression patterns of *nppa* and *bmp4* were unaffected in MZ*dicer*+430 mutants (Supplemental Fig. I), demonstrating

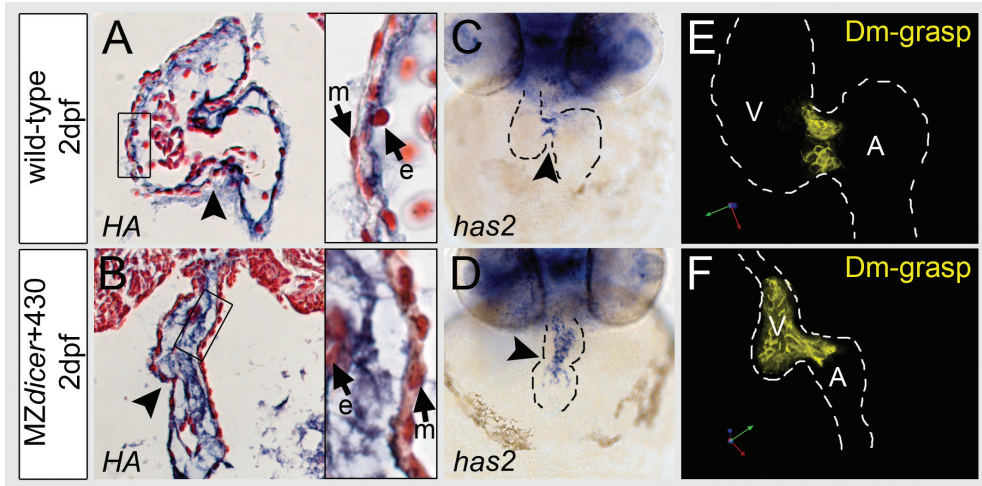


**Figure 1: MiRNAs are required to restrict endocardial cushion differentiation**

A and B, left, Hyaluronic acid (HA) staining (blue) at 2 dpf in wild-type (A) and MZ*dicer*+430 (B) embryos counter-stained with neutral red. A and B, right, HA staining in ventricle wall (boxed in A and B). Myocardial cell is indicated as m; endocardial cell, e.

Restricted endocardial expression of *has2* in wild-type endocardial cushions (C) and ectopic *has2* expression in MZ*dicer* mutant chambers (D). E and F, Three-dimensional projections of endocardial-specific Dm-grasp expression (yellow) marks endocardial cushion cells. V=ventricle, A=atrium.

correct patterning of the myocardium. Next, we analyzed differentiation of the endocardium. Expression of *nfatc1* (*nuclear factor of activated T-cells, cytoplasmic, calcineurin-dependent 1*) in MZ*dicer*+430 mutant embryos demonstrated the presence of an endocardial lining throughout the heart tube (Supplemental Fig. I). Normally, a small population of endocardial cells located at the AVC form ECs, marked by *has2* expression (Fig. 1C). Consistent with the increased levels of HA in the cardiac jelly in MZ*dicer*+430 mutants, we found that *has2* expression was no longer restricted to AVC endocardium but was expanded into the endocardium lining the chambers (n=37/39, Fig. 1D). Ectopic *has2* expression was observed in both chambers but was most prominent in the ventricle. For *osteopontin* or *secreted phosphoprotein 1* (*spp1*), another marker for differentiated ECs<sup>22</sup>, low levels were observed in wild-type ECs, whereas ectopic and high levels of *spp1* were observed in MZ*dicer* mutant embryos (Supplemental Fig. I). Formation of the ECs in zebrafish is accompanied by endocardial cell-shape changes, from squamous to cuboidal, and expression of the cell adhesion molecule, Dm-grasp/Alcama<sup>8</sup>. We examined spatial Dm-grasp expression in wild-type and MZ*dicer*+430 mutant embryos carrying the *Tg(kdr-l:GFP)* transgene, in which all endothelial cells are labeled by GFP. In wild-type embryos, Dm-grasp was expressed in all myocardial cells and endocardial cells located in the AV region (Supplemental Fig. II). In MZ*dicer*+430 mutant embryos, however, we observed ectopic Dm-grasp expression in endocardial cells lining the chambers with preference for the ventricle (Supplemental Fig. II). On quantification of the ratio of endocardial cells that express Dm-grasp, we found a 2-fold increase of Dm-grasp-positive endocardial cells in MZ*dicer*+430 mutants (Dm-grasp

expression index in wild-type,  $0.21 \pm 0.01$ ,  $n=6$ , and in *MZdicer+430*,  $0.41 \pm 0.03$ ,  $n=7$ ;  $p < 0.01$ ) (Supplemental Fig. II). To analyze the structure of the endocardial cushions, we made 3D reconstructions of the endocardial Dm-Grasp expression by omitting its myocardial expression. In the 3D reconstruction of endocardial Dm-Grasp in a wild-type heart, compact superior and inferior cushion structures were observed (Fig. 1E). In *MZdicer+430* mutants, Dm-Grasp-expressing cells did not form separated cushions but instead formed a large structure composed of both AVC and chamber endocardial cells (Fig. 1F). In addition to the ectopic Dm-grasp expression, we also observed a change in endocardial cell shape. In wild-type embryos, AVC endocardial cells are cuboidal with cytoplasmic protrusions, whereas chamber endocardial cells are flat and squamous (Supplemental Fig. II). Interestingly, in *MZdicer+430* mutant embryos, chamber endocardial cells were like wild-type AVC cells, also cuboidal with cytoplasmic projections (Supplemental Fig. II). Furthermore, we observed in *MZdicer+430* mutant embryos ( $n=3/15$ ) endothelial cells that resided in the extracellular space of the cardiac jelly (Supplemental Fig. II). We never observed such cells in wild-type hearts ( $n=0/10$ ). Together, these results reveal that a loss of miRNAs has a significant impact on regional endocardial differentiation during AV valve formation independent of myocardial patterning.

### Loss of miR-23 results in enhanced EC formation

To identify the mechanism responsible for the observed ectopic expression of *has2* and remodeling of ECs in *MZdicer+430* mutants, we searched for miRNAs that are expressed in the heart. We injected antisense MOs, targeting the mature sequence of 9 miRNA families for which cardiac expression had been reported<sup>23</sup> (for a complete list, see Online Supplement experimental procedures). MO-injected embryos were examined morphologically at 2 and 3 dpf for blood pooling on the yolk and thickness of the cardiac jelly and by *in situ* hybridization for *has2* expression (data not shown). Only the injection of a miR-23 MO resulted in cardiac defects similar to what we observed in *MZdicer+430* mutants (described further below). There are 5 copies of miR-23 family members in the zebrafish genome, all of which reside in polycistronic clusters together with miR-24 and miR-27 family members (Supplemental Fig. III). The MO designed to target miR-23 family members targets all 5 members, resulting in an efficient knockdown (Fig. 2A through 2C). Interestingly, on miR-23 knockdown, we observed enhanced expression of *has2* at 2 dpf ( $n=21/24$ ) and 3 dpf ( $n=27/33$ ) (Fig. 2D through 2G). Besides an increase in *has2* expression level, we also observed ectopic *has2* expression in the chambers, although this expansion was less pronounced compared with *MZdicer+430* mutant embryos. Concomitant with the enhanced *has2* expression, we observed a thickening of the cardiac jelly containing HA fibers in miR-23 morphants ( $n=8$ ) (Fig. 2H and 2I). Injection of *p53* MOs, which has no reported phenotype<sup>24</sup>, did not alter *has2* ( $n=16/16$ ) or HA expression ( $n=5/5$ ) (Supplemental Fig. IV). Patterning of myocardial cells in the AVC appeared normal on loss of miR-23 (Supplemental Fig. IV). In agreement with our previous observations in *MZdicer+430* mutant embryos, we observed a significant increase in endocardial Dm-grasp expression in miR-23 knockdown embryos (Dm-grasp expression index in miR-23 MO,  $0.36 \pm 0.02$ , versus  $0.21 \pm 0.01$  in wild-type embryos;  $p < 0.01$ ) (Fig. 2J through 2L). These results demonstrate that the loss of miR-23 results in endocardial defects, which are comparable to those observed in *MZdicer+430* mutants.

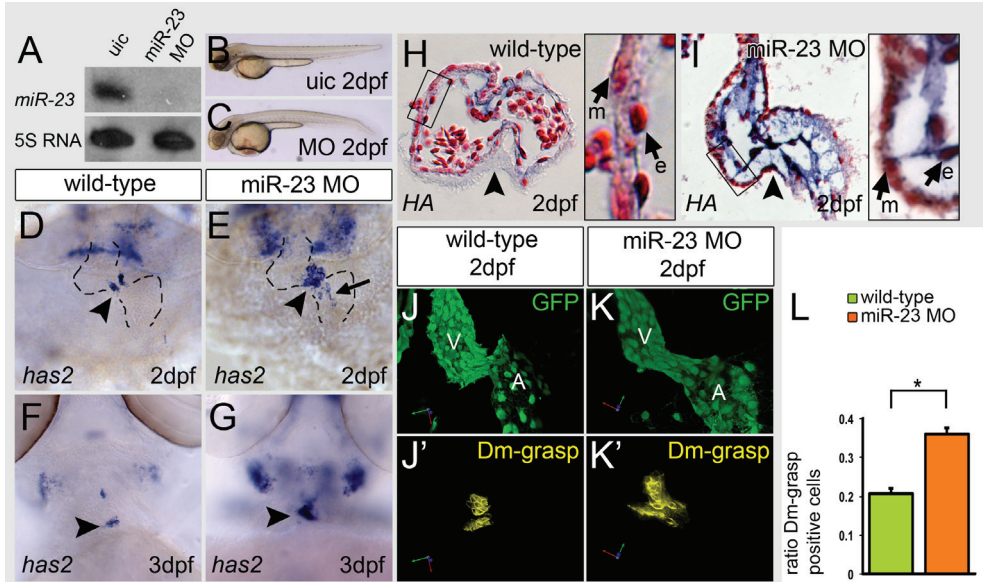


**Figure 2: Mir-23 knockdown results in endocardial defects**

(A) Northern blot analysis for miR-23 expression (top) in total RNA isolated from wild-type and miR-23 knockdown embryos. 5S RNA is used as a loading control (bottom). Bright-field images of a wild-type (B) and miR-23 knockdown (C) embryo at 2 dpf. *In situ* hybridization for *has2* in wild-type (D and F) and miR-23 knockdown (E and G) embryos at 2 dpf (D and E) and 3 dpf (F and G). Arrowheads indicate *has2* expression in ECs. Arrow in E points to ectopic *has2* expression on miR-23 knockdown. H and I, left, HA staining (blue) at 2 dpf in wild-type (H) and miR-23 knockdown (I) embryos counterstained with neutral red. H and I, right, HA staining in enlarged view of the ventricle wall (boxed in H and I). Myocardial cell is indicated as m; endocardial cell, e. Three-dimensional projections of the endocardium (*Tg(kdr-1:GFP)*, green) of wild-type (J) and miR-23 knockdown (K) heart tubes at 2 dpf with corresponding endocardial-specific *Dm-grasp* expression (yellow) (J' and K'). L, Ratio of *Dm-grasp* expressing endocardial cells in wild-type (n=6) and miR-23 morphant (n=5) embryos at 2 dpf. Error bars represent mean $\pm$ SEM; t-test analyses resulted in statistically significant differences, with \*p<0.01.

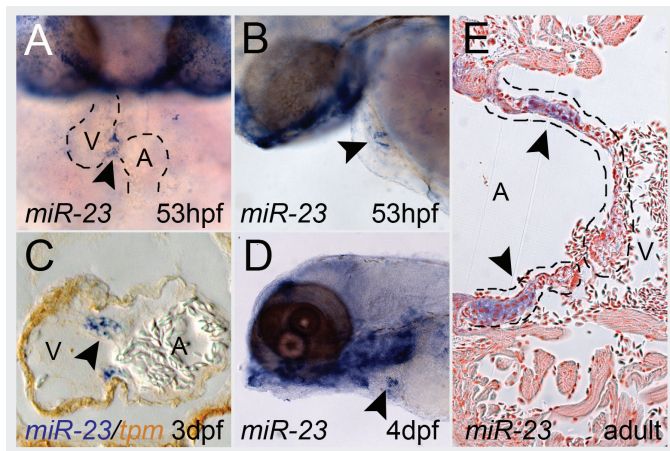


**Figure 3: MiR-23 is expressed in ECs and valves**

A and B, MiR-23 expression (black arrowheads) was detected by *in situ* hybridization in ECs at 53 hpf (A, anterior view; B, lateral view). C, Transverse section of a miR-23 *in situ* hybridization (blue) in wild-type ECs (black arrowhead) at 3 dpf combined with anti-tropomyosin antibody staining (myocardium, brown). D, Robust miR-23 expression in ECs at 4 dpf (lateral view). E, MiR-23 expression in valve leaflets of the adult zebrafish heart (indicated by arrowheads). Dotted lines indicate the myocardial outline of the heart tube (A) and valve leaflets (E). Ventricle, V; atrium, A.

## Reexpressing miR-23 rescues ectopic EC differentiation in *MZdicer* mutants

By *in situ* hybridization, we observed that cardiac expression of miR-23 starts at 2 dpf. Interestingly, expression of miR-23 was confined to the ECs (n=20/25, Fig. 3A through 3D) and was still detected in the adult valve leaflets (n=3) (Fig. 3E). To address whether a loss of miR-23 was indeed causative for the observed ectopic expression of *has2* and *Dm-grasp* in *MZdicer*+430 mutant embryos, we coinjected *MZdicer* embryos not only with miR-430 but also with an miR-23 mimic. Reintroducing miR-23 in *MZdicer*+430 mutant embryos resulted in a clear reduction (n=8/23) or loss (n=15/23) of *has2* expression (Fig. 4A and 4B and Supplemental Fig. IV). Injection of miR-27 mimics or mutated miR-23 mimics, however, did not rescue ectopic *has2* expression (Supplemental Fig. IV). Reduction in *has2* expression on miR-23 overexpression was accompanied by a strong reduction in cardiac jelly size and HA production (n=6/6) (Fig. 4C and 4D). In addition, miR-23 mimic injection in *MZdicer*+430 mutant embryos led to a rescue of the ratio of endocardial cells expressing *Dm-grasp* to

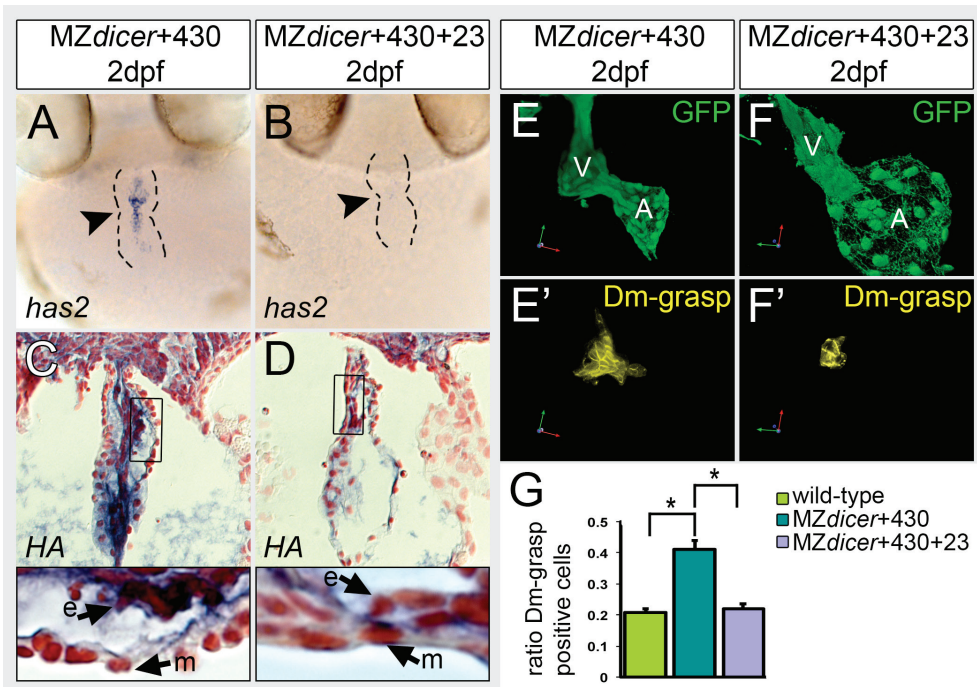


**Figure 4: MiR-23 rescues endocardial defects in *MZdicer* mutants**

A and B, *in situ* hybridization for *has2* (blue) in *MZdicer*+430 (A) and *MZdicer*+430+23 (B) hearts at 2 dpf showing a loss of *has2* expression on miR-23 mimic injection. C and D, top, HA staining (blue) at 2 dpf in *MZdicer*+430 (C) and *MZdicer*+430+23 (D) embryos counterstained with neutral red. C and D, bottom, HA staining in ventricle wall (boxed in C and D). Myocardial cell is indicated by m; endocardial cell, e.

E and F, Three-dimensional projections of the endocardium (*Tg(kdr-l:GFP)*, green) of *MZdicer*+430 (E) and *MZdicer*+430+23 (F) heart tubes at 2 dpf with corresponding endocardial specific *Dm-grasp* expression (yellow) (E' and F'). G, Ratio of *Dm-grasp* expressing endocardial cells in *MZdicer*+430 (n=7) and *MZdicer*+430+23 (n=3) embryos at 2 dpf. Error bars represent mean ± SEM; t-test analyses resulted in statistically significant differences, with \*p < 0.01.

wild-type values (MZ*dicer*+430+23, 0.22±0.02, versus wild-type, 0.21±0.01) (Fig. 4E through 4G). Together, these results demonstrate that miR-23 exerts a restricting effect on *has2* and Dm-grasp expression and extracellular HA production in the endocardium.

## **MiR-23 inhibits TGF- $\beta$ -induced endothelial-to-mesenchymal transition in mouse endothelial cells**

In mouse and chick embryos, EC cells undergo a TGF- $\beta$ -induced endothelial-to-mesenchymal transition (Endo-MT), which requires HA production by *Has2*<sup>6</sup>. To examine the role of miR-23 during TGF- $\beta$ -induced Endo-MT, we used cultured mouse embryonic endothelial cells (MEECs). TGF- $\beta$ -stimulation of MEEC induced the expression of  $\alpha$ -Smooth muscle actin ( $\alpha$ -SMA), a protein expressed by mesenchymal and fibroblast-like cells (Fig. 5A). In addition, other Endo-MT-related genes such as *Snail1*, *Has2*, and *Fibronectin*, were also upregulated in MEECs after treatment with TGF- $\beta$  (Fig. 5B). Platelet endothelial cell adhesion molecule-1 (Pecam-1) expression conversely decreased, indicative of a reduction in endothelial cell-cell interactions and a loss of endothelial cell morphology (Fig. 5A). TGF- $\beta$ -treated cells exhibited a fibroblast-like morphology compared with their rounded, cobblestone appearance in the absence of TGF- $\beta$  (Fig. 5C and 5D). In addition, loss of endothelial intercellular connections results in remodeling of the actin cytoskeleton. During Endo-MT, cortical f-actin translocates to intracellular stress fibers of transformed mesenchymal cells (Fig. 5G and 5H). Transfection of MEECs with miR-23 mimics before the TGF- $\beta$ -stimulation prevented upregulation of  $\alpha$ -SMA, *Snail1*, *Has2*, and TGF- $\beta$ -induced factor (*Tgif*) (Fig. 5A and 5B). Furthermore, miR-23-transfected MEECs did not obtain a fibroblast-like morphology, and f-actin remained at the cortical surface of the cells (Fig. 5E, 5F, 5I, and 5J). Together, these results demonstrate that in mouse endothelial cells, ectopic miR-23 inhibits TGF- $\beta$ -induced Endo-MT.

## **Identification of novel miR-23 target genes**

To identify putative miR-23 target-genes that would explain how miR-23 might exert its regulation of cardiac valve formation, we set up an *in silico* screen. We identified genes specifically expressed in mouse embryonic hearts at E10.5<sup>25</sup>. Next, we computationally selected those genes that also contained miR-23 recognition sequences defined by strict target prediction criteria using TargetScan software, resulting in 122 candidate genes (Online Table I). Since we observed that miR-23 inhibits TGF- $\beta$ -induced EMT in mouse endothelial cells, we selected those candidate genes that are expressed during early stages of EMT. By RT-PCR analysis on unstimulated and TGF- $\beta$ -stimulated MEECs, we identified 48 candidate genes that are upregulated during TGF- $\beta$ -induced EMT (Fig. 6A and Online Table I). To identify which of these cardiac genes are true miR-23 target genes, we selected 15 candidate genes for which the zebrafish homologue also contains an miR-23 binding site. We amplified 3'UTR regions surrounding these miR-23 sites and placed them each individually downstream of an eGFP coding sequence for use in a GFP silencing assay. We only observed strong silencing of the GFP signal with miR-23 mimics when the *has2*, *icat*, and *tmem2* 3'UTR sequences were present (Fig. 6B through G, Supplemental Fig. V, and Online Table I). Silencing of these GFP-3'UTR mRNAs was miR-23-dependent, because no silencing was observed after coinjecting mutated miR-23 mimics (Fig. 6H through J) or after mutating 2 nucleotides within the seed sequence of miR-23 target sites (Supplemental Fig. V).



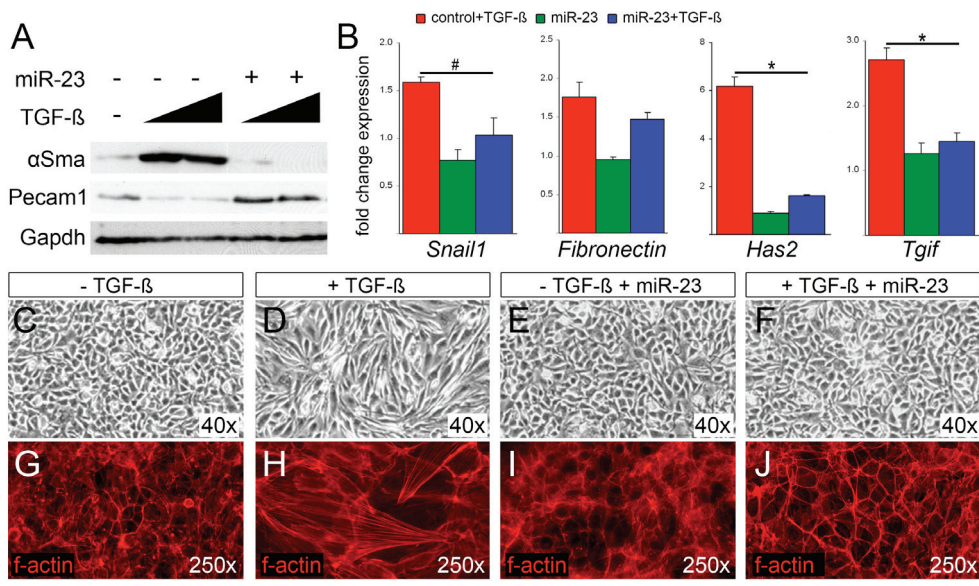


**Figure 5: MiR-23 inhibits TGF-β-induced Endo-MT in mouse embryonic endothelial cells**  
A, Western blot analysis for α-SMA (top) and Pecam-1 (middle) protein expression in unstimulated MEECs or MEECs stimulated with 1 or 5 ng of TGF-β and/or miR-23. GAPDH protein levels were used as a loading control (bottom). B, Quantitative RT-PCR analysis of *Snail1*, *Fibronectin*, *Has2*, and *Tgif* expression relative to unstimulated MEECs (n=3 experimental replicates). Error bars represent mean±SEM; t-test analyses resulted in statistically significant differences, with \*p<0.01 and #p=0.05. C through F, Bright-field images (x40) showing fibroblast-like transformation on TGF-β stimulation. G through J, Phalloidin staining of f-actin (red). Cortical f-actin in unstimulated MEECs (G) translocates to stress fibers of mesenchymal cells on TGF-β stimulation (H). F-actin remained at the cortical surface of the cells when transfected with miR-23 mimics (I and J).

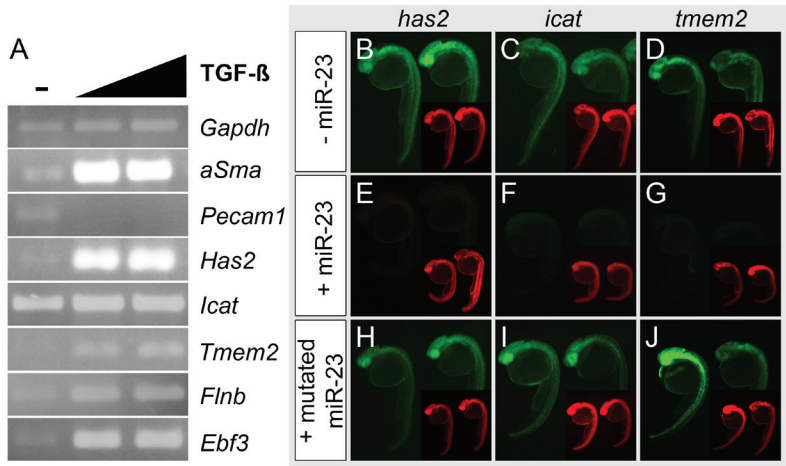


**Figure 6: Identification of *has2*, *icat*, and *tmem2* as miR-23 target genes**  
A, RT-PCR expression analysis in unstimulated MEECs (-) versus MEEC stimulated with 1 or 5 ng/mL of TGF-β. B through J, MiR-23 silencing assays. Injection of synthetic mRNA containing the coding region for GFP and 3'UTR sequences with the predicted target sites of zebrafish *has2*, *icat*, and *tmem2*. The synthetic mRNA was injected alone (B through D), in combination with miR-23 mimic (E through G), or with a mutated miR-23 mimic (H through J). Effective silencing of the GFP was only observed when a wild-type miR-23 mimic was coinjected. mRNA encoding RFP (red) was always coinjected as an injection control.

Together, these data reveal that miR-23 targets several transcripts expressed in the embryonic heart.

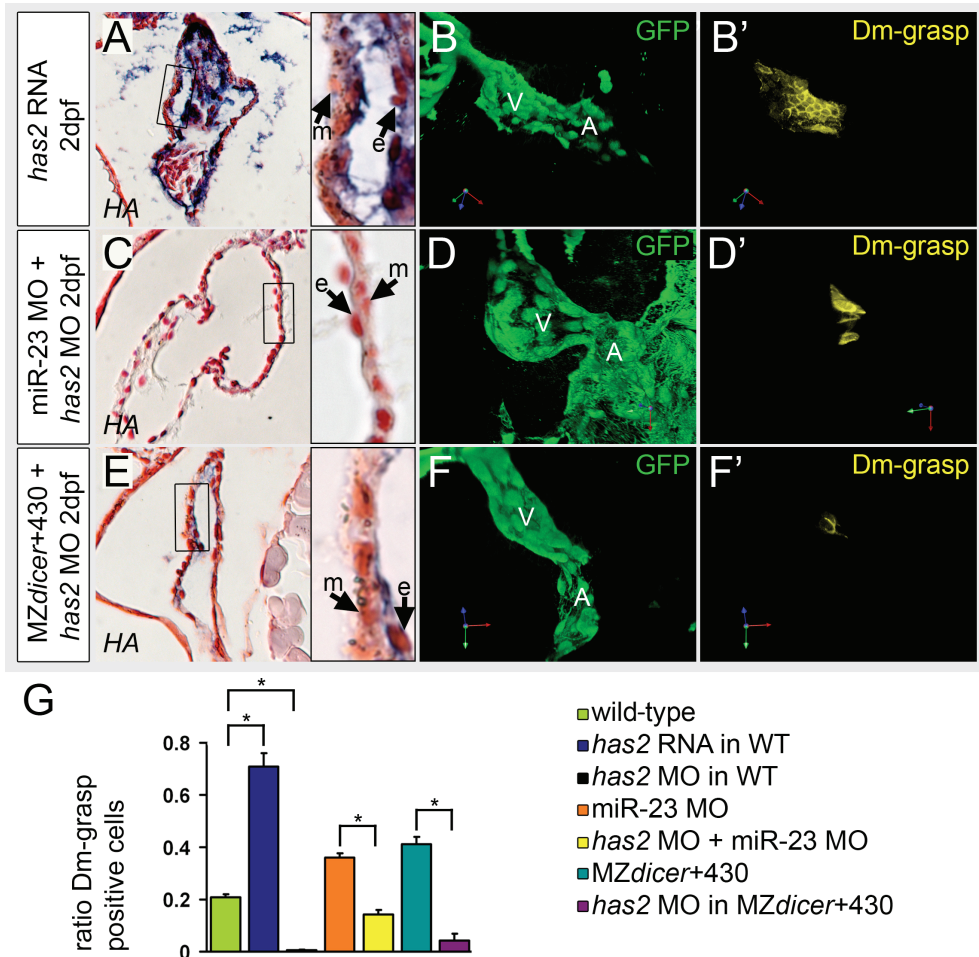


**Figure 7: *has2* knockdown prevents EC formation in MZ*dicer* mutant hearts**

A, left, HA staining of wild-type embryo injected with *has2* RNA. A, right, Magnification of boxed area of the ventricle wall. B, Three-dimensional projection of the endocardium (*Tg(kdr-l:GFP)*, green) of a wild-type embryo injected with *has2* mRNA, which induced ectopic Dm-grasp labeling in ventricular endocardium (yellow, B'). C, left, HA staining of wild-type embryo coinjected with miR-23 MO and *has2* MO. C, right, Magnification of boxed area of the ventricle wall. D, Three-dimensional projection endocardial cells (*Tg(kdr-l:GFP)*, green) of a wild-type embryo coinjected with *has2* and miR-23 MOs, which prevented ectopic endocardial Dm-grasp expression (yellow, D'). E, left, HA staining of MZ*dicer* mutant injected with miR-430 and *has2* MO. E, right, Magnification of boxed area of the ventricle wall. F, Three-dimensional projection of MZ*dicer*+430 mutant endocardial cells (*Tg(kdr-l:GFP)*, green) injected with *has2* MOs, which prevented ectopic endocardial Dm-grasp expression (yellow, F'). G, Ratio of Dm-grasp-positive endocardial cells versus all endocardial cells in wild-type (n=6), *has2* RNA in wild-type embryos (n=4), *has2* MO in wild-type embryos (n=4), miR-23 morphant (n=4), *has2* MO in miR-23 morphants (n=5), MZ*dicer*+430 mutants (n=7), and *has2* MO in MZ*dicer*+430 mutants (n=4) at 2 dpf. Error bars represent mean±SEM; t-test analyses resulted in statistically significant differences, with \*p<0.01.

## Ectopic *has2* expression in MZ*dicer* mutants is responsible for excessive EC formation

Because we identified *has2* as an miR-23 target gene and *has2* expression was upregulated both in MZ*dicer* mutant and miR-23 knockdown hearts, we investigated its expression in more detail. We observed that in the linear heart tube of zebrafish embryos, *has2* was expressed in few endocardial cells already at 30 hpf (Supplemental Fig. VI). This early endocardial *has2* expression precedes the previously described Dm-Grasp expression and cellular changes initiating EC formation at 36 hpf<sup>8</sup>. To address whether ectopic *has2* can induce Dm-Grasp expression in the endocardium, synthetic *has2* mRNA was injected into 1-cell stage embryos. As a consequence of ectopic *has2* expression, we observed thickening of the cardiac jelly, which stained positive for HA (n=8/8) (Fig. 7A). In addition, injection of *has2* mRNA into wild-type embryos significantly induced Dm-grasp expression throughout the endocardium (wild-type,  $0.22\pm 0.01$ , versus *has2* RNA,  $0.71\pm 0.05$ ;  $p<0.01$ ) (Fig. 7B, B', and 7G). We subsequently investigated whether Has2 is required to induce Dm-grasp expression in ECs of wild-type embryos by injecting previously characterized *has2* morpholinos. We observed in *has2* MO-injected embryos retrograde blood flow from the ventricle back to the atrium, suggestive for compromised EC formation. When we examined Dm-grasp expression in *has2* knockdown embryos, we observed a near complete loss of Dm-grasp expression in the endocardium (Fig. 7G and Supplemental Fig. VII) (wild-type,  $0.22\pm 0.01$ , versus *has2* MO,  $0.01\pm 0.01$ ;  $p<0.01$ ). In addition, endocardial cells located in the AVC remained squamous (Supplemental Fig. VII). Finally, we examined whether Has2 was required for the enhanced cardiac jelly production and ectopic Dm-Grasp expression observed in miR-23 knockdown and MZ*dicer* mutant embryos. Therefore, the *has2* MO was either coinjected with the miR-23 MO in wild-type embryos or coinjected with the miR-430 mimic in MZ*dicer* mutant embryos. In both cases, the *has2* knockdown caused a reduction in cardiac jelly and HA production (miR-23+*has2* MO, n=6/6; MZ*dicer*+430+*has2* MO, n=5/5) (Fig. 7C, 7E, 1B, and 2I). In addition, the *has2* knockdown in MZ*dicer* mutant or in miR-23 knockdown embryos caused a significant reduction in the ratio of endocardial cells expressing Dm-grasp (miR-23 MO,  $0.36\pm 0.02$ , versus  $0.14\pm 0.02$  in miR-23+*has2* MO coinjected embryos; MZ*dicer*+430,  $0.41\pm 0.03$ , versus MZ*dicer*+430+*has2* MO,  $0.04\pm 0.03$ ;  $p<0.01$ ) (Fig. 7D and 7D', 7F and 7F', 7G, 1F, 2K and 2K'). In summary, these results demonstrate that Has2 is required and sufficient to induce Dm-Grasp expression in the endocardium and that the ectopic Has2 activity observed in MZ*dicer* mutant hearts is the most likely cause of the excessive number of Dm-Grasp-positive EC cells in MZ*dicer* mutant hearts.

## CONCLUSIONS

To summarize, we have characterized the endocardial defect in *dicer* mutant zebrafish embryos and thereby identified excessive EC formation caused by a loss of miR-23 activity. We conclude that miR-23 is required to restrict EC formation by restricting *has2* expression and HA production. Unexpectedly, both miR-23 and its target *has2* are expressed in EC cells, suggesting the existence of an intrinsic negative feedback mechanism in the ECs

that controls the size of the ECs (see model in Supplemental Fig. VIII). The first visually recognizable process during AV valve formation in the zebrafish heart is a change in cell shape of endocardial cells in the AV region<sup>8</sup>. The transition from squamous to cuboidal cells is first apparent at 36 hpf and is accompanied by expression of the cell adhesion molecule Dm-grasp/Alcam<sup>8</sup>. We showed that endocardial *has2* expression is already detected at 30 hpf and thereby precedes the endocardial cell shape changes and Dm-grasp expression, suggesting a role for *has2* in this process. Indeed, we observed that in *has2* knockdown embryos, Dm-grasp expression was nearly lost, whereas ectopic expression of *has2* induced Dm-grasp expression. At 2 dpf, the superior and inferior ECs become apparent in the AVC, and at this stage, miR-23 expression was first observed in the ECs. The level of endocardial miR-23 expression increased over time and was still present in the valve leaflets of the adult heart. Simultaneously with the increase in miR-23 expression in the ECs, the level of *has2* expression declines resulting in very low expression at 3 dpf (Supplemental Fig. VI). At 3 dpf, Dm-grasp expression is downregulated and the ECs start to form valve leaflets through a process of invagination<sup>8,10</sup>. Interestingly, we observed that in embryos lacking miR-23, the downregulation of *has2* expression in ECs at 3 dpf did not occur. Because we found that *has2* is a direct target for miR-23, it suggests that miR-23 in the ECs is required to downregulate Has2 function during the process of valve formation, resulting in a negative feedback mechanism (Supplemental Fig. VIII). Consistently, in MZ*dicer* mutant or miR-23 knockdown embryos, recognizable valve leaflets were never formed. Instead, the endocardial cells remained cuboidal-shaped and loosely attached to each other, resulting in endocardial ruptures and allowing blood cells to invade the cardiac jelly (A.K.L. and J.B., unpublished data).

Although cardiac expression of miR-23 was restricted to the ECs, we observed ectopic *has2* and Dm-grasp expression in endocardial cells outside of the AVC in MZ*dicer* mutant and miR-23 knockdown embryos. Possibly, this non-cell-autonomous role for miR-23 is explained by the autoregulatory loop between *has2* and its product extracellular HA. In epithelial cells, extracellular HA stimulates the PI3K pathway through the CD44 receptor, and activation of the PI3K pathway results in increased *Has2* expression and extracellular HA production<sup>26,27</sup>. In addition, the HA/CD44/ErbB2 interaction induces  $\beta$ -catenin activation, which results in the induction of *Has2* expression<sup>28–31</sup>. In the avian and mammalian heart, endocardial cells overlaying the ECs undergo Endo-MT, which can be induced by TGF- $\beta$  and requires *Has2* activity<sup>1,6</sup>. Our data demonstrate that miR-23 inhibits the TGF- $\beta$ -induced Endo-MT in mouse embryonic endothelial cells, suggesting a conserved role for miR-23 in restricting EC formation and highlighting the need for future investigations into the role of miR-23 during mammalian valve formation.

## Acknowledgments

We thank V. Christoffels for analyzing the microarray data; S. Chocron, E. N. Kouwenhoven, and J. Korving for technical assistance; A. Giraldez for technical advice and providing reagents for use in this study; E. Noël for text editing; and B. Hogan for discussions and critical reading of the manuscript. The Dm-grasp antibody developed by B. Trevarrow was obtained from the Developmental Studies Hybridoma Bank, developed under the auspices of the NICHD and maintained by The University of Iowa, Department of Biological Sciences, Iowa City, IA.

## Sources of funding

Work in J. Bakkers's laboratory was supported by the Royal Dutch Academy of Arts and Sciences (KNAW) and the Netherlands Organization for Scientific Research (NWO/ALW) grant 864.08.009.

## Supplemental data

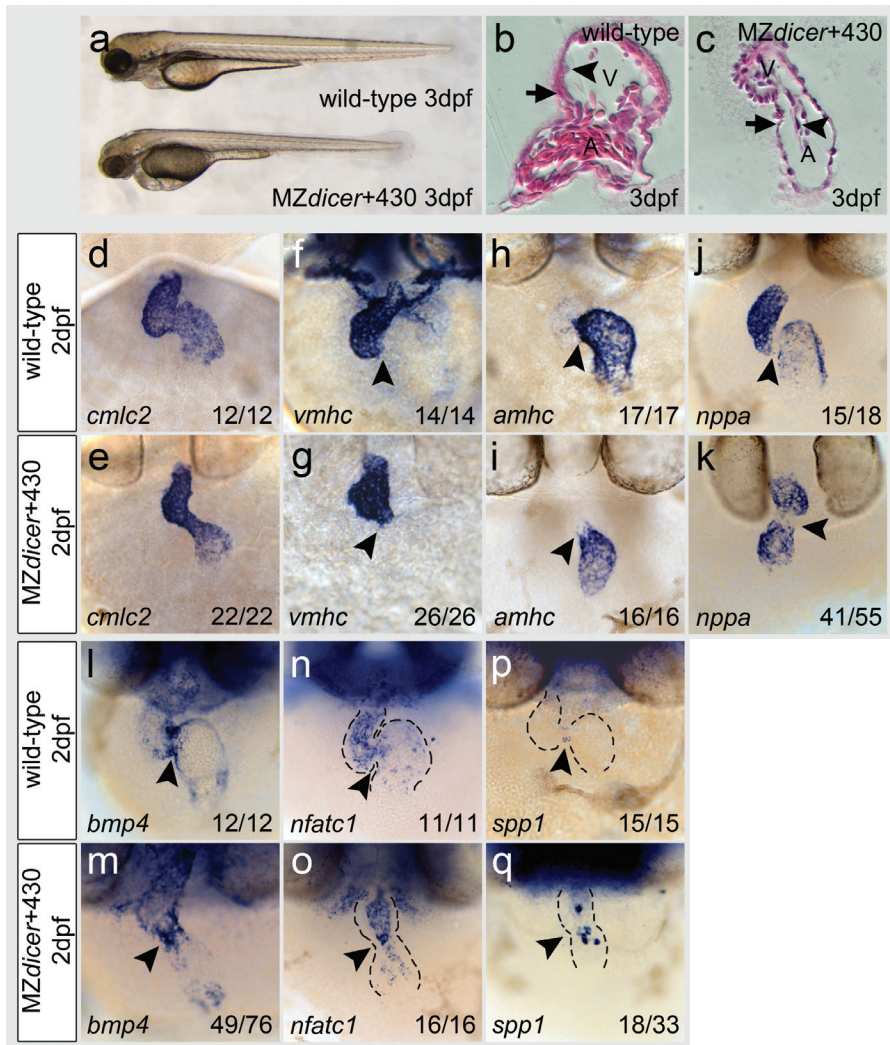
See <http://circres.ahajournals.org> for Online Supplemental Material and Methods and Online Table I.

## REFERENCES

1. Combs MD, Yutzey KE. Heart valve development: regulatory networks in development and disease. *Circ Res*. 2009;**105**:408–421.
2. Ma L, Lu MF, Schwartz RJ, Martin JF. Bmp2 is essential for cardiac cushion epithelial-mesenchymal transition and myocardial patterning. *Development*. 2005;**132**:5601–5611.
3. Rivera-Feliciano J, Tabin CJ. Bmp2 instructs cardiac progenitors to form the heart-valve-inducing field. *Dev Biol*. 2006;**295**:580–588.
4. Wang J, Sridurongrit S, Dudas M, Thomas P, Nagy A, Schneider MD, Epstein JA, Kaartinen V. Atrioventricular cushion transformation is mediated by ALK2 in the developing mouse heart. *Dev Biol*. 2005;**286**:299–310.
5. Smith KA, Joziassie IC, Chocron S, van Dinther M, Guryev V, Verhoeven MC, Rehmann H, van der Smagt JJ, Doevendans PA, Cuppen E, Mulder BJ, Ten Dijke P, Bakkers J. Dominant-negative ALK2 allele associates with congenital heart defects. *Circulation*. 2009;**119**:3062–3069.
6. Camenisch TD, Spicer AP, Brehm-Gibson T, Biesterfeldt J, Augustine ML, Calabro A Jr, Kubalak S, Klewer SE, McDonald JA. Disruption of hyaluronan synthase-2 abrogates normal cardiac morphogenesis and hyaluronan-mediated transformation of epithelium to mesenchyme. *J Clin Invest*. 2000;**106**:349–360.
7. Toole BP. Hyaluronan: from extracellular glue to pericellular cue. *Nat Rev Cancer*. 2004;**4**:528–539.
8. Beis D, Bartman T, Jin SW, Scott IC, D'Amico LA, Ober EA, Verkade H, Frantsve J, Field HA, Wehman A, Baier H, Tallafuss A, Bally-Cuif L, Chen JN, Stainier DY, Jungblut B. Genetic and cellular analyses of zebrafish atrioventricular cushion and valve development. *Development*. 2005;**132**:4193–4204.
9. Chang C-P, Neilson JR, Bayle JH, Gestwicki JE, Kuo A, Stankunas K, Graef IA, Crabtree GR. A field of myocardial-endocardial NFAT signaling underlies heart valve morphogenesis. *Cell*. 2004;**118**:649–663.
10. Scherz PJ, Huisken J, Sahai-Hernandez P, Stainier DY. High-speed imaging of developing heart valves reveals interplay of morphogenesis and function. *Development*. 2008;**135**:1179–1187.
11. Timmerman LA, Grego-Bessa J, Raya A, Bertra'n E, Perez-Pomares JM, Díez J Aranda S, Palomo S, McCormick F, Izpisua'a-Belmonte JC, de la Pompa JL. Notch promotes epithelial-mesenchymal transition during cardiac development and oncogenic transformation. *Genes & Development*. 2004;**18**:99–115.
12. Winter J, Jung S, Keller S, Gregory RI, Diederichs S. Many roads to maturity: microRNA biogenesis pathways and their regulation. *Nat Cell Biol*. 2009;**11**:228–234.
13. Zhou L, Seo KH, He HZ, Pacholczyk R, Meng DM, Li CG, Xu J, She JX, Dong Z, Mi QS. Tie2cre-induced inactivation of the miRNA-processing enzyme Dicer disrupts invariant NKT cell development. *Proc Natl Acad Sci U S A*. 2009;**106**:10266–10271.
14. Wienholds E, Koudijs MJ, van Eeden FJ, Cuppen E, Plasterk RH. The microRNA-producing enzyme Dicer1 is essential for zebrafish development. *Nat Genet*. 2003;**35**:217–218.
15. Giraldez AJ, Cinalli RM, Glasner ME, Enright AJ, Thomson JM, Baskerville S, Hammond SM, Bartel DP, Schier AF. MicroRNAs regulate brain morphogenesis in zebrafish. *Science*. 2005;**308**:833–838.
16. Dong PD, Munson CA, Norton W, Crosnier C, Pan X, Gong Z, Neumann CJ, Stainier DY. Fgf10 regulates hepatopancreatic ductal system patterning and differentiation. *Nat Genet*. 2007;**39**:397–402.

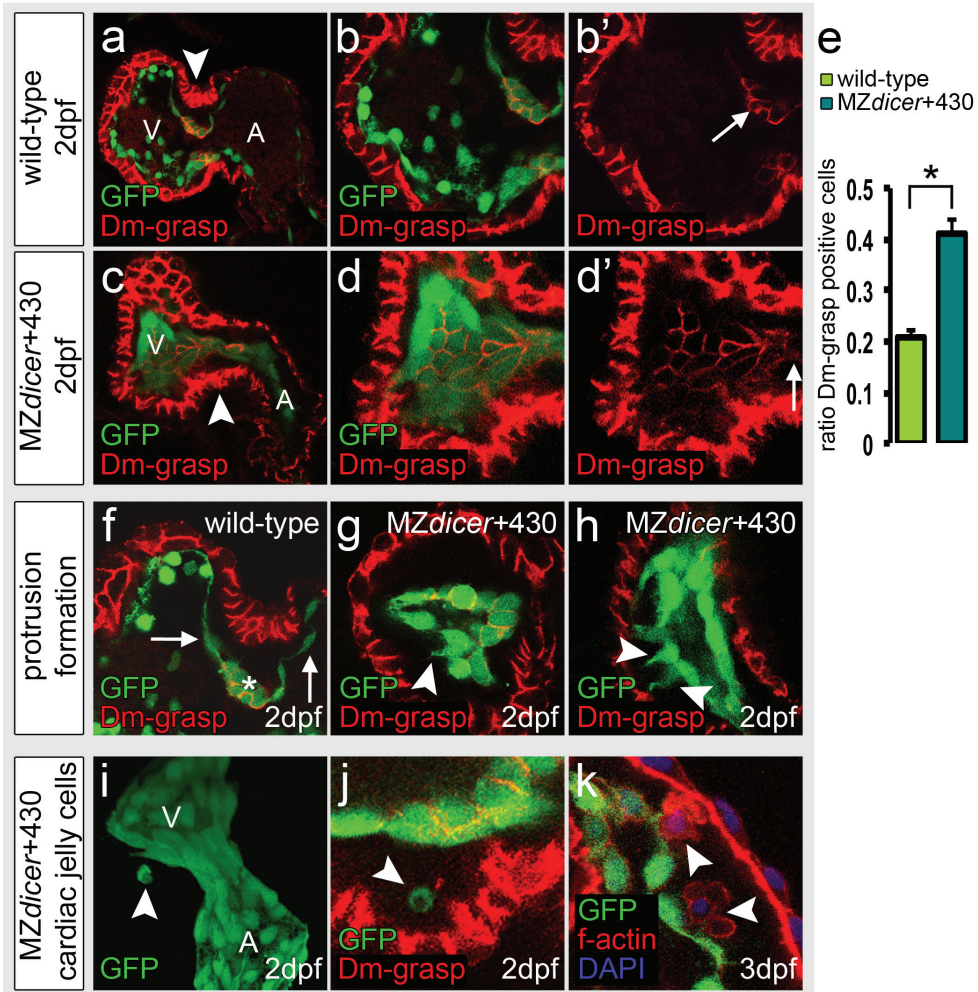
17. Westerfield M. *The Zebrafish Book: A Guide for the Laboratory Use of Zebrafish (Danio rerio)*. Eugene: University of Oregon Press; 2000.
18. Kloosterman WP, Wienholds E, de Bruijn E, Kauppinen S, Plasterk RH. In situ detection of miRNAs in animal embryos using LNA-modified oligonucleotide probes. *Nat Methods*. 2006;**3**:27–29.
19. Pena JT, Sohn-Lee C, Rouhanifard SH, Ludwig J, Hafner M, Mihailovic A, Lim C, Holoch D, Berninger P, Zavolan M, Tuschl T. miRNA in situ hybridization in formaldehyde and EDC-fixed tissues. *Nat Methods*. 2009;**6**:139–141.
20. Bakkers J, Kramer C, Pothof J, Quaedvlieg NE, Spaik HP, Hammerschmidt M. Has2 is required upstream of Rac1 to govern dorsal migration of lateral cells during zebrafish gastrulation. *Development*. 2004;**131**:525–537.
21. Larsson J, Goumans MJ, Sjostrand LJ, van Rooijen MA, Ward D, Leveen P, Xu X, ten Dijke P, Mummery CL, Karlsson S. Abnormal angiogenesis but intact hematopoietic potential in TGF-beta type I receptor-deficient mice. *EMBO J*. 2001;**20**:1663–1673.
22. Peal DS, Burns CG, Macrae CA, Milan D. Chondroitin sulfate expression is required for cardiac atrioventricular canal formation. *Dev Dyn*. 2009;**238**:3103–3110.
23. Wienholds E, Kloosterman WP, Miska E, Alvarez-Saavedra E, Berezikov E, de Bruijn E, Horvitz HR, Kauppinen S, Plasterk RH. MicroRNA expression in zebrafish embryonic development. *Science*. 2005;**309**:310–311.
24. Robu ME, Larson JD, Nasevicius A, Beiraghi S, Brenner C, Farber SA, et al. p53 activation by knockdown technologies. *PLoS Genetics*. 2007;**3**:e78.
25. Horsthuis T, Buermans HP, Brons JF, Verkerk AO, Bakker ML, Wakker V, Clout DE, Moorman AF, 't Hoen PA, Christoffels VM. Gene expression profiling of the forming atrioventricular node using a novel tbx3-based node-specific transgenic reporter. *Circ Res*. 2009;**105**:61–69.
26. Kamikura DM, Khoury H, Maroun C, Naujokas MA, Park M. Enhanced transformation by a plasma membrane-associated met oncoprotein: activation of a phosphoinositide 3'-kinase-dependent autocrine loop involving hyaluronic acid and CD44. *Mol Cell Biol*. 2000;**20**:3482–3496.
27. Zoltan-Jones A, Huang L, Ghatak S, Toole BP. Elevated hyaluronan production induces mesenchymal and transformed properties in epithelial cells. *J Biol Chem*. 2003;**278**:45801–45810.
28. Bourguignon LY, Gilad E, Peyrollier K. Heregulin-mediated ErbB2-ERK signaling activates hyaluronan synthases leading to CD44-dependent ovarian tumor cell growth and migration. *J Biol Chem*. 2007;**282**:19426–19441.
29. Bourguignon LY, Xia W, Wong G. Hyaluronan-mediated CD44 interaction with p300 and SIRT1 regulates beta-catenin signaling and NFkappaB-specific transcription activity leading to MDR1 and Bcl-xL gene expression and chemoresistance in breast tumor cells. *J Biol Chem*. 2009;**284**:2657–2671.
30. Camenisch TD, Schroeder JA, Bradley J, Klewer SE, McDonald JA. Heart-valve mesenchyme formation is dependent on hyaluronan-augmented activation of ErbB2-ErbB3 receptors. *Nat Med*. 2002;**8**:850–855.
31. Hurlstone AF, Haramis AP, Wienholds E, Begthel H, Korving J, Van Eeden F, Cuppen E, Zivkovic D, Plasterk RH, Clevers H. The Wnt/beta-catenin pathway regulates cardiac valve formation. *Nature*. 2003;**425**:633–637.

## SUPPLEMENTAL FIGURES



**Supplemental Figure 1: Loss of miRNA function does not alter myocardial patterning but does induce ectopic differentiation of endocardial cushion cells**

(a) Live images of a wild-type (top) and MZdicer+430 mutant embryo (bottom) at 3 dpf. (b,c) Hematoxylin and eosin staining on transversal sections of a wild-type (b) and MZdicer+430 mutant heart (c). Ventricle (V), atrium (A). Myocardial cell (black arrow), endocardial cell (black arrowhead). Blood cells occupy the atrial lumen of the wild-type heart. (d-i) Myocardial expression of the myosin genes *cmlc2* (d,e), *vmhc* (f,g) and *amhc* (h,i) at 2 dpf in wild-type (d,f,h) and MZdicer+430 mutant (e,g,i) embryos. (j,k) Patterning of the myocardium in working myocardium (*nppa* expression in j and k) and AVC myocardium (no *nppa* expression, indicated with black arrowheads in j and k) was not affected in MZdicer+430 mutant embryos. (l,m) Myocardial *bmp4* expression at 2 dpf in wild-type (l) and MZdicer+430 mutant (m) embryos. Black arrowheads indicate the AV boundary and dotted lines outline the heart tube; the arterial pole (outflow) is to the top and the venous pole (inflow) to the bottom. (n-q) Endocardial expression of *nfatc1* (n,o) and *spp1* (p,q) at 2 dpf. In wild-type EC cells (p) *spp1* was very low while in MZdicer+430 mutant embryos (q) *spp1* expression was increased and at ectopic places.

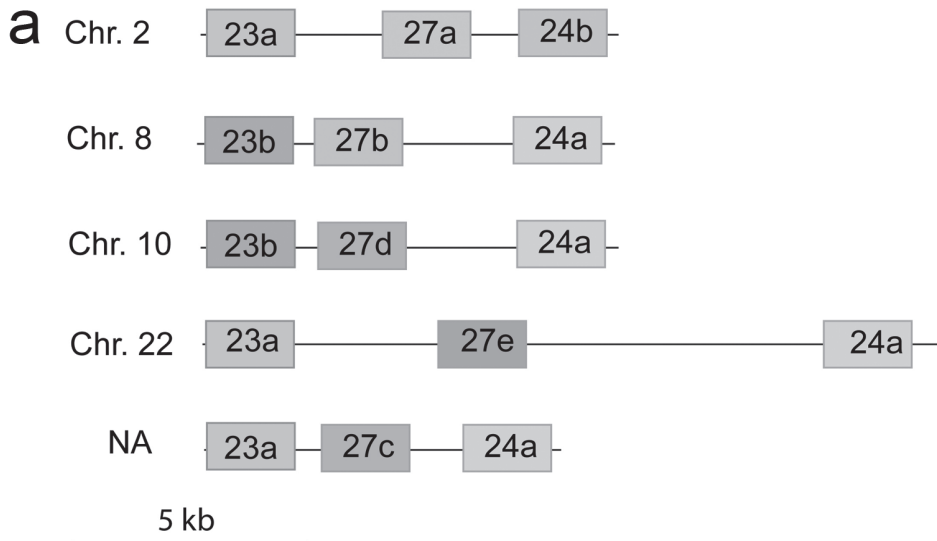


Supplemental Figure II: Ectopic *Dm-grasp* expression in accompanied by aberrant endocardial cell morphology in *MZdicer* mutants

(a-d'). Immunofluorescence staining for *Dm-grasp* (red, myocardium and endocardial cushion cells) in *Tg(kdr-I:GFP)* hearts (green, endocardium) of wild-type (a-b') and *MZdicer+430* (c-d') embryos at 2 dpf. Ventricle (V), Atrium (A). Panels b, b', d and d' show single confocal images of the ventricle with the AVC to the right. AVC (white arrowheads in a and c). Endocardial cushion cells located at the AVC (white arrows in b' and d'). (e) Ratio of *Dm-grasp* expressing endocardial cells in wild-type (n=6) and *MZdicer+430* (n=7) embryos at 2 dpf. Error bars represent means  $\pm$  s.e.m. *t*-test analyses resulted in statistically significant differences with  $p < 0.01$  (\*).

(f) In wild-type hearts endocardial cells positioned in the ECs (*Dm-grasp* positive, indicated with white asterisk) appeared cuboidal, while neighboring endocardial cells located in the chambers appeared squamous (white arrows in f). (g,h) *MZdicer+430* ventricular endocardial cells appeared cuboidal and made extensive cytoplasmic protrusions (white arrowheads in g and h) into the cardiac jelly. (i) 3D projection of *MZdicer+430* mutant endocardium showing a group of cells located outside the endocardial lining (white arrowhead); ventricle (V), atrium (A). (j) Individual cell (white arrowhead) from *MZdicer* heart shown in i located in the cardiac jelly between the endocardium (green cells) and myocardium (red cells). (k) Phalloidin staining for f-actin (red) on *Tg(kdr-I:GFP)* (green) *MZdicer+430* mutant embryo counterstained for DAPI (blue) at 3 dpf. White arrowheads indicate two clusters of f-actin positive cells located in within the cardiac jelly.





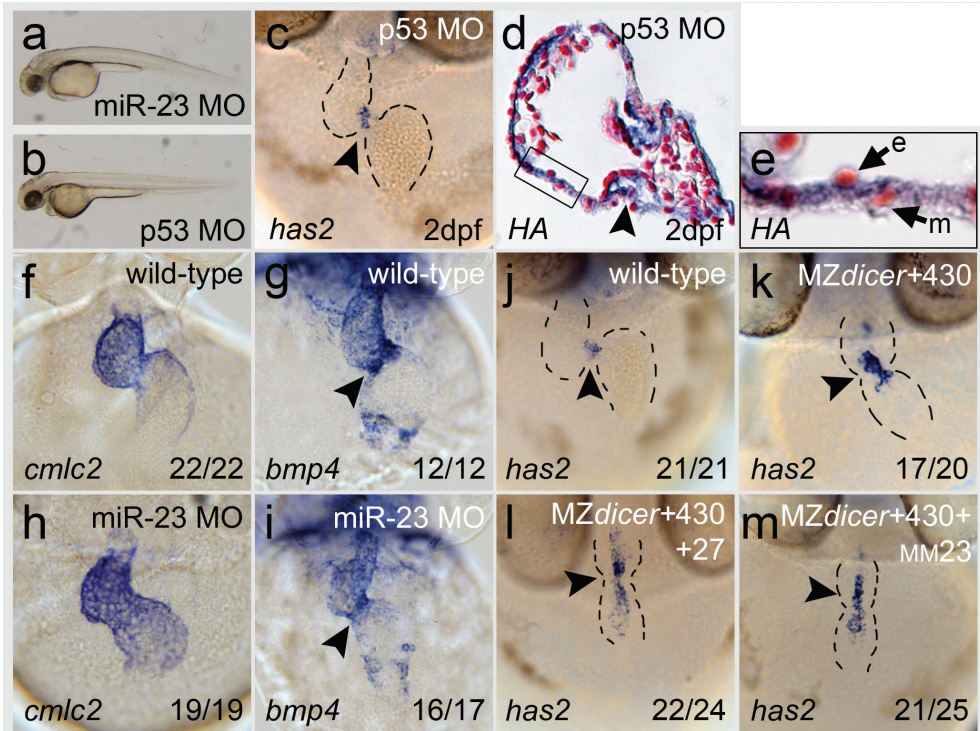
**b**

**mature miRNA sequences**

miR-23a	AUCACAUUGCCAGGGAUUUCCA
miR-23b	AUCACAUUGCCAGGGAUUACCA
miR-24a	UGGCUCAGUUCAGCAGGAACAG
miR-24b	UGGCUCAGUUCAGCAGGAACCG
miR-27a	UUCACAGUGGCUAAGUUCGCU
miR-27b	UUCACAGUGGCUAAGUUCUGCA
miR-27c	UUCACAGUGGUUAAGUUCUGC
miR-27d	UUCACAGUGGCUAAGUUCUUCA
miR-27e	UUCACAGUGGCUAAGUUCAGUG

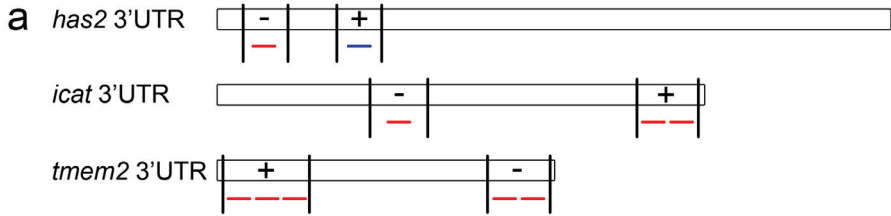
*Supplemental Figure III: Schematic representation of zebrafish miR-23-24-27 clusters*

(a) In the zebrafish genome 5 miR-23-24-27 clusters can be identified positioned on different chromosomes. (b) RNA sequences of mature miRNAs residing in all miR-23-24-27 clusters. Sequence variation amongst copies occurs in the last 4 bases at the 3'end.

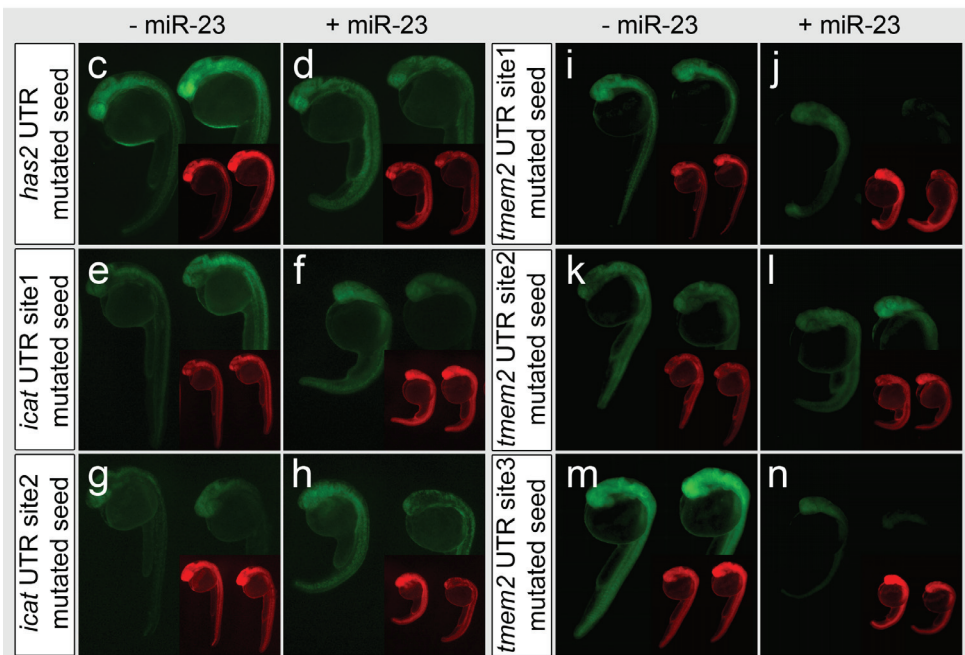


Supplemental Figure IV: MiR-23 is not required for myocardial patterning but can rescue abnormalities in endocardial patterning

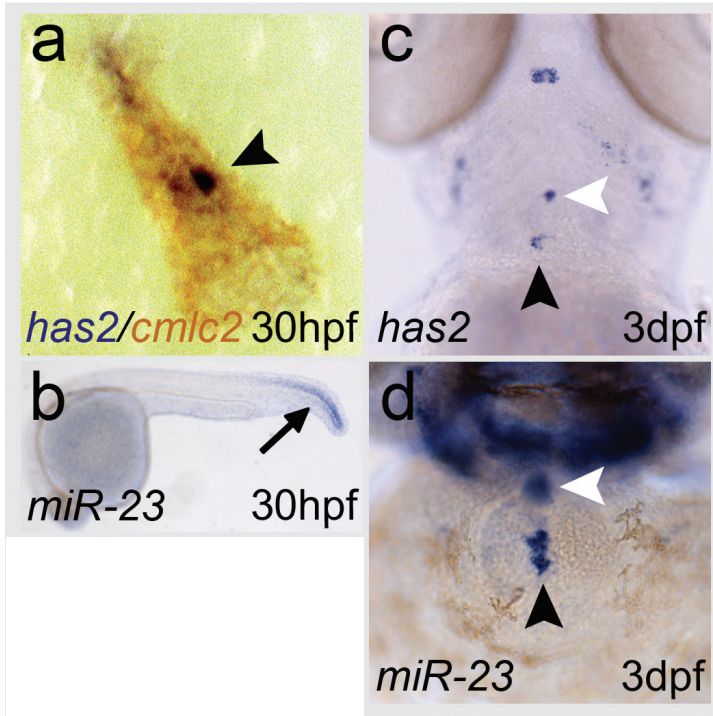
(a,b) Brightfield images of a miR-23 knock-down (a) and a *p53* knock-down (b) embryo at 2 dpf. (c) *in situ* hybridization showing wild-type levels of *has2* expression in *p53* knock-down embryo at 2 dpf. (d) Hyaluronic acid (HA) staining (blue) at 2 dpf in *p53* morphant counter stained with neutral red. (e) HA staining in ventricle wall (boxed in d) of *p53* knock-down embryo. Myocardial cell (m), endocardial cell (e). (f,i) Myocardial expression of *cmlc2* (f,h) and *bmp4* (g,i) at 2 dpf in wild-type (f,g) and miR-23 knock-down embryos (h,i). Black arrowheads indicate restricted *bmp4* expression in the AVC. (j-m) *has2* expression in wild-type ECs (j) compared to ectopic expression in MZdicer+430 mutants (k), MZdicer+430 mutants injected with miR-27 mimics (l) and MZdicer+430 mutants injected with mutated miR-23 mimics (m). Black arrowheads indicate the AV boundary and dotted lines outline the heart tube; the arterial pole (outflow) is to the top and the venous pole (inflow) to the bottom. All panels show *has2* expression at 2 dpf.



**b** D. rerio miR-23a/b ACCWUUAGGGACCGUUACACUA  
 D. rerio *has2* 3'UTR GCCUAUCUGACCAAAAUGUGAA  
 Human *has2* 3'UTR AAAAAUCCUGCCCAAAAUGUGAA  
 Mouse *has2* 3'UTR AUUAACCUGCCCAAAAUGUGAA  
 Frog *has2* 3'UTR UUUAAACUGGCCAAAAUGUGAA

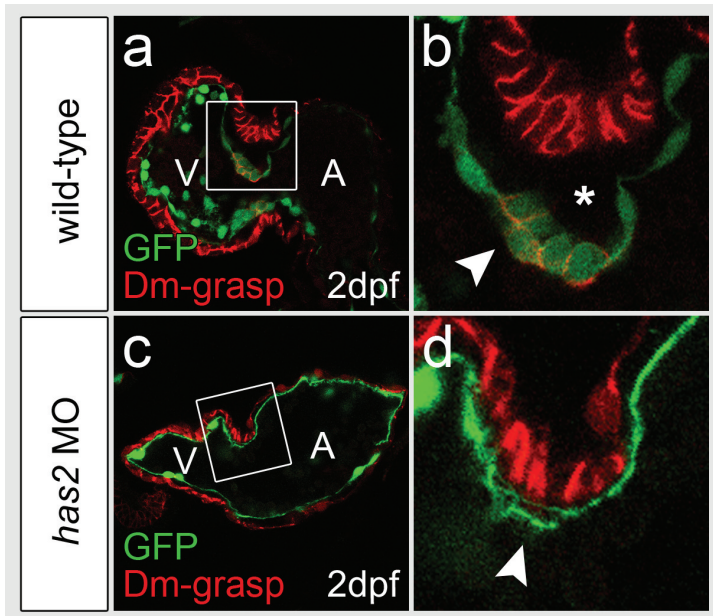


**Supplemental Figure V: miR-23 interacts with specific sequences within the zebrafish *has2*, *icat* and *tmem2* 3'UTRs**  
 (a) Schematic representation of *has2*, *icat* and *tmem2* 3'UTRs. Location of miR-23 seed sequences (minimal sequence underlined in b) in red and blue. Results of miR-23 silencing assays of 3'UTR regions (between lines) indicated by - (no silencing) and + (silenced). (b) Conservation of miR-23 seed sequence in *has2* 3'UTR (blue in a). Injection of synthetic mRNA containing the coding region for GFP and the 3'UTR sequences of zebrafish *has2* (c,d), *icat* (e-h) and *tmem2* (i-n) with a single putative target site mutated. The synthetic mRNA was injected alone (c,e,g,i,k,m) and in combination with miR-23 mimic (d,f,h,j,l,n). No effective silencing of the GFP was observed when a wild-type miR-23 mimic was co-injected upon mutation all the individual putative target sites. mRNA encoding RFP (red) was always coinjected as an injection control.



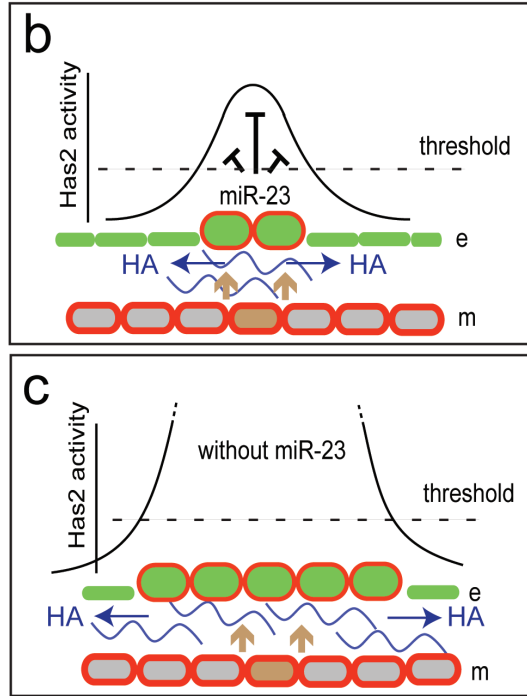
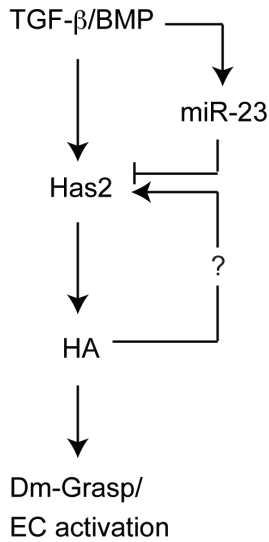
Supplemental Figure VI: *Has2* expression precedes *miR-23* in the ECs

(a) Combined *in situ* hybridization for *has2* (blue) and *cmlc2* (red) in a wild-type embryo at 30 hpf already showing AVC restricted *has2* expression. (b) *MiR-23* is not expressed in the heart at 30 hpf but can only be detected in the tail (black arrow). (c) Low levels of *has2* expression in the ECs of a wild-type embryo at 3 dpf. (d) Prominent *miR-23* expression in the ECs of a wild-type embryo at 3 dpf. Black arrowheads indicate the AVC ECs. White arrowheads indicate the outflow tract ECs.



Supplemental Figure VII: *Has2* loss of function prevents induction of AVC endocardial cell shape changes

(a-d) Single confocal images of immunofluorescence staining for *Dm-grasp* (red) in *Tg(kdr::GFP)* hearts (green, endocardium) of wild-type (a,d) and *has2* knock-down embryos (c,d) at 2 dpf. (a,b) Wild-type EC cells are cuboidal and *Dm-grasp* positive (boxed in a, white arrowhead in b). The cardiac jelly enlarges at the wild-type AVC (asterisks in b). (c,d) Upon *has2* knock-down endocardial cells at the AVC remained squamous and are *Dm-grasp* negative (boxed in c, white arrowhead in d).

**a**

Supplemental Figure VIII: Model for regulation of *Has2* by miR-23 in ECs

(a) Cartoon showing regulation of *Has2* expression by both positive and negative feedback mechanisms. (b,c) Proposed mechanism how miR-23 restricts EC formation to the AVC region. (b) In the AVC signals from the myocardium, such as TGF-β growth factors (blue arrows), induce *has2* expression in the endocardial cells and thereby enhance *Has2* enzyme activity (represented by solid curved line). *Has2* produces extracellular HA (blue ribbons) resulting in the activation of endocardial cushion cells and Dm-Grasp expression (indicated by red cell outlines). miR-23 is expressed in the ECs, where it provides a negative feedback mechanism for *Has2* activity. (c) Without miR-23 expression this negative regulation on *Has2* activity is lost and as a consequence *Has2* activity will increase resulting in more HA production and increase of the cardiac jelly. HA above a threshold (dashed line) induces Dm-grasp expression (indicated by red cell outlines) and cell shape changes. Since *Has2* activity is also regulated via an auto-regulatory and positive feedback mechanism (see discussion for explanation) *has2* expression and its activity will increase even more and expand outside the AV canal region. e, endocardium, m, myocardium.



# TRANSMEMBRANE PROTEIN 2 (TMEM2) IS REQUIRED TO REGIONALLY RESTRICT ATRIO- VENTRICULAR CANAL BOUNDARY AND ENDOCARDIAL CUSHION DEVELOPMENT

K.A. Smith<sup>1,2</sup>, A.K. Lagendijk<sup>1</sup>, A.D. Courtney<sup>2</sup>, H. Chen<sup>2</sup>, S. Paterson<sup>2</sup>,  
B.M. Hogan<sup>2</sup>, C. Wicking<sup>2</sup> and J. Bakkers<sup>1,3</sup>.  
*Development*. 2011 Oct;**138**(19):4193-8.

1. Hubrecht Institute, KNAW & Iniversity Medical Center, Utrecht, The Netherlands.
2. Institute for Molecular Bioscience, The University of Queensland, Brisbane, Australia.
3. Interuniversity Cardiology, Institute of the Netherlands, Utrecht, The Netherlands

4

## ABSTRACT

The atrio-ventricular canal (AVC) physically separates the atrial and ventricular chambers of the heart and plays a crucial role in the development of the valves and septa. Defects in AVC development result in aberrant heart morphogenesis and are a significant cause of congenital heart malformations. We have used a forward genetic screen in zebrafish to identify novel regulators of cardiac morphogenesis. We isolated a mutant, named *wickham* (*wkm*), that was indistinguishable from siblings at the linear heart tube stage but exhibited a specific loss of cardiac looping at later developmental stages. Positional cloning revealed that the *wkm* locus encodes *transmembrane protein 2* (*tmem2*), a single-pass transmembrane protein of previously unknown function. Expression analysis demonstrated myocardial and endocardial expression of *tmem2* in zebrafish and conserved expression in the endocardium of mouse embryos. Detailed phenotypic analysis of the *wkm* mutant identified an expansion of expression of known myocardial and endocardial AVC markers, including *bmp4* and *has2*. By contrast, a reduction in the expression of *spp1*, a marker of the maturing valvular primordia, was observed, suggesting that an expansion of immature AVC is detrimental to later valve maturation. Finally, we show that immature AVC expansion in *wkm* mutants is rescued by depleting Bmp4, indicating that Tmem2 restricts *bmp4* expression to delimit the AVC primordium during cardiac development.



## INTRODUCTION

During mammalian embryonic development, the primitive linear heart tube undergoes dynamic morphogenesis to give rise to the looped heart. This process begins as an asymmetric positioning of the heart tube followed by subsequent ballooning of the developing chambers and constriction of the AVC. The AVC partitions the atrial and ventricular chambers and gives rise to the endocardial cushions (ECs), which later contribute to the developing valves and septa of the heart. The AVC remains in an undifferentiated state, in contrast to the differentiating chamber myocardium, and uses a defined genetic programme to establish and maintain this spatially discrete region<sup>1</sup>. Developmental defects arising from improper AVC formation give rise to atrio-ventricular septal defects. These malformations constitute the largest subset of human congenital heart malformations and can have devastating consequences for the affected individual<sup>2</sup>. Identifying and characterising the molecular regulators of AVC development are crucial to understanding and managing this group of diseases.

For more than a decade, the zebrafish has successfully been used as a model to identify regulators of cardiac morphogenesis, including the AVC. Mutants for genes such as *ugdh* (*jeekyll*)<sup>3</sup>, *notch1*<sup>4</sup> and *foxn4* (*slipjig*)<sup>5</sup> exhibit a loss or diminution of EC development. In contrast, mutations in *apc*<sup>6</sup>, *tbx5* (*heartstrings*)<sup>7,8</sup> or *hey2* (*gridlock*)<sup>9</sup> result in an expansion of the AVC. In this latter category of mutants, the AVC-chamber boundary is compromised. Whilst the AVC defects in these mutants are phenotypically and molecularly diverse, each case is accompanied by cardiac looping defects, suggesting that appropriate patterning of the AVC is essential for correct looping and morphogenesis of the heart.

Here we describe a novel zebrafish mutant (*wickham* - *wkm*) identified in a forward genetic screen by a defect in cardiac looping. We show that the *wkm* mutant harbours a mutation in *tmem2*, a previously undescribed regulator of cardiac development that is expressed in the zebrafish and mammalian heart.

## MATERIALS AND METHODS

### Fish and mouse lines and fish mutagenesis

Fish were kept under standard conditions as previously described<sup>10</sup>. The *tg(myl7:dsRed)* and *tg(kdrl:gfp)* lines were previously described<sup>11-13</sup>. Pregnant wild-type CD1 mice were sacrificed and embryos dissected at the required stages.

ENU mutagenesis was performed as previously described<sup>14</sup>. F1 progeny from mutagenised Tuebingen Longfin males were crossed to an AB strain to produce F2 families. Subsequent incrossing of F2 progeny generated F3 embryos that were screened for cardiac morphogenesis defects. All animal work conformed to ethical guidelines and was approved by the relevant animal ethics committees at the Hubrecht Institute and the University of Queensland.

### Positional cloning of *wkm*

The *tmem2*<sup>hu4800</sup> allele was mapped using standard meiotic mapping with simple sequence length polymorphisms (SSLPs). The primer sequences used for SSLP markers

depicted in Fig. 1 are available on request. Linkage for the *tmem2*<sup>hu5935</sup> allele was also performed using SSLP markers. Subsequent genotyping of the *tmem2*<sup>hu5935</sup> allele was performed by sequencing using the primer pair 5'-ATGTCTTGACCTTCCTCAC-3' (forward) and 5'-AGAACAGAGTATAAAGCCCTCTG-3' (reverse). The genomic region was analysed with reference to Ensembl assembly zv8, release 55, December 2008.

### **Probe sequence and MO injections**

A 1500bp fragment of zebrafish *spp1* (Image clone 5602411, Imagenes) was cloned into pBluescript+ (Stratagene) for RNA probe synthesis. MO oligonucleotides (MO; Gene Tools) were dissolved in water and injected at 1 nl per embryo. The *tmem2* MO was targeted to the 5th exon donor site with the sequence: 5'-ACAAACCAAAGCCATCTCACCTTGA-3'. The splice-targeting *bmp4* MO was as previously described<sup>15</sup>. Standard *p53* MO control from Genetools was used.

### ***In situ* hybridization (ISH), immunohistochemistry and sectioning**

ISH analysis of zebrafish was carried out as previously described<sup>10</sup>. For sectioning, embryos were mounted in Technovit 8100 (Heraeus Kulzer) and sectioned at 7 µm thickness. Wholemount ISH analysis of mouse embryos was as described previously<sup>16</sup>. Immunohistochemistry was performed as previously described<sup>17</sup>. Hyaluronic acid staining was performed on paraffin sections as described previously<sup>18</sup>.

### **BAC recombineering**

BAC recombineering was performed as previously described<sup>19</sup>, integrating the Cherry coding sequence in place of the *tmem2* stop codon in CHORI BAC clone CH73-204I21. Homologous targeting sequences used for primers are available upon request.

### **Heart rate quantitation**

Heartbeats of 15 (alternating) sibling and mutant embryos were counted over a one-minute period using a dissecting microscope.

### **Imaging and image analysis**

Confocal imaging was performed using Leica SP2 and Zeiss 510 confocal laser scanning microscopes with 40x magnification. Embryos were mounted in ProLong Gold. Imaris (Bitplane) (Fig. 1 and 2) and Volocity software (Improvision) (Fig. 3 and 4) software were used for image analysis. ImageJ software was employed to remove myocardial Alcama expression in Fig. 3 and 4. Statistical analyses were performed in Excel (Microsoft).

# RESULTS & DISCUSSION

## Identification of the *wkm* mutant

To identify genetic regulators of cardiac morphogenesis and EC development, a forward genetic screen for zebrafish mutants with defective heart looping was performed. Embryos were screened at 26-32 hours post fertilization (hpf), to ensure normal formation and asymmetry of the cardiac tube, and at 48-54 hpf, to identify mutants with defective looping. Two alleles of the recessive lethal *wkm* (*wkm*<sup>hu4800</sup> and *wkm*<sup>hu5935</sup>) mutant were identified resulting in mutants indistinguishable from siblings at 26 hpf but displaying an unlooped heart at 48 hpf (Fig. 1A-C'). Heterozygous fish of each allele crossed together failed to complement (27% affected transheterozygotes), confirming that these two mutations are allelic (Fig. 1I-I'). The gross morphology of *wkm* mutants was relatively normal compared with siblings. The cardiac looping defect was accompanied by cardiac oedema and accumulation of blood above the ventral tail fin. By 4 days post fertilization (dpf), massive pericardial oedema was observed (data not shown) and from 5 dpf onward, lethality resulted.

## *wkm* mutant hearts fail to undergo looping morphogenesis but appear otherwise normal

Morphology of the heart was examined by *in situ* hybridization analysis. A reduction in the S-loop shape of the heart accompanied by diminished constriction of the AVC were observed in both whole-mount ISH and frontally-sectioned embryos stained with *cardiac myosin light chain 2* (*cmhc2/myl7*) and *atrial myosin heavy chain* (*amhc/myh6*) (Fig. 1C-D'). Chamber myocardium was specified normally in *wkm* mutants as determined by *ventricular myosin heavy chain* (*vmhc*) and *myh6* expression (Fig. 1E-F'). Pacemaker activity was also unchanged in *wkm* mutants, when beats per minute at 50 hpf was measured in mutant and sibling embryos (see Fig. S1A in the supplementary material). At later stages (>56 hpf), heart rate and cardiac contractility became impaired (data not shown) however this occurred subsequent to the looping defect and was, therefore, secondary to the morphogenetic defect. No alteration in overall myocardial cell number in *wkm* mutants was observed at 50 hpf compared with sibling embryos (see Fig. S1B in the supplementary material). The overall morphology of *wkm* hearts was examined by confocal imaging of embryos immunostained for Alcama (also known as Dm-grasp, which labels the myocardium and ECs<sup>20</sup>) on the transgenic background, *kdrl:GFP* (expressing GFP in all endocardial cells). The myocardium and endocardium were intact in the *wkm* heart, forming distinct layers. The presence of the endocardium was further confirmed by ISH staining for *nfatc1* (see Fig. S2 in the supplementary material) and the overall laterality of the embryo was normal, as determined by the direction of gut looping (see Fig. S2 in the supplementary material). Taken together these data indicate that myocardial patterning, cell number and function and endocardial specification were unaffected in *wkm* mutants at 50 hpf, suggesting that the cardiac morphogenesis defect was highly specific.

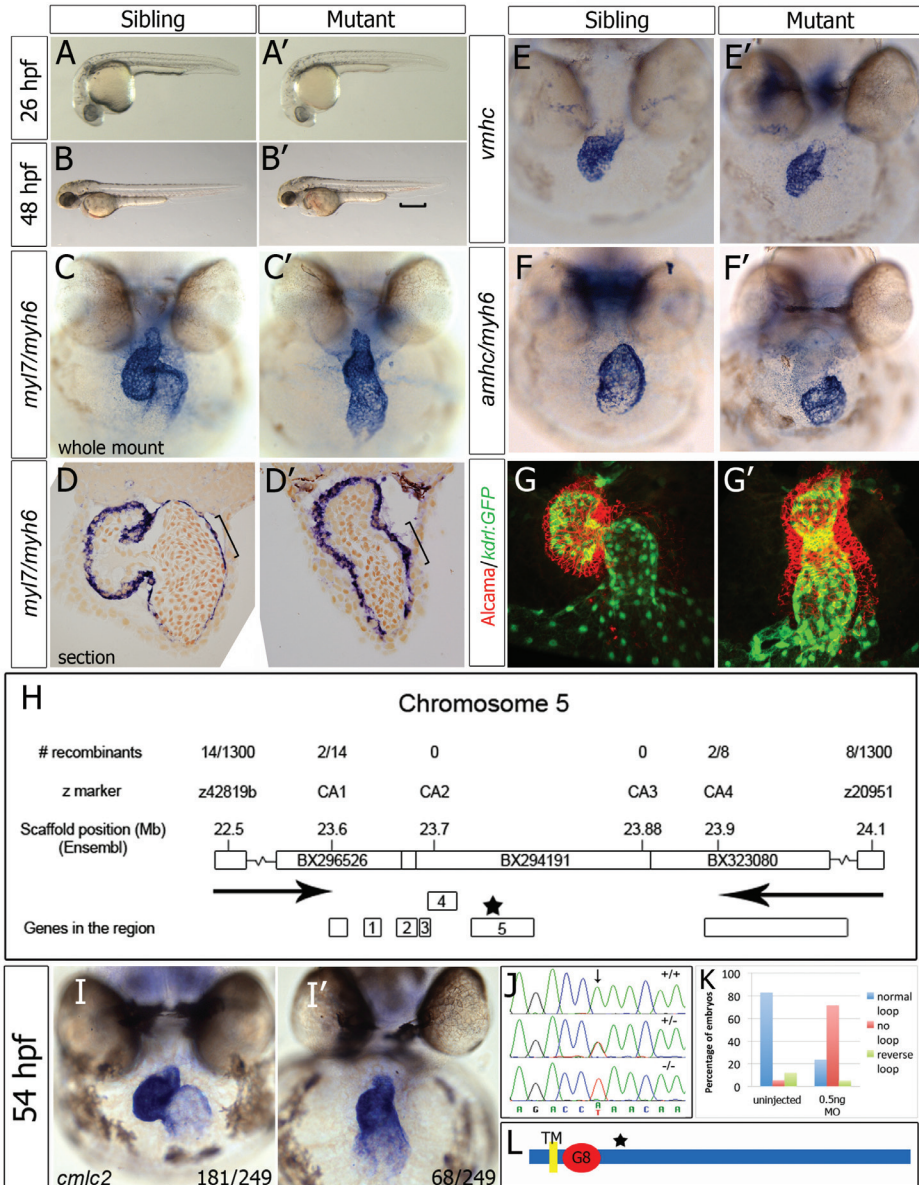


**Figure 1:** *wkm* has abnormal cardiac looping and encodes the novel protein, Transmembrane protein 2 (*Tmem2*) (A-B') Bright field images of *wkm* mutants and siblings. (C-D') Whole mount *in situ* hybridization (ISH) (C,C') and sectioning (D,D') of *wkm* sibling and mutant embryos for *cmlc2/myl7* and *amhc/myh6*. (E-F') ISH staining for *vmhc* (E,E') and *amhc/myh6* (F,F') at 52 hpf. G-G'. Confocal z-stacks of whole-mount, Alcama/Dm-grasp (red)-immunostained *kdr1:GFP* (green) transgenic embryos at 50 hpf. (H) Positional cloning of *wkm* (allele *tmem2*<sup>hu4800</sup>) on chromosome 5 (Ensembl, zv8). (I-I') ISH for *myl7/cmlc2* on embryos from a *wkm*<sup>hu5935</sup> x *wkm*<sup>hu4800</sup> transheterozygote cross. (J) Exon sequencing revealed an A>T transversion in the *wkm*<sup>hu5935</sup> allele, resulting in the stop codon (K329X) of *tmem2*. (K) 0.5ng of morpholino against *tmem2* reproduced the *wkm* phenotype in 72% of injected embryos at 48 hpf. (L) Protein schematic depicting the predicted single transmembrane domain (TM), the G8 domain and the location of the premature stop codon (black star).

## ***wkm* encodes Tmem2, a single-pass transmembrane domain containing protein**

To determine the gene responsible for the *wkm* phenotype, positional cloning using traditional genetic mapping with SSLP markers was performed. The mutation responsible for one of the *wkm* alleles (*wkm*<sup>hu4800</sup>) was localised to a genetic interval of 0.3Mb on Chromosome 5 containing 5 genes (Fig. 1H) however sequencing of the coding regions failed to identify any causative mutations. For the second allele (*wkm*<sup>hu5935</sup>), linkage on Chromosome 5 was confirmed. Sequencing the coding regions of all five genes in the genetic interval for *wkm*<sup>hu5935</sup> revealed an A to T transition at position 985 in the 3rd exon of the 23 exon gene, *transmembrane protein 2* (*tmem2*; Accession # NM\_001099449). This mutation is predicted to introduce a stop codon (K329X) leading to a prematurely truncated protein (Fig. 1J). To confirm that the lesion in *tmem2* is responsible for the *wkm* phenotype, MO (MO) knockdown of *tmem2* was performed and robustly reproduced the *wkm* cardiac phenotype (Fig. 1K). Thus, genetic linkage, the identification of a premature stop codon and MO phenocopy confirm that disruption of the *tmem2* gene results in the *wkm* phenotype (see Fig. S3 in the supplementary material). The 4173 nucleotides *tmem2* transcript is predicted to encode a 1,390 amino acid protein that harbours a single transmembrane domain, in close proximity to the N-terminus, and a G8 domain, which is hypothesised to be involved in ligand binding and catalysis (Fig. 1L; 21). The long C-terminal region of the protein is predicted to reside extracellularly<sup>22</sup>. Until now, no functional role had been ascribed to Tmem2.

## ***Tmem2* is expressed in the developing zebrafish and mouse heart**

*Tmem2* expression was examined in zebrafish and found to be present at the 2-cell stage (data not shown), indicating maternal deposition, and at the 22-somite stage, when it is ubiquitously expressed (Fig. 2A). By 48 hours, expression is restricted to the brain and head mesenchyme, otic vesicles, fin buds, caudal vein and the heart (Fig. 2B). Within the heart *tmem2*-positive regions included the outflow tract, ventricular regions and outer curvature of the atrium (Fig. 2C). Sectioned hearts counter-stained with tropomyosin (to label the myocardium) revealed both myocardial and endocardial expression (Fig. 2D). To expand on these analyses, a recombinered bacterial artificial chromosome (BAC) containing the *tmem2* locus, with an in-frame insertion of the cherry coding sequence, replacing the *tmem2* stop codon, (resulting in a fusion of Cherry to the Tmem2 C-terminus) was created. Injection of BAC DNA into 1-cell stage zebrafish embryos resulted in mosaic expression of Tmem2-Cherry protein. In the developing heart, fusion protein expression localised to both myocardial and endocardial cells at 48 hpf, consistent with *tmem2* RNA expression at the same stage (Fig. 2E&F). These approaches confirm that *tmem2* is transcribed and expressed in both endocardium and myocardium during the morphogenesis of the zebrafish heart.

To investigate possible conservation of function in mammals, we investigated expression of *Tmem2* by whole-mount ISH analysis in mouse embryos. At early stages of development, *Tmem2* showed ubiquitous expression (Fig. 2G&H), although enriched, punctate staining was evident in the developing heart, particularly from E9.5 (Fig. 2J). Sagittal sections of stained E9.5 embryos revealed expression restricted to endocardial cells lining the ventricles

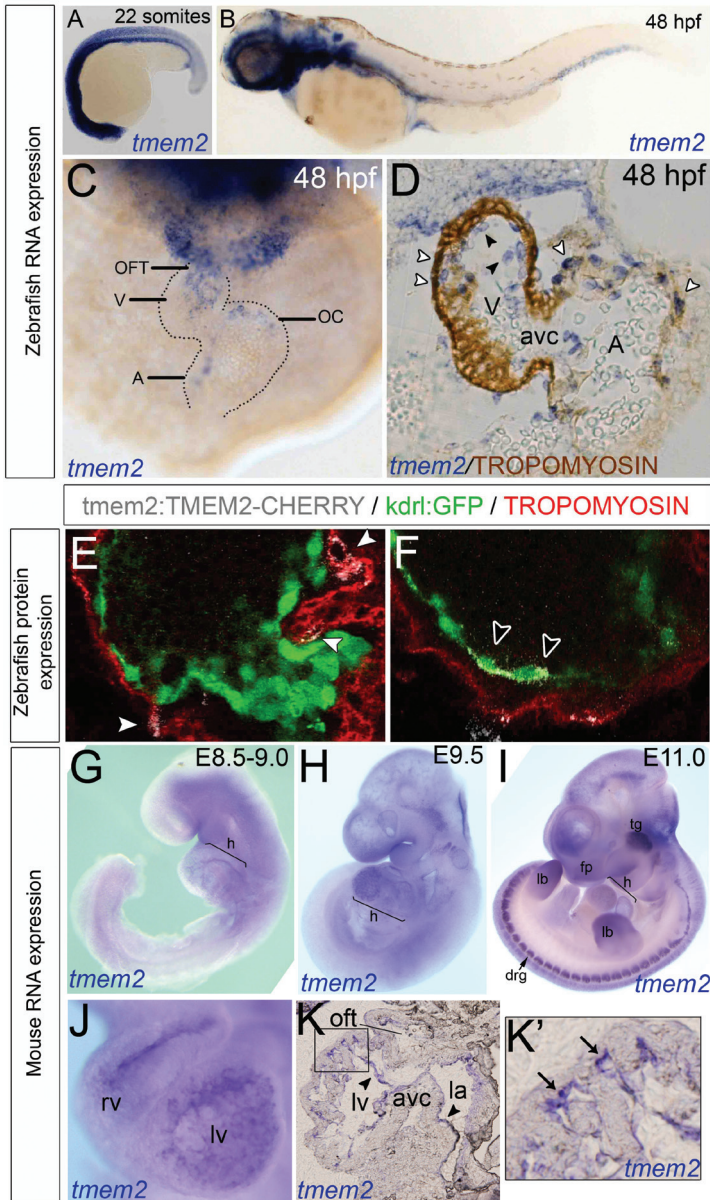


**Figure 2: *Tmem2* expression in endocardial cells of zebrafish and mouse hearts and myocardial cells of zebrafish hearts**  
 A-C. ISH for *tmem2* expression at 22-somite (A) and 48 hpf (B,C) shown as lateral (A,B) or frontal (C) view (outflow tract (OFT), ventricle (V), outer curvature (OC) and atrium (A)). D. Cross section of *tmem2* ISH with tropomyosin counterstaining (white arrowheads, myocardial expression, black arrowheads, endocardial expression). E,F. Transient expression from a *Tmem2*-Cherry BAC construct (white arrowheads, myocardial *Tmem2*-Cherry, black arrowheads, endocardial *Tmem2*-Cherry). G-K'. ISH of mouse embryos stained for *Tmem2* at embryonic day 8.5-9.0 (E8.5-9.0), H,J. E9.5 and I. E11.0. K. Sagittal sectioning revealed expression in the endocardium K'. Enlargement of boxed region from K. A, atrium; avc, atrio-ventricular canal; drg, dorsal root ganglion; fp, facial prominences; h, heart; la, left atrium; lb, limb buds; lv, left ventricle; OC, outer curvature; OFT, outflow tract; tg, trigeminal ganglion; V, ventricle

and atria (Fig. 2K&K'). In an analogous manner to the zebrafish, *tmem2* expression became progressively restricted at later stages of mouse development (E11.0; Fig. 2I). Although the morphology of zebrafish and mammalian hearts ultimately differ, many of the underlying molecular and cellular patterning events are conserved. The finding that *Tmem2* has enriched expression in the mouse heart suggests a potential conservation of function.

### ***wkm* affects cardiac looping via a distinct genetic pathway distinct from *tbx5***

The *tbx5* mutant has been shown to exhibit a specific cardiac looping defect similar to *wkm* mutants<sup>8</sup>. To determine whether the looping defect observed in *wkm* mutants was related to the *tbx5* genetic pathway, reciprocal expression analysis was performed on both mutants. No obvious difference in *tbx5* expression was observed in *wkm* mutants relative to sibling embryos (see Fig. S4A, A' in the supplementary material). Likewise, no difference in *tmem2* expression was observed in *tbx5* mutant embryos (see Fig. S4B, B' in the supplementary material), suggesting that these genes operate in distinct genetic pathways to affect cardiac looping.

### ***tmem2* is required to restrict endocardial cushion development**

To more clearly define the cardiac defect in *wkm* mutants, the expression of a number of regionalized cardiac markers was examined. The myocardial chamber marker, *anf/nppa*, was expressed in the chambers but excluded from the AVC of *wkm* mutants (Fig. 3A&A'), although the area of *anf*-negative myocardial cells appeared to be broader than in siblings. Strikingly, the myocardial AVC markers, *bmp4* and *tbx2b*, were found to be upregulated and expanded, notably with *bmp4* expression expanded throughout the entire ventricle in *wkm* mutants (Fig. 3B-C'). As with markers of the AVC myocardium, the AVC endocardial marker *hyaluronic acid synthase 2 (has2)*, was expanded into the chambers (Fig. 3D&D'). Concordantly, an increase in hyaluronic acid (HA) in the chambers was also observed (see Fig. S5A, A' in the supplementary material). *notch1b* expression in the AVC was less condensed but otherwise unchanged in mutants (see Fig. S5B, B' in the supplementary material); however expression of the Notch target, *hey2*, was expanded (see Fig. S5C, C' in the supplementary material). Immunofluorescence analysis of the EC marker, Alcama, also showed a dramatic expansion in ECs (Fig. 3E&E'), confirming an expansion of the EC region in *wkm* mutants. Intriguingly, whilst the suite of early AVC development markers showed expansion of their expression domain, the marker *spp1/osteopontin* showed a substantial reduction in expression (Fig. 3F&F'). *spp1* marks the developing cardiac valves at later stages of formation<sup>23</sup>, suggesting that, whilst the EC primordium is expanded, there is a failure to progress to valve maturation.

### **AVC expansion in *tmem2* mutants is driven by Bmp4**

Bmp signaling is essential for the formation of the AVC<sup>24</sup>. *bmp2/4* have restricted expression in the AVC and outflow tract and have been demonstrated to promote cardiac jelly formation, epithelial-to-mesenchymal transition and patterning of the AVC<sup>25</sup>. Given this role, we hypothesized that the ectopic expression of *bmp4* in *wkm* mutants may be responsible for the expanded AVC phenotype. To test this, Bmp4 was depleted in sibling and

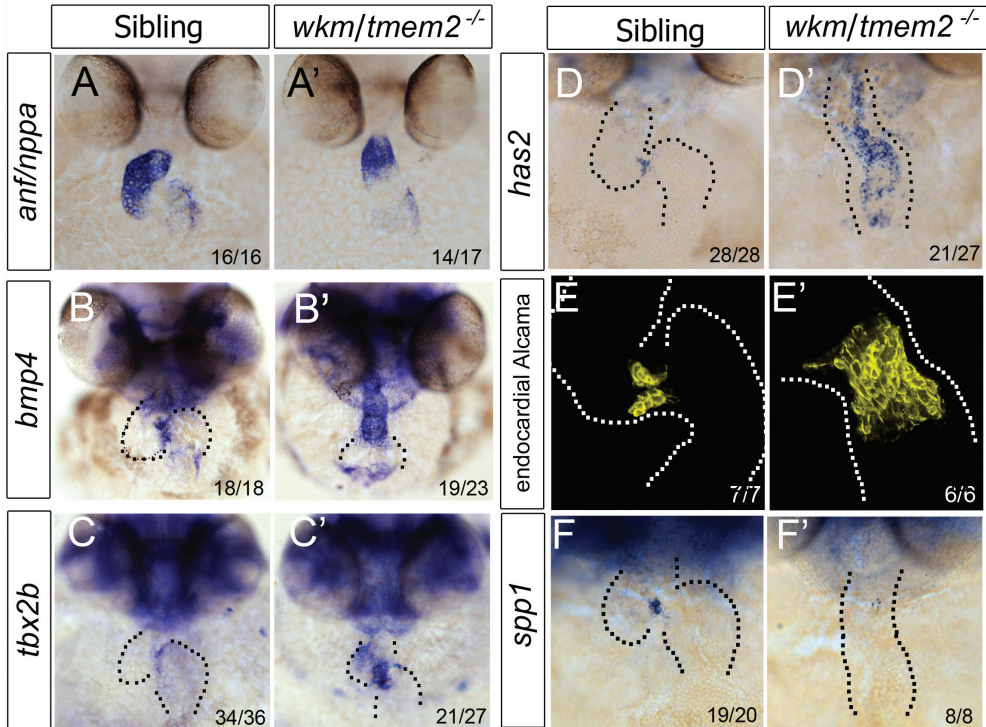


Figure 3: *wkm/tmem2* is required to restrict the AVC

A-D'. ISH for *anf/nppa* (A,A'), *bmp4* (B,B'), *tbx2b* (C,C') and *has2* (D,D') at 52 hpf in *wkm/tmem2* sibs and mutants. E-E'. 3D projections of endocardial-specific Alcama expression in *wkm/tmem2* sibs and mutants (50 hpf). F-F'. *osteopontin/spp1* expression in *wkm/tmem2* sibs and mutants (50 hpf). Numbers of embryos was recorded in lower right corners.

mutant embryos by MO knockdown and ECs examined. *has2* expression was unchanged in sibling and mutant embryos injected with control *p53* MO in that an expansion of *has2* was evident (Fig. 4A-A'). In contrast, whilst injection of *bmp4* MO had no effect on *has2* expression in sibling embryos, a rescue of the ectopic expression of *has2* in *wkm* mutants was observed (Fig. 4B-B'). A similar rescue was observed for Alcama staining in ECs (Fig. 4C-F'), indicating that the expanded EC phenotype in *wkm* mutants is Bmp4-dependent. It is noteworthy that the AVC expression of *has2* and Alcama is not abolished in *bmp4* morphants, suggesting that this region is not under the sole regulation of Bmp4. The expanded AVC phenotype of *wkm* is phenotypically indistinguishable from the defect seen in zebrafish *tbx5*, *apc* and *hey2* mutants. In these cases, an expansion of *bmp4* expression throughout the ventricular myocardium is observed and associated with EC marker expansion. Here we show that, downstream of *tmem2*, ectopic *bmp4* expression is functionally responsible for the expansion of the immature AVC. Bmp signaling is known to activate *tbx2* expression in the AVC<sup>26,27</sup> and, in turn, *tbx2* inhibits the chamber myocardial differentiation program via repression of genes, such as *anf*<sup>8</sup>. The boundary between the AVC and chambers is kept in check by chamber-specific genes, such as *Hesr1* and *Hesr2*<sup>29</sup>. Clearly *tbx5*, *apc*, *hey2* and, now, *tmem2*, are instrumental in determining this AVC boundary and regionally restricting EC development.



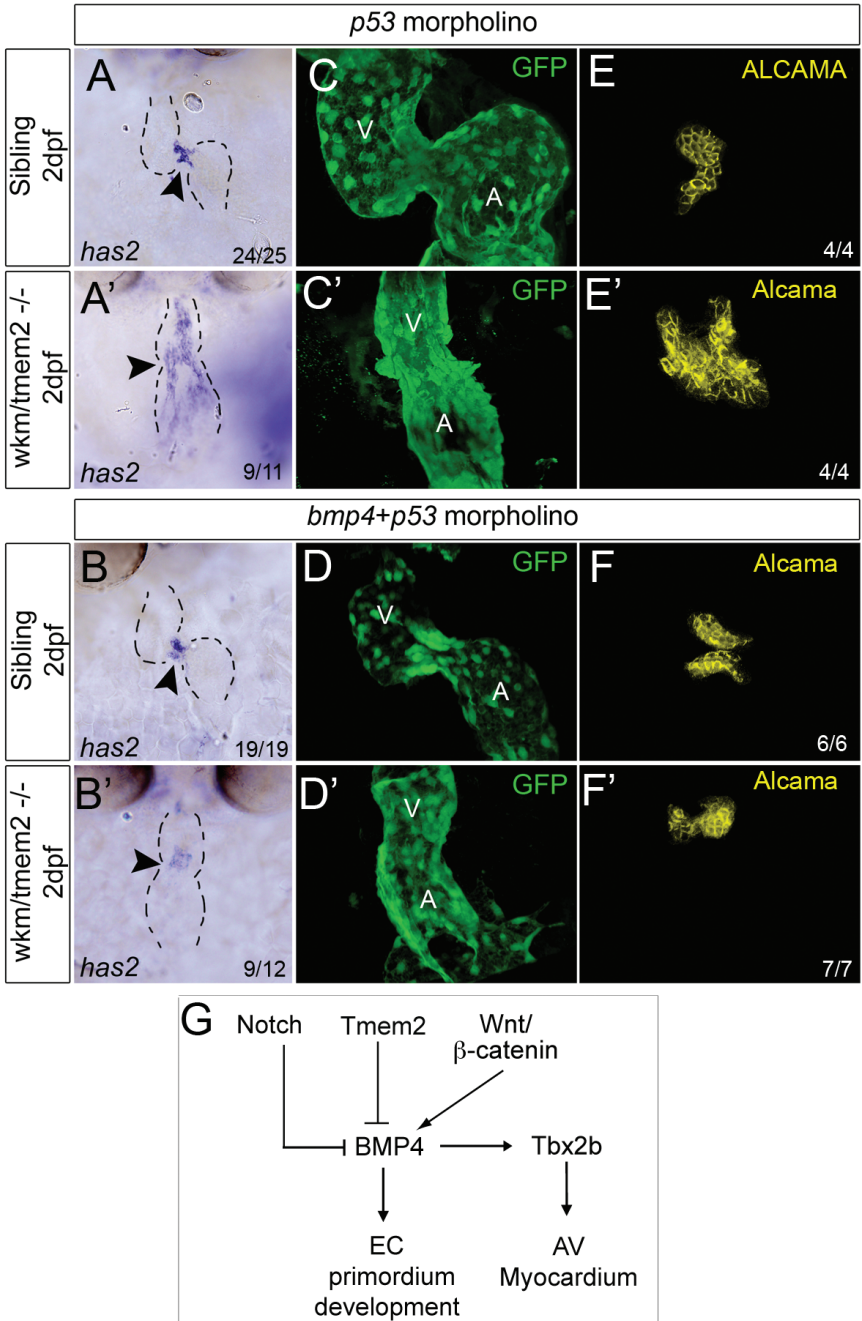


Figure 4: The endocardial expansion in *wkm/tmem2* mutants is *bmp4*-driven  
A-B'. ISH for *has2* in *p53* MO (A) or *p53* + *bmp4* MO injected *wkm/tmem2* mutants at 52 hpf. C-F'. Endothelial *kdr1:GFP* (C-D') or endocardial Alcama (E-F') expression in *p53* or *p53*+*bmp4* MO injected *wkm/tmem2* mutants.  
G. Model of AVC boundary regulation. In zebrafish, Bmp4 can drive EC primordium development in the AVC. Tmem2 restricts EC cushion formation to the AVC by inhibiting Bmp4.

## Acknowledgements

The authors would like to thank the Hubrecht Screen Team and Jeroen Korving for technical assistance and Dr. David Pennisi for useful discussions.

## Sources of funding

This work was supported by the Research Council for Earth and Life Sciences (ALW) from the Netherlands Organization for Science (NWO) to J.B. K.S. was supported by a UQ Postdoctoral Fellowship, Concordia Fellowship, an Institute for Molecular Bioscience (IMB) Development Grant and National Health and Medical Research Council (NHMRC) of Australia Project Grant. B.M.H is an Australian Research Council (ARC) Future Fellow and C.W is a NHMRC senior research fellow. Confocal microscopy was performed at the ACRF Cancer Biology Imaging Facility at the IMB, established with the generous support of the Australian Cancer Research Foundation (ACRF).

## Supplemental data

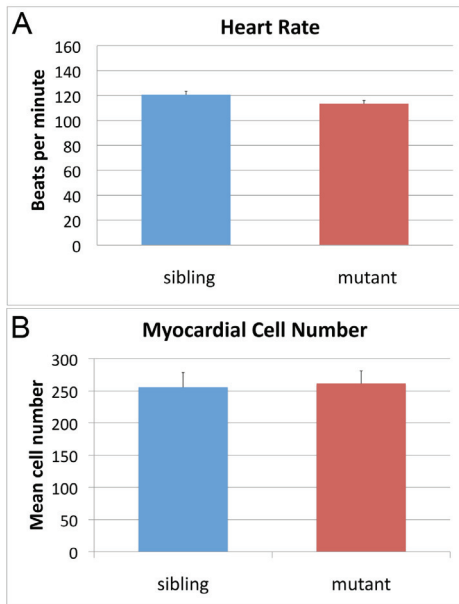
Supplementary Table 1 is available at <http://dev.biologists.org/lookup/suppl/doi:10.1242/dev.065375/-/DC1>

## REFERENCES

1. A. F. Moorman, V. M. Christoffels, Cardiac chamber formation: development, genes, and evolution. *Physiol Rev* **83**, 1223 (Oct, 2003).
2. A. K. Lagendijk, K. A. Smith, J. Bakkers, Genetics of congenital heart defects: a candidate gene approach. *Trends Cardiovasc Med* **20**, 124 (May, 2010).
3. E. C. Walsh, D. Y. Stainier, UDP-glucose dehydrogenase required for cardiac valve formation in zebrafish. *Science* **293**, 1670 (Aug 31, 2001).
4. L. A. Timmerman et al., Notch promotes epithelial-mesenchymal transition during cardiac development and oncogenic transformation. *Genes Dev* **18**, 99 (Jan 1, 2004).
5. N. C. Chi et al., Foxn4 directly regulates tbx2b expression and atrioventricular canal formation. *Genes Dev* **22**, 734 (Mar 15, 2008).
6. A. F. Hurlstone et al., The Wnt/beta-catenin pathway regulates cardiac valve formation. *Nature* **425**, 633 (Oct 9, 2003).
7. T. Camarata et al., Pdlim7 (LMP4) regulation of Tbx5 specifies zebrafish heart atrio-ventricular boundary and valve formation. *Dev Biol* **337**, 233 (Jan 15, 2010).
8. D. M. Garrity, S. Childs, M. C. Fishman, The heart strings mutation in zebrafish causes heart/fin Tbx5 deficiency syndrome. *Development* **129**, 4635 (Oct, 2002).
9. J. B. Rutenberg et al., Developmental patterning of the cardiac atrioventricular canal by Notch and Hairy-related transcription factors. *Development* **133**, 4381 (Nov, 2006).
10. M. Westerfield, *The Zebrafish Book - A guide for laboratory use of zebrafish (Brachydanio rerio)*. (University of Oregon Press, Oregon, 1995).
11. C. J. Huang, C. T. Tu, C. D. Hsiao, F. J. Hsieh, H. J. Tsai, Germ-line transmission of a myocardium-specific GFP transgene reveals critical regulatory elements in the cardiac myosin light chain 2 promoter of zebrafish. *Dev Dyn* **228**, 30(Sep,2003).
12. N. D. Lawson, B. M. Weinstein, In vivo imaging of embryonic vascular development using transgenic zebrafish. *Dev Biol* **248**, 307 (Aug 15, 2002).
13. J. D. Mably, M. A. Mohideen, C. G. Burns, J. N. Chen, M. C. Fishman, heart of glass regulates the concentric growth of the heart in zebrafish. *Curr Biol* **13**, 2138 (Dec 16, 2003).
14. E. Wienholds, S. Schulte-Merker, B. Walderich, R. H. Plasterk, Target-selected inactivation of the

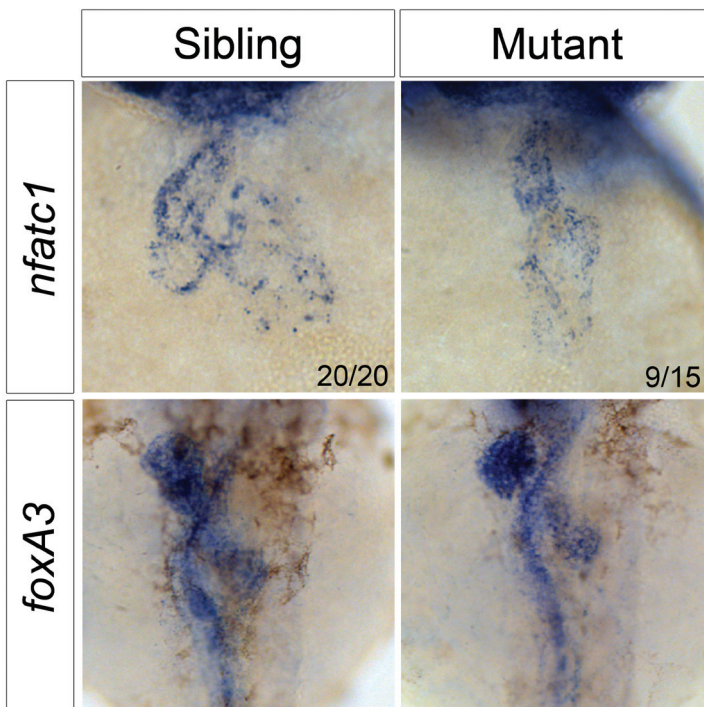
- zebrafish rag1 gene. *Science* **297**, 99 (Jul 5, 2002).
15. S. Chocron, M. C. Verhoeven, F. Rentzsch, M. Hammerschmidt, J. Bakkers, Zebrafish Bmp4 regulates left-right asymmetry at two distinct developmental time points. *Dev Biol* **305**, 577 (May 15, 2007).
  16. L. F. Fowles et al., Genomic screen for genes involved in mammalian craniofacial development. *Genesis* **35**, 73 (Feb, 2003).
  17. K. A. Smith et al., Rotation and asymmetric development of the zebrafish heart requires directed migration of cardiac progenitor cells. *Dev Cell* **14**, 287 (Feb, 2008).
  18. J. Bakkers et al., Has2 is required upstream of Rac1 to govern dorsal migration of lateral cells during zebrafish gastrulation. *Development* **131**, 525 (Feb, 2004).
  19. B. M. Hogan et al., Ccbe1 is required for embryonic lymphangiogenesis and venous sprouting. *Nat Genet* **41**, 396 (Apr, 2009).
  20. D. Beis et al., Genetic and cellular analyses of zebrafish atrioventricular cushion and valve development. *Development* **132**, 4193 (Sep, 2005).
  21. Q. Y. He et al., G8: a novel domain associated with polycystic kidney disease and non-syndromic hearing loss. *Bioinformatics* **22**, 2189 (Sep 15, 2006).
  22. M. C. Hogan et al., PKHD1, a homolog of the autosomal recessive polycystic kidney disease gene, encodes a receptor with inducible T lymphocyte expression. *Hum Mol Genet* **12**, 685 (Mar 15, 2003).
  23. D. S. Peal, C. G. Burns, C. A. Macrae, D. Milan, Chondroitin sulfate expression is required for cardiac atrioventricular canal formation. *Dev Dyn* **238**, 3103 (Dec, 2009).
  24. B. van Wijk, A. F. Moorman, M. J. van den Hoff, Role of bone morphogenetic proteins in cardiac differentiation. *Cardiovasc Res* **74**, 244 (May 1, 2007).
  25. L. Ma, M. F. Lu, R. J. Schwartz, J. F. Martin, Bmp2 is essential for cardiac cushion epithelial-mesenchymal transition and myocardial patterning. *Development* **132**, 5601 (Dec, 2005).
  26. M. Yamada, J. P. Revelli, G. Eichele, M. Barron, R. J. Schwartz, Expression of chick Tbx-2, Tbx-3, and Tbx-5 genes during early heart development: evidence for BMP2 induction of Tbx2. *Dev Biol* **228**, 95 (Dec 1, 2000).
  27. R. Singh et al., Tbx20 interacts with smads to confine tbx2 expression to the atrioventricular canal. *Circ Res* **105**, 442 (Aug 28, 2009).
  28. P. E. Habets et al., Cooperative action of Tbx2 and Nkx2.5 inhibits ANF expression in the atrioventricular canal: implications for cardiac chamber formation. *Genes Dev* **16**, 1234 (May 15, 2002).
  29. H. Kokubo, S. Tomita-Miyagawa, Y. Hamada, Y. Saga, Hes1 and Hes2 regulate atrioventricular boundary formation in the developing heart through the repression of Tbx2. *Development* **134**, 747 (Feb, 2007).

## SUPPLEMENTAL FIGURES



*Supplemental Figure S1: The heart rate and myocardial cell number are unaltered in *wkm* mutants*

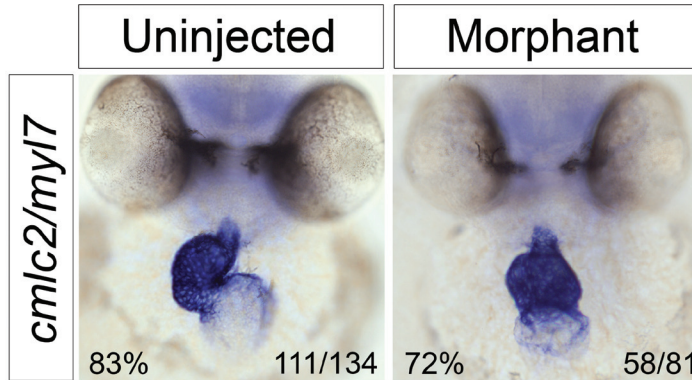
(A) The heart rate is not significantly different in mutant embryos compared with siblings (n=15) at 50 hpf, indicating no affect of the *wkm* mutation on pacemaker activity. (B) Myocardial cell counts showed no significant difference between *wkm* sibling and mutant embryos at 50 hpf, indicating that myocardial cell number is not contributing to the defective looping phenotype of *wkm* mutants. Counts were performed on confocal z-stacks of *wkm* mutant and sibling embryos (n=5-6) on a *myl7:dsRed* transgenic background. Statistical significance was determined by *t*-test, bars represent mean ± SEM.



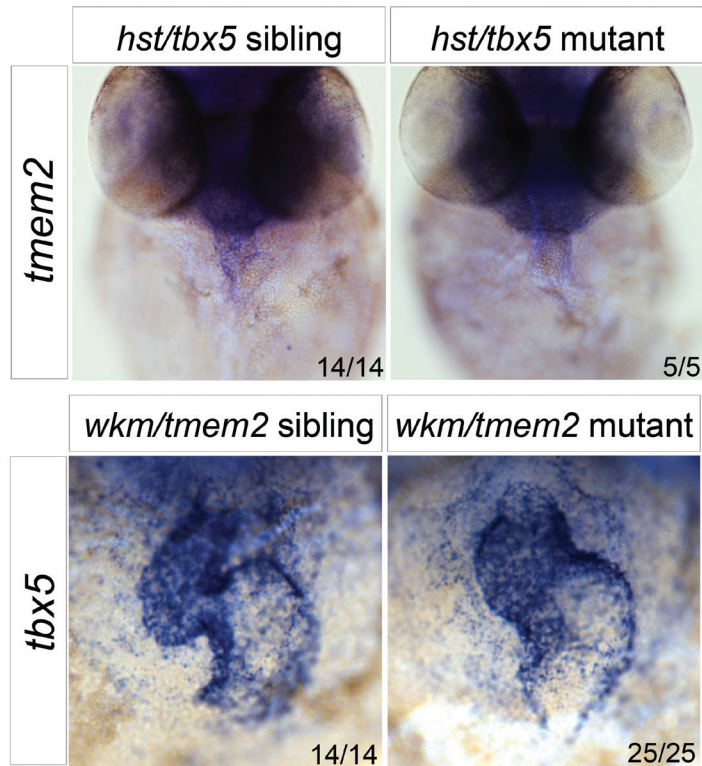
*Supplemental Figure S2: *nfatc1* expression and embryonic laterality are normal in *wkm* mutants*

(Top) *nfatc1* expression is unaltered in *wkm* mutants at 52 hpf reiterating that, as seen in Figure 1G, the endocardium is intact.

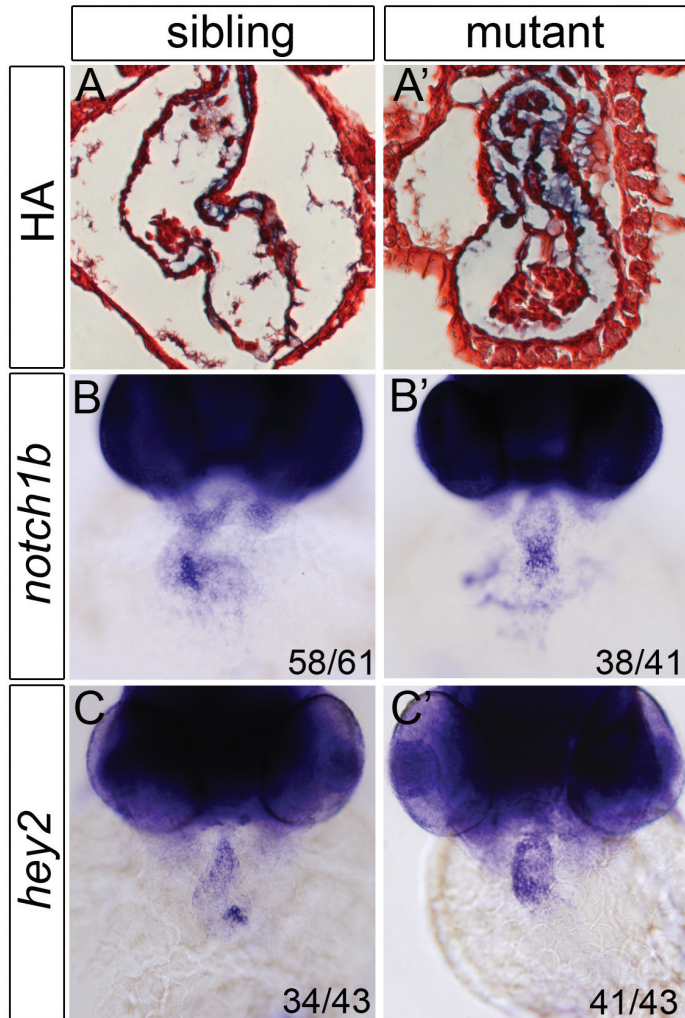
(Bottom) *foxA3* ISH staining labeling the developing gut, liver and pancreas at 52 hpf. These organs are present and loop normally, indicating that overall laterality is unaffected in *wkm* mutant embryos and therefore not responsible for the cardiac looping defect.



Supplemental Figure S3: Cardiac looping is disturbed in *tmem2* morphant embryos *cmlc2/myl7* ISH staining showing the cardiac looping phenotype at 48 hpf of uninjected embryos (left) and embryos injected with 0.5 ng of morpholino against *tmem2* (right).



Supplemental Figure S4: Expression of *tbx5* in *wkm* mutants and *tmem2* expression in *tbx5* mutants is unchanged (Top) *tmem2* expression is unchanged in *tbx5* mutants compared with siblings at 49 hpf. (Bottom) Reciprocally, *tbx5* staining in sibling and *wkm* mutant embryos show no difference in expression at 52 hpf, demonstrating that *tmem2* and *tbx5* are regulated differently at the transcriptional level. Numbers of embryos scored are in the lower right corner.



*Supplemental Figure S5: HA production and hey2 expression is expanded in wkm mutants*  
 (A&A') Staining for HA on sectioned hearts showed an increase and expansion of HA staining. (B&B') *notch1b* expression in the AVC was less condensed and but otherwise unchanged in mutants. (C&C') *hey2*, a Notch target, was expanded in *wkm* mutant embryos compared with siblings. Numbers of scored embryos are recorded in the lower, right corner.

# 4

## TMEM2, A NOVEL VALVE RESTRICTING GENE





# ZEBRAFISH LOOPING MORPHOGENESIS: INVESTIGATING THE INFLUENCE OF CONTRACTILITY, FLOW AND ATRIO-VENTRICULAR CANAL PATTERNING

A.K. Lagendijk<sup>1</sup>, F. Tessadori<sup>1</sup>, E.S. Noël<sup>1</sup>, K.A. Smith<sup>1,3</sup>, F.K. Kruse<sup>1</sup> and  
J. Bakkers<sup>1,2</sup>.

1. Hubrecht Institute, KNAW & Iniversity Medical Center, Utrecht,  
The Netherlands.
2. Interuniversity Cardiology, Institute of the Netherlands, Utrecht,  
The Netherlands
3. Institute for Molecular Bioscience, The University of Queensland,  
Brisbane, Australia.

# 5

## **ABSTRACT**

Asymmetric movements during cardiac development are required to position cardiac chambers relative to the great vessels. Discrepancies in this process induce congenital malformation resulting in cardiac dysfunction. To identify genes that regulate cardiac looping we have employed classical forward genetic screens. As a result we identified 5 zebrafish mutants that can be divided into 3 different groups that display cardiac looping defects. Embryos derived from a mutant representing the first group lack cardiac contraction and therefore have no circulating blood. Analysis of this mutant indicates that contraction is not required for the directional looping, although potential secondary effects can still disrupt the looping process. We describe two looping mutants representing a second group with clear atrio-ventricular patterning defects, suggesting a relation between cardiac looping and myocardial patterning. Two additional looping mutants from the third group displaying minor changes in differentiation of the AVC implying that additional, thus far unknown, factors are required for looping morphogenesis.

## INTRODUCTION

Correct positioning of internal organs relative to the embryonic left-right (L-R) axis is a crucial process during vertebrate development. Laterality defects can influence positioning of all organs simultaneously, like *situs inversus*, a complete reversal of all internal organs<sup>1</sup>. However, organ specific L-R asymmetry defects also occur. Incorrect L-R patterning of the embryonic heart can induce an array of congenital heart defects (CHDs), like transposition of the great arteries (TGA) which is life threatening due to a failure of oxygenating blood by transportation through the lungs<sup>2</sup>.

The zebrafish heart breaks symmetry by moving into a leftward direction starting around 24 hours post fertilization (hpf). This leftward displacement of the linear heart tube (LHT) is also referred to as cardiac jogging<sup>3</sup>. It is well known that this leftward displacement is highly dependent on correct signaling of early L-R genetic cues, including Bmp and Nodal signaling (reviewed in Bakkers et al.<sup>2</sup>). At 2 days post fertilization (dpf) cardiac looping has been completed and the LHT has transformed into an S-shaped heart, with the ventricle positioned next to the atrium separated by the atrio-ventricular canal (AVC). The exact mechanism of cardiac looping however is not well understood. Extrinsic signals that determine L-R patterning affect early leftward positioning of the LHT and also result in defects in the direction of cardiac looping<sup>3,4</sup>. However, early studies using explanted chick hearts showed that the heart can bend autonomously which suggests intrinsic cardiac signals to be required for the C-looping process<sup>5</sup>. The presence of actin bundles in myocardial cells positioned on the right side of the chick LHT were shown to be necessary for looping morphogenesis<sup>6,7</sup>. Later studies showed that actin polymerization and not cytoskeletal contraction was required for the looping process to occur<sup>8-10</sup>. Also in zebrafish *silent heart (sih)* mutants, that lack cardiac contraction due to a mutation in *cardiac troponin T2a*, cardiac looping was reported as normal<sup>11,12</sup>. However, biomechanical forces induced by blood flow have been reported to direct the looping process in zebrafish<sup>13</sup>. Therefore, even though most evidence points to the intrinsic capacity of the LHT to undergo the initial steps of looping, the influence of contractility and resulting blood flow is debatable. Another component believed to direct looping is the process of ventricular torsion<sup>9</sup>. Due to torsion in chick the curved ventricular tube transforms into a helically wound loop<sup>9</sup>. In zebrafish torsional rotation just prior to cardiac looping has also been described<sup>4,14</sup>.

To identify novel intrinsic and/ or extrinsic players required for cardiac looping several classical forward genetic screens in zebrafish have been conducted in the Bakkers laboratory. We phenotypically analyzed five cardiac looping mutants identified from such screens; *ca304*<sup>hu5753</sup>, *wickham(wkm)/tmem2*<sup>hu5935</sup>, *oudegracht(ogr)/tbx5a*<sup>hu6499</sup>, *ca004*<sup>hu6912</sup> and *ca172*<sup>hu7077</sup>. All mutants showed normal leftward jogging but were defective in subsequent cardiac looping. Characterization of mutant embryos resulted in the classification of the mutants into three different groups. In the first group, representing mutant *ca304*<sup>hu5753</sup> embryos lacked cardiac contraction and therefore were used to address the role of biomechanical forces for the looping process. In the second group, representing *wkm/tmem2*<sup>hu5935</sup> and *ogr/tbx5a*<sup>hu6499</sup> mutant embryos myocardial patterning is affected characterized by an extended AVC. In the third group, representing *ca004*<sup>hu6912</sup> and *ca172*<sup>hu7077</sup>, no additional defects were observed suggesting another yet unknown factor that contributes to cardiac looping.

# MATERIAL AND METHODS

## Fish lines

Fish were kept under standard conditions as previously described<sup>40</sup>. ENU mutagenesis was performed as previously described<sup>15</sup>. F1 progeny from mutagenised Tuebingen Longfin males were crossed to an AB strain to produce F2 families. Subsequent inbreeding of F2 progeny generated F3 embryos that were screened for cardiac morphogenesis defects. Mutant alleles used for this study; *ca304*<sup>hu5753</sup>, *wkm/tmem2*<sup>hu5935</sup>, *ogr/tbx5a*<sup>hu6499</sup>, *ca004*<sup>hu6912</sup> and *ca172*<sup>hu7077</sup>.

## In situ hybridization

Whole mount *in situ* hybridizations on zebrafish embryos and were performed as described previously<sup>16,17</sup>. Embryos were cleared in methanol (MeOH) and mounted in benzylbenzoate/benzylalcohol (2:1) before pictures were taken. Riboprobes were generated by transcription in the presence of digoxigenin-11-UTP from linearized templates of *cmlc2*, *amhc*<sup>18</sup>, *nppa*<sup>19</sup>, *bmp4*<sup>3</sup>, *tbx2b*, *has2*<sup>20</sup>, and *spp1*<sup>19</sup>.

## Positional cloning

Mapping and cloning analysis of the *wkm/tmem2*<sup>hu5935</sup> allele has been described previously<sup>21</sup>. The *ogr/tbx5a*<sup>hu6499</sup> locus was mapped close to the telomere of linkage group 5. Isolated DNA of homozygous *ogr* embryos was tested against individual microsatellite markers and analysis of 1552 meioses narrowed the critical interval to 0,26 centiMorgan (cM) Subsequent cDNA sequencing revealed a G to A substitution at base pair 441, resulting in a nonsense mutation and conversion of a Tryptophan to a premature STOP codon (W147STOP) (Tessadori et al., manuscript in preparation).

# RESULTS & DISCUSSION

## Zebrafish cardiac looping stages

Since the morphological changes during zebrafish cardiac looping stages have not been described in detail thus far, we examined the transformation of the LHT into a looped heart in wild-type embryos. We fixed embryos at 30 hpf, 36 hpf, 48 hpf and 53 hpf and performed *in situ* hybridisations probing for *cardiac myosin like chain 2* (*cmlc2*) and *atrial myosin heavy chain* (*amhc*) to clearly outline the entire myocardium. At 30 hpf we observed the LHT extended in a leftward direction (Fig. 1A). At 36 hpf the LHT was positioned more anteriorly and closer to the midline of the embryo (Fig. 1B). In addition ventricular cells, located on the right, had bulged outwards, which can be appreciated as the initial bending of the LHT (Fig. 1B, white arrowhead). A similar primitive ventricular bending has been well described to be the initial sign of looping in chick hearts<sup>22</sup>. At 48 hpf the heart was no longer linear, atrium and ventricle were separated by a constriction representing the presumptive AVC and an S-shape was distinguished (Fig. 1C). A few hours later, at 53 hpf, looping was completed

and the atrium (left) was positioned next to the ventricle (right) (Fig. 1D). Notably, the atrio-ventricular constriction was oriented in a 90° angle referenced to a horizontal line at the venous pole (Fig. 1B-D, black and white bars). During the looping process, both chambers start to balloon outward, a process that continues after the looping process has been completed<sup>23</sup>. Since *natriuretic peptide precursor a (nppa/anf)* is expressed in the elongated outer curvature cells during chamber ballooning we investigated its expression during the different looping stages. Interestingly, *nppa* is detected mostly in the ventricle at 30 hpf (Fig. 1E), prior to the initial ventricular bending of the tube, similar to what has been reported by Auman and colleagues<sup>23</sup>. Afterwards, *nppa* expression increases in the ventricle and at 48 hpf and 53 hpf can be detected in the outer curvature of the atrium (Fig. 1F-H). At this stage myocardial cell of the AVC are *nppa* negative (Fig. 1G and H, black arrowheads). Together these results demonstrate that cardiac looping in the zebrafish embryos starts around 36 hpf with the rightward bending of the ventricle, which is preceded by the expression of *nppa* at 30 hpf (Fig. 1B and F, white arrowheads).

### Forward genetic screen identifying cardiac looping mutants

To identify mutants defective in cardiac morphogenesis several forward genetic screens were performed in our laboratory. F3 generation embryos were screened live at 1 dpf and 2 dpf for the direction of cardiac displacement and cardiac looping abnormalities (Fig. 2A and B). In addition, putative mutant and sibling embryos were fixed at 2 dpf for subsequent *forkhead box a3 (foxa3)* *in situ* hybridization. *foxa3* Staining was used as a marker for the developing gut tube, liver and pancreas. The direction of gut looping and positioning of the liver and pancreas relative to the gut tube is applied to distinguish heart specific laterality mutants from mutants having general L-R asymmetry defects. Finally, all mutants were classified into three classes. Class I mutants having general randomization defects, not only in the direction of cardiac displacement and looping but also randomisation in the direction of gut looping. Class II mutants were proven to be more heart specific mutants, showing defects in the direction of cardiac displacement and looping while gut asymmetry was not affected. Finally, Class III mutants exclusively displayed defective heart looping while normal leftward displacement was observed and also gut looping was unaffected.

We selected five Class III looping mutants for phenotypic analysis; *ca304*<sup>hu5753</sup>, *wkm/tmem2*<sup>hu5935 21</sup>, *ogr/tbx5a*<sup>hu6499</sup>, *ca004*<sup>hu6912</sup> and *ca172*<sup>hu7077</sup> (Table 1). We observed that *ca304*<sup>hu5753</sup> mutants were deficient of cardiac contractility. Genetic mapping of *ca304*<sup>hu5753</sup> revealed linkage in proximity to the *cardiac troponin Ta (tnnt2a)* gene (Table 1), previously shown to be causative for the *silent heart (sih)* mutation<sup>11</sup>. This suggests that *ca304*<sup>hu5753</sup> is a novel *sih* allele. Causative mutations for the *wkm* and *ogr* phenotypes have been identified in the *tmem2* and *tbx5a* genes respectively (Table 1 and Material and Methods). Concomitantly to cardiac looping defects, additional phenotypes have also been observed for both *wkm* and *ogr* (Table 1). Likewise, in *ca004*<sup>hu6912</sup> mutants we observed a randomized gut looping accompanied by uncompleted heart looping (Table 1). Since, this combination of phenotypes was not observed previously and cardiac jogging was not affected we decided to categorize *ca004*<sup>hu6912</sup> in Class III. No other additional phenotypes have been observed thus far up to 2 dpf by live inspection for the *ca004*<sup>hu6912</sup> mutants. Also, *ca172*<sup>hu7077</sup> mutant embryos have a wild-type appearance apart from uncompleted heart looping (Table 1).

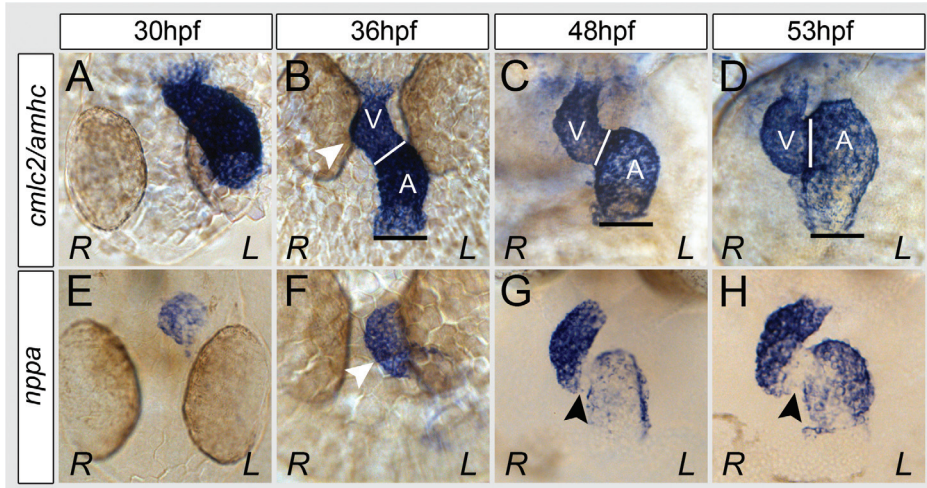


**Figure 1: Zebrafish looping morphogenesis**

(A-D) *In situ* hybridization for *cmlc2* and *amhc* expression at 30 hpf (A, n=27), 36 hpf (B, n=22), 48 hpf (C, n=10) and 53 hpf (D, n=25). White arrowhead in B indicates the outward bending of ventricular cells. Black bars in B-D show the 0° reference point at the atrial venous pole that was used to determine the relative orientation of the AVC (white bars in B-D). V=ventricle, A=atrium. (E-F) *In situ* hybridization for *nppa* expression at 30 hpf (A, n=20), 36 hpf (B, n=13), 48 hpf (C, n=11) and 53 hpf (D, n=6). White arrowhead in B denotes the outward bending of ventricular cells, accompanied by high levels of *nppa* expression (white arrowhead in F). Black arrowheads in G and H indicate *nppa* negative myocardial cells at the AVC. R=right. L=left.

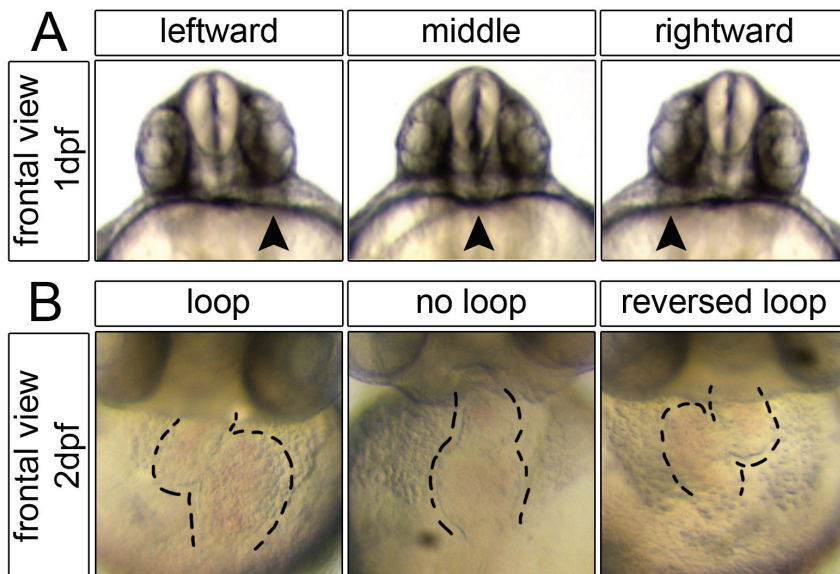


**Figure 2: Phenotypes analysed during forward genetic heart laterality screen**

(A) Frontal views at 1 dpf. The positioning of the LHT relative to midline was scored upon live inspection. Black arrowheads in A show positioning of the heart tube under the left eye (wild-type situation, left image), a heart that fails to undergo displacement and remains at the midline (middle image) and a LHT displaced under the right eye (right image). (B) Frontal views of at 2 dpf with the heart outlined by dotted lines. Left: Wild-type S-shaped heart. Middle: A non-looped or incomplete looped heart. Right: looped heart in the reversed orientation.

	heart looping	gut looping	LG	mutated gene	additional phenotypes
<i>ca304</i> <sup>hu5753</sup>	incomplete (phenotype not fully penetrant)	unaffected	23	unknown	loss of contraction
<i>wkm</i> <sup>hu5935</sup>	incomplete	unaffected	5	<i>tmem2</i>	blood accumulation above ventral tail fin
<i>ogr</i> <sup>hu6499</sup>	incomplete	unaffected	5	<i>tbx5a</i>	reduced contractility loss of pectoral fins
<i>ca004</i> <sup>hu6912</sup>	incomplete	randomized	-	unknown	none
<i>ca172</i> <sup>hu7077</sup>	incomplete	unaffected	-	unknown	none

Table 1: Overview of the looping mutants described in this study

## Myocardial morphology of looping mutants

To confirm looping discrepancies identified in all five mutant while screening, we fixed mutant and sibling embryos for *in situ* hybridisation analysis for *cmlc2*. For *ca304*<sup>hu5753</sup>, *wkm* and *ogr*, the *cmlc2* marker was complemented with *amhc* to enhance expression in the atrium.

Firstly, we observed that the loss of contraction in *ca304*<sup>hu5753</sup> was accompanied by incomplete cardiac looping in 14 out of 23 mutant embryos. In the remaining mutant embryos (n=9/23) looping appeared to be completed and an S-shaped heart could be observed, suggesting the identified reduced looping is not fully penetrant in this mutants (Fig. 3A and B).

In *wkm*, *ogr*, *ca004*<sup>hu6912</sup> and *ca172*<sup>hu7077</sup> wild-type like S-shaped hearts were not observed, all mutant embryos represented incomplete cardiac looping (Fig. 3C-J). To investigate whether chamber morphology during looping was affected we used *nppa* as a marker for the elongated outer curvature cells of the myocardium. In *ca304*<sup>hu5753</sup> mutant embryos *nppa* expression was reduced in the ventricle while upregulated in the atrium (n=5/5) (Fig. 3K and L). In addition, *nppa* was ectopically expressed in the AVC region of *ca304*<sup>hu5753</sup> mutant embryos (Fig. 3K and L). Both for *wkm* and *ogr* we observed an expansion of the AVC *nppa* negative cell population (Fig. 3M-P, black bars). In addition, overall intensity of *nppa* expression in *ogr* *-/-* was reduced (Fig. 3P). Noteworthy, *Tbx5* has previously been shown to be required for *Nppa*/*Anf* transcription, in synergy with *Nkx2.5* or *Gata4*<sup>24-26</sup>. We observed a mild expansion of the *nppa* negative AVC area in *ca004*<sup>hu6912</sup> mutants (Fig. 3Q and R) while in *ca172*<sup>hu7077</sup> mutants less *nppa* negative AVC cells were observed (Fig. 3S and T).

## Loss of cardiac contraction is accompanied by incomplete cardiac looping

Since we noticed variation in looping morphology amongst *ca304*<sup>hu5753</sup> mutants we continued to measure the degree of looping in this contractility deficient mutant. We observed that the loss of contractility does not affect leftward displacement of the LHT and subsequent outward bending of the ventricular cells at 36 hpf (Fig. 4A and B). To define the degree of looping in *ca304*<sup>hu5753</sup> mutants at 53 hpf we measured the angle of AVC orientation. Since all pictures were taken as a full frontal view, the horizontal axis of all images was taken as the

0° reference point (Fig. 4C-K). We measured the degree of looping in *ca304*<sup>hu5753</sup> mutants that did not develop a S-shaped heart (n=3). We found an average AVC orientation of 44.8° in these embryos, which was significantly different from the average AVC degree of 84.5° in sibling (n=3) embryos ( $p < 0.01$ ). Similarly, AVC angle measurement were conducted in *ca304*<sup>hu5753</sup> mutants that appeared to have completed looping (n=3). Indeed, the average AVC orientation of 83.2° in these mutants was not significantly different compared to sibling embryos ( $p = 0.86$ ). To conclude, these data showed that when contraction is lost, the majority of *ca304*<sup>hu5753</sup> mutant hearts fail to loop completely (n=14/23). Nevertheless, completed looping is possible (n=9/23) which suggest that contractility and thus flow are not required for cardiac looping.

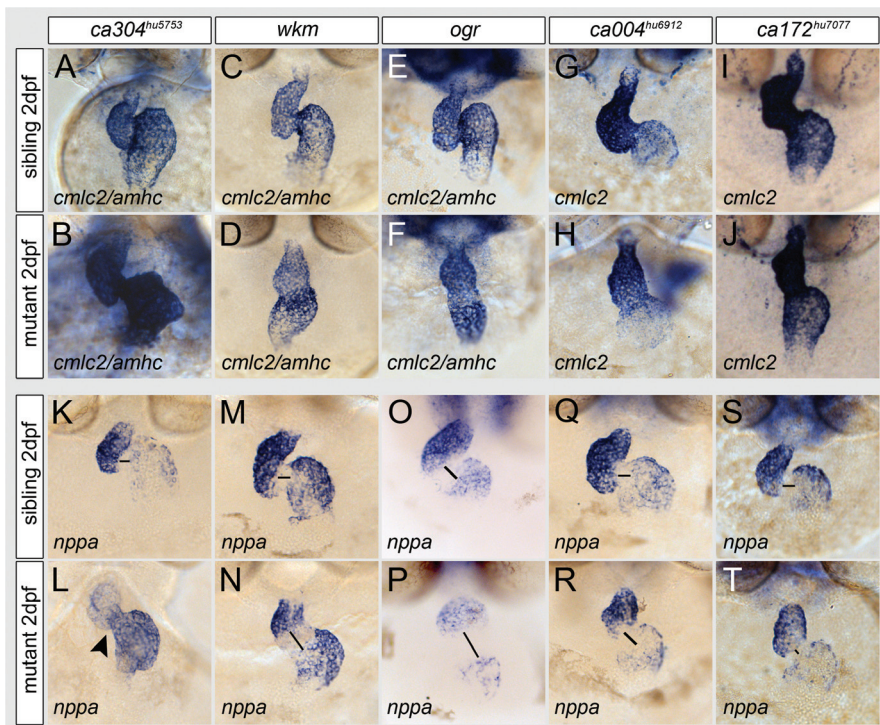


**Figure 3: Myocardial morphology of looping mutants**

(A-J) Sibling (A, C, E, G and I) and mutant (B, D, F, H and J) embryos stained for the cardiomyocyte marker *cmlc2* (complemented with *amhc* in A-F) at 2 dpf. In *ca304*<sup>hu5753</sup> mutants both S-shaped hearts (n=9, shown in B) as well as incomplete looped hearts (n=14, Fig. 4I-K) were observed. In *wkm* <sup>-/-</sup> (D, n=17), *ogr* <sup>-/-</sup> (F, n=10), *ca004*<sup>hu6912</sup> <sup>-/-</sup> (G, n=7) and *ca172*<sup>hu7077</sup> <sup>-/-</sup> (H, n=9), looping was incomplete.

(K-T) *nppa* expression analysis in sibling (K, M, O, Q and S) and mutant (L, N, P, R and T) embryos at 2 dpf. In sibling hearts *nppa* expression marks elongated myocardial cells mostly at the ventricular and atrial outer curvatures. *nppa* expression is repressed at the AVC, leaving a gap of *nppa* negative cells, indicated by black bars. (L) *ca304*<sup>hu5753</sup> mutants (n=5) showed reduced *nppa* expression in the ventricle and enhanced *nppa* expression in the atrium. Also *nppa* was ectopically expressed in the AVC of *ca304*<sup>hu5753</sup> mutants (L, black arrowhead). (N and P) In *wkm* (n=20) and *ogr* (n=10) mutants embryos an increased *nppa* negative gap was observed at the AVC. (P) Overall intensity of *nppa* is strongly reduced in *ogr* mutants. Both for *ca004*<sup>hu6912</sup> (R, n=8) and *ca172*<sup>hu7077</sup> (T, n=6) mutants, expression of *nppa* in the outer curvatures was similar to sibling embryos (Q, n=20 and S, n=18). (R) In *ca004*<sup>hu6912</sup> mutants the *nppa* negative gap at the AVC was slightly enlarged. (T) In *ca172*<sup>hu7077</sup> mutants the *nppa* negative gap at the AVC was slightly reduced.



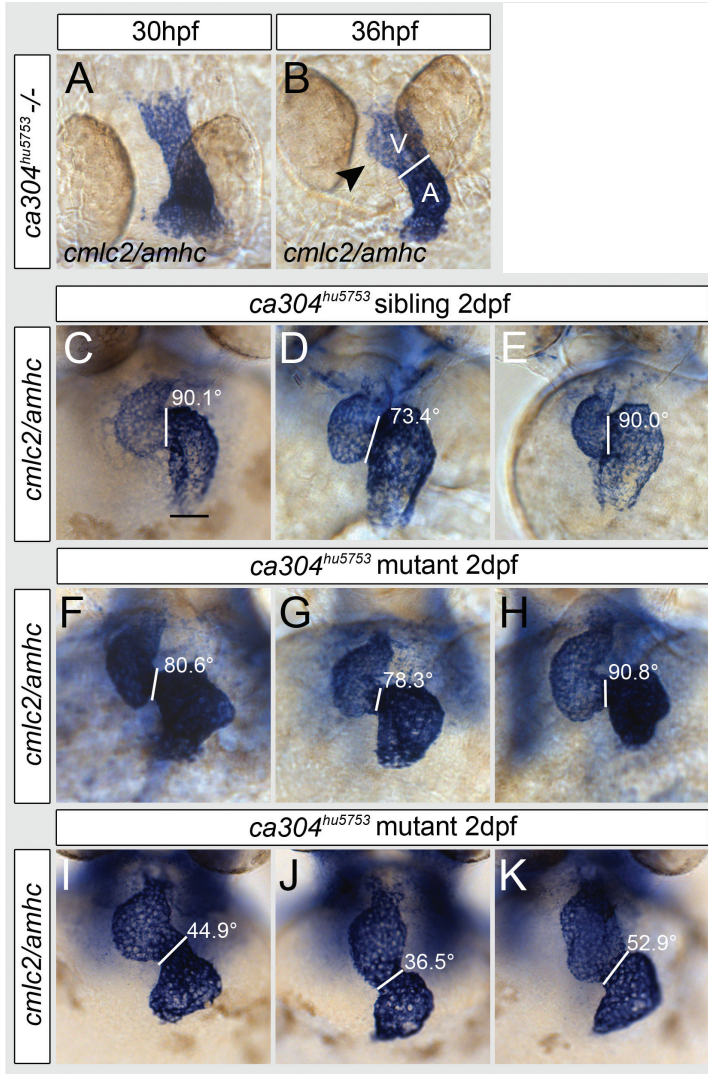


**Figure 4: Cardiac contractility is not required for cardiac looping**

(A-B) *cmlc2* and *amhc* expression analysis in *ca304<sup>hu5753</sup>* contractility deficient mutants at 30 hpf (A, n=13) and 36 hpf (B, n=6). Black arrowhead in B indicates the outward bending of ventricular cells, comparable to wild-type (Fig. 1B). Black bar in C shows the 0° reference at the atrium used for AVC orientation (white bars in B). V=ventricle, A=atrium. (C-E) *ca304<sup>hu5753</sup>* looped sibling hearts at 2 dpf stained for *cmlc2* and *amhc*, numbers represent the angle of the AVC relative to imaginary horizontal axis. (F-H) *ca304<sup>hu5753</sup>* mutant hearts at 2 dpf stained for *cmlc2* and *amhc*, with comparable AVC orientations to sibling hearts. (I-K) *ca304<sup>hu5753</sup>* mutant hearts at 2 dpf stained for *cmlc2* and *amhc*, with uncompleted looping as measured by the AVC orientation.

## Differential myocardial AVC patterning amongst looping mutants

Since we observed variable *nppa* expression patterns amongst all five looping mutants we were interested to examine expression of upstream regulators of *nppa* in the AVC, providing more information on overall AVC patterning.

A known repressor of *nppa* expression in the AVC is *tbx2b*, which is induced by *bmp4*<sup>27-30</sup>.

We conducted *in situ* hybridization analysis for these AVC markers at 2 dpf.

In *ca304*<sup>hu5753</sup> mutants we observed that *bmp4* and *tbx2b* were spatially restricted to the AVC, however expression of both genes appeared to be slightly reduced (Fig. 5A-B and 5K-L). Noteworthy, *bmp4* expression has been reported previously to be unaffected in contraction deficient *sih* mutants<sup>12</sup>. Nevertheless, *tbx2b* was found to be present at the AVC (Fig. 5L), suggesting that a loss of *tbx2b* is not responsible for the diffuse *nppa* expression in *ca304*<sup>hu5753</sup> mutants.

In *wkm* mutants, instead of AVC restricted *bmp4* expression, we detected *bmp4* ectopically in the chamber myocardium (Fig. 5B and C)<sup>21</sup>. Interestingly, the expanded *bmp4* expression domain is not completely reflected by enhanced *tbx2b* expression and a loss of *nppa* in these cells (Fig. 5N and 3N). Nevertheless, complete restriction of *tbx2b* to the AVC was also not evident in *wkm* mutant hearts, when compared to the *tbx2b* expression pattern in *wkm* sibling embryos (Fig 5M and N). In *ogr* mutants we observed a different pattern, clear decrease in chamber *nppa* expression, as shown previously (Fig. 3P) was accompanied by generally AVC restricted *bmp4* expression (Fig. 5F). Still, diffuse *bmp4* and *tbx2b* expression was observed in chamber myocardial cells of *ogr* <sup>-/-</sup> hearts (Fig 5E-F and 5O-P).

In *ca004*<sup>hu6912</sup> mutants, *bmp4* and *tbx2b* expression was restricted although slightly more diffuse in the AVC myocardium (Fig. 5G-H and 5Q-R). Finally, in *ca172*<sup>hu7077</sup> mutants we observed a striking decrease in *bmp4* expression (Fig. 5I and J). Expression analysis for *tbx2b* still remains to be performed for this mutant.

## Restricted endocardial cushion differentiation is not required for cardiac looping

Myocardial AVC expressed genes, including *bmp4*, initiate endocardial AVC differentiation of endocardial cushion (EC) cells<sup>31</sup>. Previously, it has been shown histologically that ECs fail to form when contraction is lost<sup>12</sup>. We could confirm these results by a loss of the EC marker *hyaluronic acid synthase 2* (*has2*) in endocardial AVC cells of *ca304*<sup>hu5753</sup> mutants (Fig. 6A and B). Since blood flow is absent when contraction is lost, this might also be causative for the loss of EC differentiation<sup>13</sup>.

In *wkm* <sup>-/-</sup> hearts *has2* expression analysis revealed a clear expansion of the EC population (Fig. 6C and D)<sup>21</sup>, which correlates with the previously observed expansion of *bmp4* in these embryos (Fig. 5C and D). Both for *ogr* and *ca004*<sup>hu6912</sup> mutants we observed a mild expansion of *has2* expression (Fig. 6E-H). Due to a shortage in embryos, further expression analysis of the *ca172*<sup>hu7077</sup> mutants remains to be performed.

To conclude based on the molecular analysis of the looping mutants selected for this study, we can divide these mutants into three different groups.

The first group is formed by *ca304*<sup>hu5753</sup>, which besides its variable looping defect lacks myocardial contraction and blood flow but displayed a rather normal myocardial patterning. The second group is formed by the *wkm* and *ogr* mutants that displayed strong looping

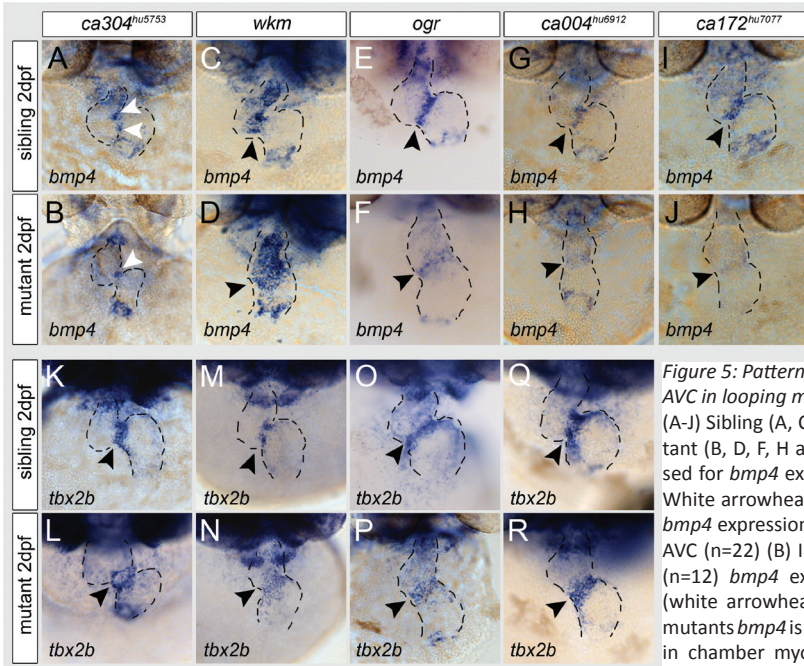


Figure 5: Patterning of the myocardial AVC in looping mutants

(A-J) Sibling (A, C, E, G and I) and mutant (B, D, F, H and J) embryos analysed for *bmp4* expression at 2 dpf. (A) White arrowheads indicate restricted *bmp4* expression in *ca304<sup>hu5753</sup>* sibling AVC (n=22) (B) In *ca304<sup>hu5753</sup>* mutants (n=12) *bmp4* expression is reduced (white arrowhead in B). (D) In *wkm* mutants *bmp4* is ectopically expressed in chamber myocardial cells (n=14).

(F) AVC restricted *bmp4* expression was observed in *ogr* mutants (n=7), yet diffuse expression in the chambers was also detected. (H) In *ca004<sup>hu6912</sup>* mutant hearts (n=5) *bmp4* was restricted to the AVC, however the overall intensity of *bmp4* expression was reduced. (J) Likewise, strongly reduced *bmp4* was detected in *ca172<sup>hu7077</sup>* mutants (n=5) compared to *ca172<sup>hu7077</sup>* sibling embryos (I, n=10). (K-T) *tbx2b* expression analysis in sibling (K, M, O, Q and S) and mutant (L, N, P, R and T) embryos at 2 dpf. (K) White arrowheads indicate AVC restricted *tbx2b* expression in *ca304<sup>hu5753</sup>* sibling (n=23), which was reduced in *ca304<sup>hu5753</sup>* mutants (n=21). (N) In *wkm* mutants *tbx2b* expression was not completely restricted to AVC myocardial cells (n=19). (P) *tbx2b* expression in *ogr* mutants (n=21) was restricted to the AVC although diffuse expression in the chambers was also visible. (R) AVC restricted *tbx2b* was observed in *ca004<sup>hu6912</sup>* mutants (n=10). The black dotted lines indicate the myocardial outline and the black arrowheads indicate the AVC.

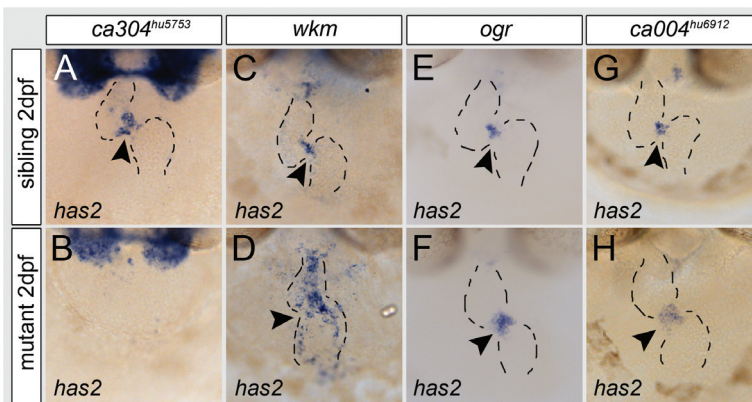


Figure 6: Endocardial cushion differentiation in looping mutants

(A) *has2* expression in *ca304<sup>hu5753</sup>* sibling endocardial cushions (n=13). (B) In *ca304<sup>hu5753</sup>* mutant embryos *has2* was not expressed in the heart (n=23). (C and D) *has2* was ectopically expressed by endocardial cells lining the chambers in *wkm* mutants (n=28) compared to restricted *has2*

expression in *wkm* siblings (n=39). In *ogr* (F, n=18) and *ca004<sup>hu6912</sup>* (H, n=20) mutants *has2* expression was detected at the AVC, possibly in a slightly broader domain compared to sibling embryos (E, n=20 and G, n=38). Black arrowheads indicate the AVC. The myocardial outline is given by the black dotted lines. All *in situ* hybridization experiments shown in this figure were conducted at 2 dpf.

defects in combination with reduced chamber but expanded AVC specification. The third group is formed by the *ca004*<sup>hu6912</sup> and *ca172*<sup>hu7077</sup> mutants that displayed very little patterning defects in combination with the observed compromised looping.

## DISCUSSION

For this study we have described zebrafish heart tube morphology at several time points during cardiac looping. In addition, we analyzed the effect of a loss in myocardial contractility and thus blood flow on the looping process. Our results are in agreement with two previous reports that contractility is not required for cardiac looping in zebrafish<sup>11,12</sup> but contradict the conclusion from another earlier report that blood flow is required for cardiac looping<sup>13</sup>. In *ca304*<sup>hu5753</sup> mutant embryos that lacked cardiac contractility, the initial ventricular bending of the heart tube occurred normally and we identified contractility mutants that loop indistinguishable from siblings. Similarly, arresting myocardial contraction of chick hearts also did not affect cardiac looping<sup>32</sup>. However, we also observed contractility deficient embryos that developed a significant uncompleted loop. We suggest that these looping defects are secondary. We have noticed a variable degree of cardiac oedema in a clutch of *ca304*<sup>hu5753</sup> mutants at 2 dpf. Possibly, oedema surrounding the heart disrupts extrinsic torsional movements resulting in uncompleted looping. Similarly, artificially blocking zebrafish blood flow by inserting beads might very well interfere with extrinsic forces required for the looping process<sup>13</sup>. A more recent study showed that by altering the stress inflicted by reversing blood flow, EC development is diminished<sup>33</sup>. Even though cardiac looping has not specifically been investigated in this study, results implicate that altering the flow did not induce cardiac looping defects. Together these data imply that cardiac looping is not dependent on contraction and subsequent blood flow.

We investigated four Class III looping mutants, identified specifically by a loss of directional looping. We have described a novel *tbx5a* mutant allele, *ogr*. Interestingly, the *hst/tbx5a* mutant phenotype<sup>34,35</sup> appears to have a stronger effect on heart morphology compared to the novel *ogr/tbx5a* allele. The *ogr/tbx5a* mutation induces a stop in the middle of the DNA binding T-box domain, while in *hst/tbx5a* the T-box is still present. Therefore, *hst/tbx5a* might act as a dominant negative protein while *ogr/tbx5a* would represent the actual *tbx5a* null phenotype (Tessadori et al., manuscript in preparation). Like previously described for *hst*, *ogr* mutant hearts develop AVC patterning defects. Similarly, *wkm/tmem2* mutants exhibit an expansion of EC like cells, again accompanied by looping defects. We can conclude therefore that looping deficiencies in these mutants are accompanied by an expansion of the AVC. Interestingly, injection of both *bmp4* and *has2* MOs in *wkm* mutants rescued ectopic differentiation of EC cells but did not rescue looping morphogenesis<sup>21</sup> (data not shown). These data suggest that ectopic differentiation of EC cells is not causative for looping defects observed in *wkm/tmem2*. In *wkm* mutants, *tbx5a* expression was shown to be normal and vice versa, in *hst* mutants *tmem2* expression was detected in a comparable pattern to wild-type<sup>21</sup>. Also, embryos deficient for both *wkm/tmem2* and *ogr/tbx5a* exhibit stronger defects in cardiac morphology. These data suggest that *tmem2* and *tbx5a* exert

a different function during the looping process (F. Tessadori, personal communication). *tbx5a* is expressed in all myocardial cells at 2 dpf (F. Tessadori, manuscript in preparation) and absent from endocardial cells. *tmem2* however was shown to be expressed in both myocardial and endocardial cells<sup>21</sup>. This might explain why a loss of *Tmem2* function exerts a strong effect in both myocardial and endocardial AVC patterning. Our observation that injection of *bmp4* MOs in *wkm* mutants did rescue ectopic EC differentiation suggests that the defects observed in the endocardium of *wkm* mutants are a consequence of the high levels of *bmp4* acting from the myocardium. However these changes in endocardial differentiation are not responsible for the cardiac looping defect. An interesting observation is that the high levels of *bmp4* in *wkm* mutant hearts was not accompanied by high levels of *tbx2b* and a strong reduction of *nppa* expression. We did observe a strong decrease in *nppa* expression in embryos deficient for both *wkm* and *ogr* at 2 dpf compared to the reduction in *nppa* expression observed in *ogr* mutants (F. Tessadori, personal communication). These data suggest that *Tmem2* and *Tbx5a* function in parallel during AVC patterning.

Based on this study we believe we need to investigate further cell shape changes and cell movements that take place from the early onset of ventricular bending at 36 hpf up to the fully looped heart at 2 dpf. It has been demonstrated that the myocardial tissue rotates during LHT stages<sup>4,14</sup>. Next it will be necessary to investigate whether there is rotational movement/ torsion during the entire looping process. We know from previous studies in chick that actin polymerization also plays an important role during the looping. Possibly, biochemical forces induced by torsional movement direct the cellular actin polarization.

Secondly, since torsion of the heart tube would inflict patterned stress in different areas loss of the heart tube it would be interesting to visualize these forces *in vivo*. Force biosensors, using a FRET based mechanism, have been proven to reproduce *in vitro* the different intensities of stress inflicted at cell-cell junctions<sup>36</sup>. Expression of such force biosensors in myocardial cells could map the biochemical forces in the looping heart tube. In addition, one could generate a transgenic line expressing *lifeact* in the myocardium to visualize the response of the actin cytoskeleton to biochemical forces<sup>37</sup>. However, a limiting factor for this type of imaging would be again the heartbeat. Especially using a FRET based stress sensor would be highly susceptible to mechanical movements inflicted by cardiac contraction. As mentioned previously, one could image contraction deficient mutants. However, we reported in this study that secondary looping defects might occur in these mutants. Another approach could be to employ selective plane illumination microscopy (SPIM)<sup>38,39</sup> to image forces in specific areas of the looping heart, like the AVC versus cells of the outer curvatures or inner curvatures. Since SPIM allows high-speed fluorescence imaging and optical sectioning with deep penetration at cellular resolution this might allow imaging while the heart still contracts.

To conclude, phenotypic characterization of newly identified looping mutants and the mechanistic insights of genes mutated in these mutants will reveal more about the intrinsic and extrinsic signals required for cardiac looping. However, we believe that careful characterization of cellular movements and dynamics in a wild-type looping heart tube will also reveal more information about the looping process.

## REFERENCES

1. M. J. Sutherland, S. M. Ware, Disorders of left-right asymmetry: heterotaxy and situs inversus. *Am J Med Genet C Semin Med Genet* **151C**, 307 (Nov 15, 2009).
2. J. Bakkers, M. C. Verhoeven, S. Abdelilah-Seyfried, Shaping the zebrafish heart: from left-right axis specification to epithelial tissue morphogenesis. *Dev Biol* **330**, 213 (Jun 15, 2009).
3. J. N. Chen et al., Left-right pattern of cardiac BMP4 may drive asymmetry of the heart in zebrafish. *Development* **124**, 4373 (Nov, 1997).
4. K. Baker, N. G. Holtzman, R. D. Burdine, Direct and indirect roles for Nodal signaling in two axis conversions during asymmetric morphogenesis of the zebrafish heart. *Proc Natl Acad Sci U S A* **105**, 13924 (Sep 16, 2008).
5. H. Stalsberg, Development and ultrastructure of the embryonic heart. II. Mechanism of dextral looping of the embryonic heart. *Am J Cardiol* **25**, 265 (Mar, 1970).
6. N. Itasaki, H. Nakamura, M. Yasuda, Changes in the arrangement of actin bundles during heart looping in the chick embryo. *Anat Embryol (Berl)* **180**, 413 (1989).
7. N. Itasaki, H. Nakamura, H. Sumida, M. Yasuda, Actin bundles on the right side in the caudal part of the heart tube play a role in dextro-looping in the embryonic chick heart. *Anat Embryol (Berl)* **183**, 29 (1991).
8. K. S. Latacha et al., Role of actin polymerization in bending of the early heart tube. *Dev Dyn* **233**, 1272 (Aug, 2005).
9. L. A. Taber, Biophysical mechanisms of cardiac looping. *Int J Dev Biol* **50**, 323 (2006).
10. G. Fenteany, S. Zhu, Small-molecule inhibitors of actin dynamics and cell motility. *Curr Top Med Chem* **3**, 593 (2003).
11. A. J. Sehnert et al., Cardiac troponin T is essential in sarcomere assembly and cardiac contractility. *Nat Genet* **31**, 106 (May, 2002).
12. T. Bartman et al., Early myocardial function affects endocardial cushion development in zebrafish. *PLoS Biol* **2**, E129 (May, 2004).
13. J. R. Hove et al., Intracardiac fluid forces are an essential epigenetic factor for embryonic cardiogenesis. *Nature* **421**, 172 (Jan 9, 2003).
14. K. A. Smith et al., Rotation and asymmetric development of the zebrafish heart requires directed migration of cardiac progenitor cells. *Dev Cell* **14**, 287 (Feb, 2008).
15. E. Wienholds, S. Schulte-Merker, B. Walderich, R. H. Plasterk, Target-selected inactivation of the zebrafish *rag1* gene. *Science* **297**, 99 (Jul 5, 2002).
16. C. Thisse, B. Thisse, T. F. Schilling, J. H. Postlethwait, Structure of the zebrafish *snail1* gene and its expression in wild-type, spadetail and no tail mutant embryos. *Development* **119**, 1203 (Dec, 1993).
17. C. Thisse, B. Thisse, High-resolution in situ hybridization to whole-mount zebrafish embryos. *Nat Protoc* **3**, 59 (2008).
18. D. Yelon, S. A. Horne, D. Y. Stainier, Restricted expression of cardiac myosin genes reveals regulated aspects of heart tube assembly in zebrafish. *Dev Biol* **214**, 23 (Oct 1, 1999).
19. A. K. Lagendijk, M. J. Goumans, S. B. Burkhard, J. Bakkers, MicroRNA-23 Restricts Cardiac Valve Formation by Inhibiting Has2 and Extracellular Hyaluronic Acid Production. *Circ Res*, **109**, 649-657.
20. J. Bakkers et al., Has2 is required upstream of Rac1 to govern dorsal migration of lateral cells during zebrafish gastrulation. *Development* **131**, 525 (Feb, 2004).
21. K. A. Smith et al., Transmembrane protein 2 (Tmem2) is required to regionally restrict atrioventricular canal boundary and endocardial cushion development. *Development* **138**, 4193 (Oct, 2011).
22. J. Manner, Cardiac looping in the chick embryo: a morphological review with special reference to terminological and biomechanical aspects of the looping process. *Anat Rec* **259**, 248 (Jul 1, 2000).
23. H. J. Auman et al., Functional modulation of cardiac form through regionally confined cell shape changes. *PLoS Biol* **5**, e53 (Mar, 2007).
24. Y. Hiroi et al., Tbx5 associates with Nkx2-5 and synergistically promotes cardiomyocyte differentiation. *Nat Genet* **28**, 276 (Jul, 2001).
25. B. G. Bruneau et al., A murine model of Holt-Oram syndrome defines roles of the T-box transcription factor Tbx5 in cardiogenesis and disease. *Cell* **106**, 709 (Sep 21, 2001).
26. V. Garg et al., GATA4 mutations cause human congenital heart defects and reveal an interaction with TBX5. *Nature* **424**, 443 (Jul 24, 2003).
27. M. C. Verhoeven, C. Haase, V. M. Christoffels, G. Weidinger, J. Bakkers, Wnt signaling regulates atrioventricular canal formation upstream of BMP and Tbx2. *Birth Defects Res A Clin Mol Teratol* **91**, 435 (Jun, 2011).
28. V. M. Christoffels et al., T-box transcription factor Tbx2 represses differentiation and formation of the cardiac chambers. *Dev Dyn* **229**, 763 (Apr, 2004).
29. M. Yamada, J. P. Revelli, G. Eichele, M. Barron, R. J. Schwartz, Expression of chick Tbx-2, Tbx-3, and Tbx-5 genes during early heart development: evidence for BMP2 induction of Tbx2. *Dev Biol*

- 228**, 95 (Dec 1, 2000).
30. Z. Harrelson et al., Tbx2 is essential for patterning the atrioventricular canal and for morphogenesis of the outflow tract during heart development. *Development* **131**, 5041 (Oct, 2004).
  31. E. J. Armstrong, J. Bischoff, Heart valve development: endothelial cell signaling and differentiation. *Circ Res* **95**, 459 (Sep 3, 2004).
  32. F. J. Manasek, R. G. Monroe, Early cardiac morphogenesis is independent of function. *Dev Biol* **27**, 584 (Apr, 1972).
  33. J. Vermot et al., Reversing blood flows act through klf2a to ensure normal valvulogenesis in the developing heart. *PLoS Biol* **7**, e1000246 (Nov, 2009).
  34. D. M. Garrity, S. Childs, M. C. Fishman, The heartstrings mutation in zebrafish causes heart/fin Tbx5 deficiency syndrome. *Development* **129**, 4635 (Oct, 2002).
  35. T. Camarata et al., Pdlim7 (LMP4) regulation of Tbx5 specifies zebrafish heart atrio-ventricular boundary and valve formation. *Dev Biol* **337**, 233 (Jan 15, 2010).
  36. C. Grashoff et al., Measuring mechanical tension across vinculin reveals regulation of focal adhesion dynamics. *Nature* **466**, 263 (Jul 8, 2010).
  37. J. Riedl et al., Lifeact: a versatile marker to visualize F-actin. *Nat Methods* **5**, 605 (Jul, 2008).
  38. J. Huisken, J. Swoger, F. Del Bene, J. Wittbrodt, E. H. Stelzer, Optical sectioning deep inside live embryos by selective plane illumination microscopy. *Science* **305**, 1007 (Aug 13, 2004).
  39. P. J. Scherz, J. Huisken, P. Sahai-Hernandez, D. Y. Stainier, High-speed imaging of developing heart valves reveals interplay of morphogenesis and function. *Development* **135**, 1179 (Mar, 2008).
  40. M. Westerfield, *The Zebrafish Book - A guide for laboratory use of zebrafish (Brachydanio rerio)*. (University of Oregon Press, Oregon, 1995).





# **AN ANTISENSE MIR-128 MORPHOLINO ENHANCES BMP SIGNALING INDEPENDENT FROM MIR-128: A STORY ENDS WITH A LESSON IN MORPHOLINO CONTROLS**

A.K. Lagendijk<sup>1</sup> and J. Bakkers<sup>1,2</sup>.

1. Hubrecht Institute, KNAW & Iniversity Medical Center, Utrecht, The Netherlands.
2. Interuniversity Cardiology, Institute of the Netherlands, Utrecht, The Netherlands

**6**

## ABSTRACT

Both in vertebrates and invertebrates Bone morphogenetic proteins (Bmps) form a crucial determinant for correct establishment of the body axis. Investigation of loss and gain of Bmp function in various zebrafish mutants has led to the description of an array of body patterning abnormalities. In a high-throughput microRNA (miRNA/miR) knockdown screen using Morpholino oligomers (MOs), we observed that loss of miR-128 function resulted in excessive tissue deposited at the ventral side of the tailfin, a phenotype reminiscent to zebrafish mutants with overactive Bmp signaling. In addition, we report that *bmp4* expression is strongly increased in the tail bud region of miR-128 MO injected embryos. Co-injection experiments using *noggin* RNA (a Bmp antagonist) restored fin morphology in miR-128 MO injected embryos. By analysing *alk1* (*violet beaugarde* (*vbg*)) and *alk8* (*lost-a-fin* (*laf*)) mutants and *bmp4* knock-down embryos we concluded that the miR-128 knock-down effect was dependent of Alk8 and Bmp4, but not Alk1. Using a targeting assay we subsequently identified a functional interaction between miR-128 and the *bmp4* 3'UTR. Finally, to control for miR-128 MO specificity we performed knockdown experiments in MZ*dicer* mutant embryos, lacking most miRNAs including miR-128. Surprisingly we still observed the tail tissue expansion upon miR-128 MO injection in *dicer* mutants, demonstrating an off target effect of the miR-128 MO sequence.

## INTRODUCTION

Bmps were initially described by Urist and colleagues as proteins that could promote *de novo* cartilage and bone formation at ectopic sites<sup>1</sup>. Much later the first Bmp molecules, each sufficient to induce bone differentiation *in vitro*, were cloned from bovine tissue and for all these molecules human orthologous were identified<sup>2</sup>. Based on sequence similarity Bmps have been classified as members of the Transforming growth factor- $\beta$  (TGF- $\beta$ ) superfamily. Apart from bone formation, Bmps are currently well known to function in a broad range of biological processes, also during embryonic development and disease of both vertebrates and invertebrates.

After translation Bmp pro-proteins dimerize when travelling through the endoplasmatic reticulum. Upon dimerization Bmps get activated when proteolytically cleaved by proteases like SPC1/Furin or SPC4/PACE4<sup>3,4</sup>. Activate Bmp dimers will subsequently bind to a heterotetrameric transmembrane receptor complex composed of two “type I” and two “type II” Bmp receptors of the Activin receptor-like kinase (Alk) family (Fig. 1) (reviewed in 5). Bmp ligand binding activates type-II receptors, which subsequently phosphorylate and activate type-I receptors present in the complex. Active type-I receptors phosphorylate receptor associated Smad proteins (R-Smads/ Smad1,5,8) that subsequently bind to a common partner Smad (co-Smad/ Smad4) resulting in a R-Smad-co-Smad complex. This Smad complex translocates to the nucleus where it functions as a transcriptional modulator of Bmp target genes. Nuclear activity of R-Smads can be repressed when R-Smads interact with inhibitory-Smads (I-Smads/ Smad6,7). During development a conserved phenomenon of graded Bmp expression is required for determination of the body axis (reviewed in 6 and 7). These gradients of Bmp activities are regulated extracellularly by diffusible Bmp antagonists like Chordin, Noggin and Follistatin (reviewed in 8). Bmp inhibitor proteins interact with Bmps to prevent binding of Bmp ligands to Alk receptors. Since full null phenotypes of Bmp signaling components often induce early lethality in higher vertebrates, the zebrafish system has provided a valuable tool to study Bmp function. Making use of zebrafish forward genetic screens a wide variety of mutants have been identified carrying mutations in Bmp signaling components<sup>9,10</sup>. Mutations inducing a loss of Bmp signaling result in a loss of ventral derived tissues, a phenotype referred to as dorsalisation. This can result in a complete loss of the tail or in more subtle defects, like a loss of ventral fin tissue, depending on the power of redundant Bmp signaling components<sup>9,10</sup>. Gain of Bmp function results in an expansion of ventral derived tissues, mostly visible by an excess of tissue at the ventral side of the tail fin<sup>11</sup>. The array of DV patterning defects observed upon a loss or gain of Bmp function have been carefully categorized by Kishimoto and colleagues, from severe dorsalisation (C5) to the most extreme ventralisation (V4)<sup>12</sup>. Due to the extensive variety of Bmp function in space and time, Bmp activity is regulated at various levels, from proteolytical cleavage of pro-Bmp proteins to interaction with Bmp antagonists or I-Smads. Since Bmp expression level changes can alter cellular identity, additional fine-tuning by miRNAs could potentially also be a mechanism to maintain Bmp gradients during development. During a previous miRNA loss of function screen using MOs<sup>13</sup> we observed loss of miR-128 function resulted in a phenotype similar to zebrafish mutants suffering from overactive Bmp signaling. In this study, we explored the possibility of miR-128 regulated Bmp signaling.

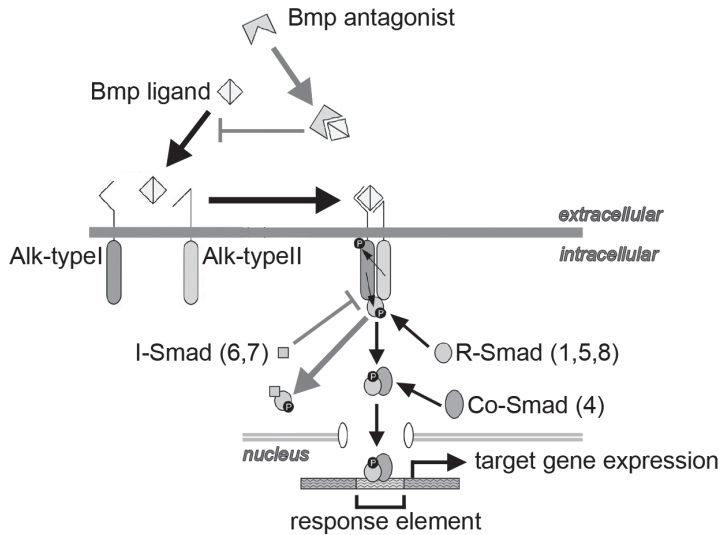


Figure 1: schematic representation of Bmp signaling cascade

Bmp dimers bind to Alk-typeI and typeII receptors. Extracellular Bmp antagonists can prevent binding of Bmp dimers to the Alk receptors. Upon ligand binding, typeII receptors transphosphorylate typeI receptors. Alk-typeI receptors subsequently phosphorylate members of the Smad family of transcription factors (R-Smads). Together with Co-Smad proteins, a R-Smad-Co-Smad complex is formed. This complex translocates to the nucleus, where they activate transcription of target genes. Inhibitory-Smads (I-Smads) regulate intracellular signaling by preventing further Smad signaling and consequent activation of gene transcription.

Adapted from Balemans and Van Hul<sup>8</sup>

## MATERIAL AND METHODS

### Fish lines

Fish were kept under standard conditions as previously described<sup>35</sup>. *Lost-a-fin/alk8* mutant allele used in this study is *laftm110b*<sup>10</sup>. *Violet beauregarde/alk1* mutant allele used is *vbgy6*<sup>14</sup>. Mutant allele for loss of dicer is *dicer*<sup>Hu869 15</sup>.

### In situ hybridization

Whole mount *in situ* hybridizations on zebrafish embryos and were performed as described previously<sup>16,17</sup>. Embryos were cleared in methanol (MeOH) and mounted in benzylbenzoat/benzylalcohol (2:1) before pictures were taken. Riboprobes were generated by transcription in the presence of digoxigenin-11-UTP from linearized templates of *bmp2b*, *bmp4*, *bmp7*, *gata1* and *pax2a*. LNA probe for miR-128 LNA probe was obtained from Exiqon and labeled using terminal transferase (Roche) and digoxigenin-11-UTP. MiR-128 *in situ* hybridizations were performed as described previously<sup>18</sup>.

### Morpholino and RNA injections

Morpholino oligonucleotides (MOs; Gene Tools) were dissolved in water to 5 mM (miRNA MOs) and 4 mM (*bmp4* splice MO<sup>19</sup>).

Sequences of used MOs were:

*bmp4* splice MO 5'-ggtgttgattgtctgaccttcacg-3'

miR-128 MO 5'-aaaagagaccgggtcactgtga-3'

miR-128-1 MO 5'-ttcactgtgagaagcctacat-3'

miR-128-2 MO 5'-ttcactgtgagacgagtggca-3'

For injection, MOs were diluted to concentrations between 0.2 mmol/l and 0.5 mmol/l, of which 1 nl was injected at the one cell stage.

Capped zebrafish *noggin* RNA<sup>20</sup> was prepared with the SP6 Message Machine kit (Ambion) and injected at 2 and 3 ng/μl.

## Luciferase silencing assay

We amplified a 887bp PCR fragment of the zebrafish *bmp4* 3'-UTR containing the predicted miR-128 target site. This PCR fragments was cloned into pCS2 (Clontech), containing the firefly luciferase cDNA sequence between restriction sites BamHI and ClaI (pCS2-eGFP). 3'UTR fragments were cloned downstream of eGFP between EcoRI and XbaI resulting in reporter construct. *Renilla* RNA, transcribed from pCS2-*renilla* plasmid, was co-injected as a control. RNA oligos for miR-128 overexpression injections were obtained from Biologio and dissolved to a concentration of 100 μM in distilled water. Oligos were annealed using a 5x buffer containing 30 mM HEPES-KOH (pH 7.4), 100 mM KCl, 2 mM MgCl<sub>2</sub>, and 50 mM NH<sub>4</sub>Ac. For injections, 1 nl of a 10 μM miR-128 duplex solution was injected.

Embryonic lysates (n=10 embryos/ lysate) were prepared at 6 hpf for subsequent luciferase assays, as described previously<sup>21</sup>.

## RESULTS

### Loss of miR-128 function is accompanied by defective ventral tail morphogenesis

We identified a single miRNA, miR-128, of which a loss of function resulted in a thickening of the ventral tail fin at 1 day post fertilization (dpf) (W.P Kloosterman and A.K. Lagendijk, personal communication) (Fig. 2H-I'), a phenotype previously related to overactive Bmp signaling<sup>11</sup>. The zebrafish genome encodes two miR-128 transcripts; miR-128-1 is located within an intron of the *r3hdm1* gene and miR-128-2 is also located intronically of an unknown transcript. The position of miR-128-1 within the *r3hdm1* intron is highly conserved amongst vertebrates. We could first detect expression of zebrafish mature miR-128 in total RNA lysates at 6 hours post fertilization (hpf) (Fig. 2A). Spatially, miR-128 expression was observed ubiquitously at 1 dpf (Fig. 2B). Subsequently, miR-128 expression is more restricted to specific areas in the developing brain from 2 dpf onwards (Fig. 2C). Injection of a MO complementary to the miR-128 mature sequence could block miR-128 expression in wild-type embryos, shown by a loss of miR-128 *in situ* expression (Fig. 2D and E). Interestingly, from 15 hpf miR-128 morphant embryos could be identified phenotypically by an enlarged tailbud (Fig. 2F and G). At 1 dpf this phenotype was even more prominent in morphant embryos, showing additional tissue present at the ventral side of the tail (Fig. 2H-I').

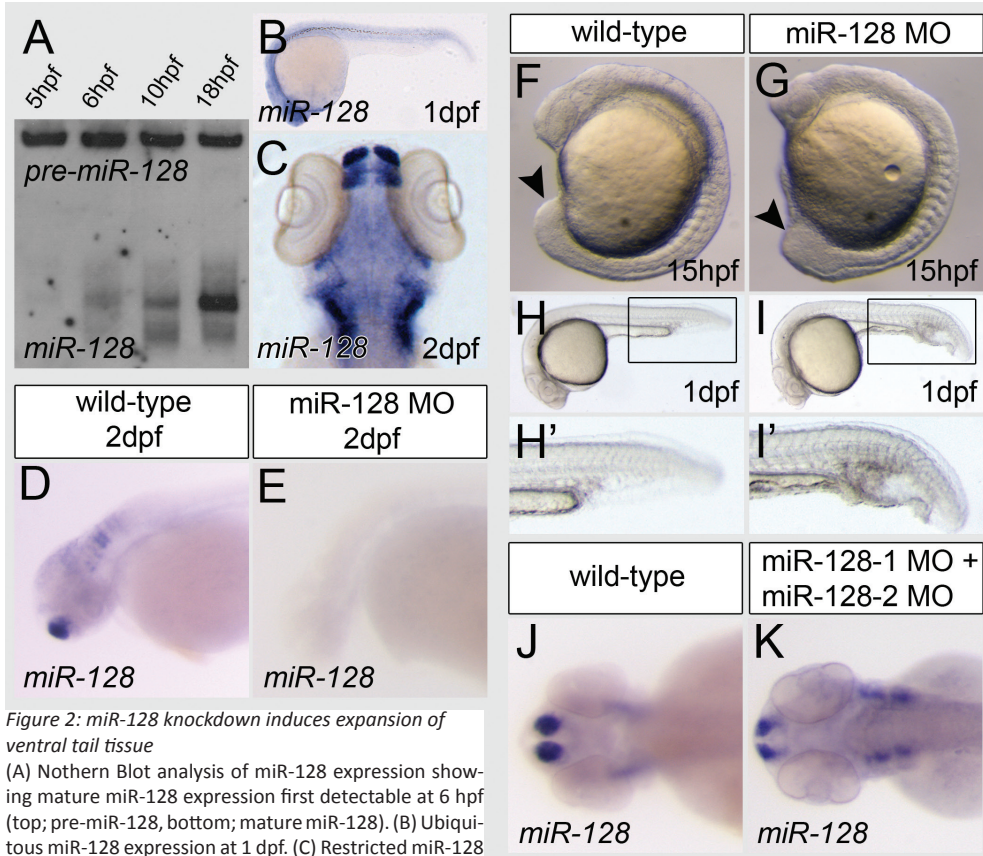


Figure 2: miR-128 knockdown induces expansion of ventral tail tissue

(A) Northern Blot analysis of miR-128 expression showing mature miR-128 expression first detectable at 6 hpf (top; pre-miR-128, bottom; mature miR-128). (B) Ubiquitous miR-128 expression at 1 dpf. (C) Restricted miR-128 expression in regions of the developing zebrafish brain at 2 dpf. (D-E) Upon injection of miR-128 MO, miR-128 expression at 2 dpf is lost (E) while expressed normally in non-injected control embryo (D). (F-G) Brightfield images showing increased tailbud structure in miR-128 MO injected embryo (G) compared to a non-injected embryo (F). Black arrowheads in F and G indicate the tailbud. (H-I) Brightfield image of a non-injected embryo (H) and a miR-128 MO injected embryo (I) at 1 dpf. MiR-128 morphants can be recognized by the appearance of additional tissue at the ventral side of the tailfin. (H'-I') Enlargement of the embryonic tail (boxed in H and I). (J-K) Co-injection of miR-128-1 and miR-128-2 MOs (K) does not generate efficient knock-down of miR-128 expression at 2 dpf (n=14/15).

	MO-miR-128 n=30	noggin RNA 2ng/ $\mu$ l n=37	MO-miR-128+ noggin RNA 2ng/ $\mu$ l n=37	noggin RNA 3ng/ $\mu$ l n=35	MO-miR-128+ noggin RNA 3ng/ $\mu$ l n=31
C5	0	1	0	0	0
C4	0	2	0	4	4
C3	0	3	3	4	1
C2	0	2	3	3	1
C1	0	15 (41%)	3	12 (34%)	9
WT	0	14	0	12 (34%)	3
V1	4	0	18 (47%)	0	10 (32%)
V2	27 (90%)	0	10	0	3

Table 1: *noggin* reduces the excess of tissue formed upon miR-128 MO injection

Left column: phenotypic classification from C5 (loss of ventral structures) to V2 (enhancement of ventral tail structures) as classified by Kishimoto et al<sup>12</sup>. Injection of miR-128 MO strongly enhances ventral tail tissue development in 90% of the injected embryos. Injection of *noggin* RNA at 2 ng/ $\mu$ l or 3 ng/ $\mu$ l

results in a mild loss of the ventral tail fin in 41% and 34% of injected embryos respectively. When miR-128 MO is injected in combination with either 2 ng/ $\mu$ l or 3 ng/ $\mu$ l of *noggin* RNA most of the embryos develop a mild increase of ventral tail tissue, 47% and 32% respectively.

Later, at 2 dpf, we occasionally observed morphant embryos that had developed two ventral tailfins (data not shown). Since two miR-128 copies can be found in the zebrafish genome, we subsequently conducted co-injection experiments of two MOs each designed to targeting one of the miR-128 copies. Simultaneous knockdown of miR-128-1 and miR-128-2 however did not induce an expansion of the tail tissue. Nevertheless, we could still detect miR-128 expression in these double MO-injected embryos, suggesting a failure to block mature miR-128 synthesis efficiently using these additional MOs (Fig. 2J and K). To conclude, mature miR-128 knock-down phenotypes suggest overactive Bmp signaling, like in zebrafish *chordino* mutants<sup>11</sup>.

### Loss of miR-128 function results in imbalanced Bmp signaling

To investigate whether the tail phenotypes observed in miR-128 morphants were a consequence of altered Bmp signaling, we performed co-injection experiments of *noggin*, a Bmp antagonist. Hypothetically, Bmp inhibition should rescue tail morphogenesis in miR-128 morphants when caused by overactive Bmp signaling. We scored all injected embryos using a previously published classification of DV patterning defects<sup>12</sup>, with V4 being severely ventralised and C5 severely dorsalised (Supplemental Fig. 1). Injection of *noggin* RNA induced a range of dorsalised phenotypes while injection of miR-128 MOs resulted mainly in V2 ventralised embryos. Co-injection of *noggin* RNA, both at 2 ng/ $\mu$ l and 3 ng/ $\mu$ l, together with miR-128 MOs resulted in V1 ventralisation and a variety of phenotypically dorsalised embryos (Table 1). These data indicate that upon miR-128 knockdown Bmp signaling activity is enhanced resulting in ectopic tissue located in the tail region.

### Gene expression analysis reveals expansion of *bmp4*, *gata1*, *pax2a* and *Tg(kdr-l:GFP)* expressing cells

To examine where mechanistically miR-128 would function within the Bmp pathway we analysed gene expression levels of Bmp ligands as well as downstream Bmp target genes by *in situ* hybridization. First we compared spatial expression of three Bmp ligands; *bmp2*, *bmp4* and *bmp7* at 12 hpf. While *bmp2* and *bmp7* expression was comparable between miR-128 morphants and non-injected controls (Fig. 3A-B and data not shown), *bmp4* was evidently expanded in morphants into a large area surrounding the tailbud (Fig. 3C-F). Excess Bmp signaling has been shown to result in an expansion of mesodermal cell lineages, like hematopoietic and vascular cells (lateral mesoderm) and pronephric cells (intermediate mesoderm)<sup>11</sup>. Therefore we examined the volume of vascular endothelial cells at 28 hpf by injecting miR-128 MOs into *Tg(kdr-l:GFP)* embryos, a transgene expressed in all endothelial cells. We observed a clear expansion of the *Tg(kdr-l:GFP)* positive endothelial population at the ventral side of the tail at 28 hpf (Fig. 3G and H). Similar to what has been shown for zebrafish *chordino* mutants, expression of *gata binding protein 1* (*gata1*), a marker for primitive blood cells and *paired box gene 2a* (*pax2a*), expressed in the pronephric duct was expanded in miR-128 MO injected embryos (Fig. 3I-L). From these results we conclude that upon miR-128 knockdown, there is an increase of *bmp4* expression accompanied by ectopic mesodermal gene expression.

### Identification of *bmp4* as a candidate miR-128 target gene

To examine how miR-128 can interfere with Bmp signaling we used a candidate gene approach

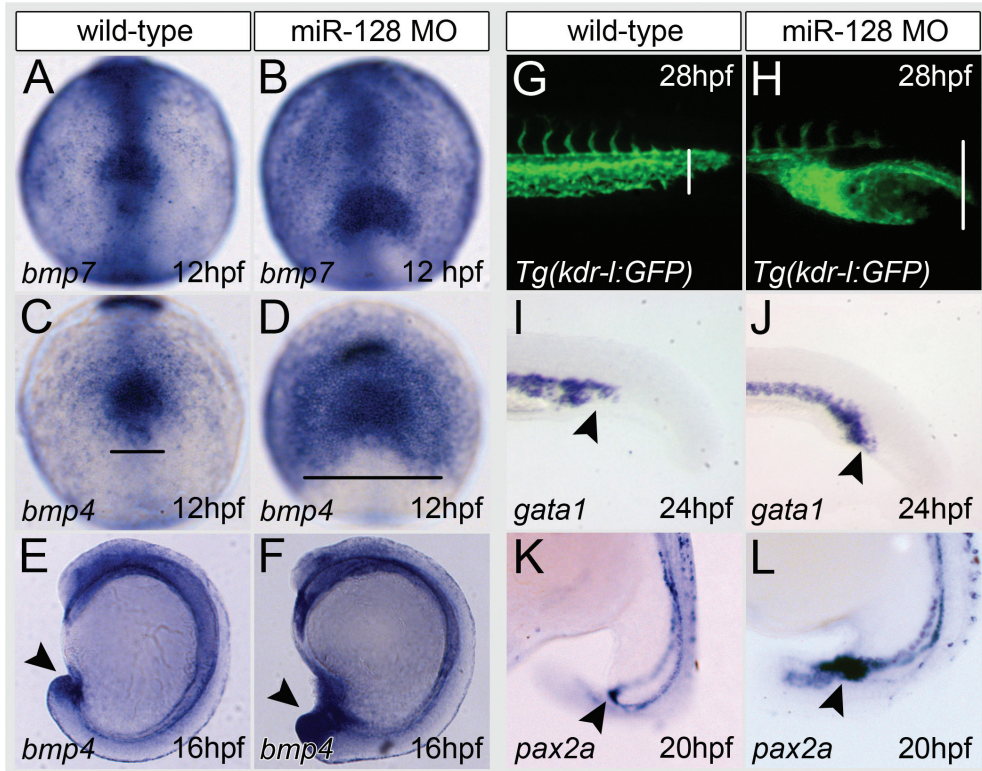


**Figure 3: Knockdown of miR-128 is accompanied by ectopic *bmp4* expression and expansion of endothelial and pronephric cells**

(A-D) miR-128 MO injection results in an expansion of *bmp4* (n=11/12) (D) but not *bmp7* (n=13/14) expression at 12 hpf (B). Enhanced *bmp4* expression in the developing tail of miR-128 morphants (F) at 16 hpf (n=16/16). (G-H) *Tg(kdr-l:GFP)* expression in the tail region of a non-injected (n=21/21) (G) and miR-128 MO injected (H) embryo at 28 hpf, showing an expansion of the endothelial cell population at the ventral side of the tail (n=40/43) (white bars indicate the area of expansion). (I-J) Ectopic expression of the primitive blood cell marker, *gata1*, in miR-128 morphants (n=9/10) at 24 hpf (I and J, black arrowhead). (K-L) More intense *pax2a* staining, marking the pronephric lineage, in the developing tail of miR-128 MO injected embryos at 20 hpf (n=10/12) (K and L black arrowhead).

to select predicted miR-128 target genes related to Bmp signaling. We first explored the online Targetscan software ([www.targetscan.org](http://www.targetscan.org)) for conserved miR-128 putative target genes related to Bmp signaling. We found several Bmp receptor genes; Activin A receptor, type IIA (ACVR2A), Activin A receptor, type IC (ACVR1C) and Bone morphogenetic protein receptor2 (BMPR2). In addition, a putative miR-128 target sequence was predicted in the 3'UTR of the ligand BMP3. We continued to manually analyze the presence of miR-128 binding sites within zebrafish 3'UTR sequences of Bmp receptors and ligands. We selected three zebrafish Bmp related genes containing at least one 3'UTR miR-128 target sequence; *activin A receptor, type I like (alk8)*, *activin A receptor type II-like 1 (alk1)* and the ligand *bmp4*. We continued to examine *in vivo*, the potential interactions between miR-128 and these target candidates. In previous mutagenesis screens zebrafish mutants have been identified for both *laf/alk8*<sup>22</sup> and *vbg/alk1*<sup>14</sup>. MiR-128 knockdown in *vbg* mutants resulted in an indistinguishable tail phenotype compared to injected *vbg* siblings (data not shown).



Alk1 thus is not required for miR-128 to inhibit Bmp signaling and therefore we excluded *alk1* as a miR-128 target. However, the miR-128 MO induced tail phenotype were not observed in *laf* mutant embryos, while in *laf* siblings a clear tail thickening was observed (Fig. 4A-D). From this we conclude that the Alk8 receptor is required for the miR-128 knockdown effect suggesting that *alk8* is a direct miR-128 target, or miR-128 targets upstream components Alk8 receptor signaling. Since we had already observed a strong up-regulation of *bmp4* expression in miR-128 morphants (Fig. 3C-F) and we also identified *bmp4* as a putative miR-128 target gene, we continued to examine a potential *bmp4*-miR-128 interaction. We first performed *bmp4* and miR-128 MO co-injection experiments. Injection of a *bmp4* splice MO<sup>19</sup> resulted in a mild dorsalisation defect, recognizable by a loss of ventral tail tissue (Fig. 4G). Double knock-down embryos for *bmp4* and miR-128 also developed dorsalis tail fins (Fig. 4H). From this we concluded that both *alk8* and the ligand *bmp4* are required for miR-128 to inhibit Bmp signaling. Since *bmp4* is the most upstream candidate that also requires the Alk8 receptor for downstream signaling we continued to investigate functional binding of miR-128 to the zebrafish *bmp4* 3'UTR. We cloned the zebrafish *bmp4* 3'UTR sequence behind the coding sequence for the firefly luciferase gene (*bmp4*-3'UTR). We injected 1-cell stage embryos with *bmp4*-3'UTR RNA and added firefly *renilla* RNA as a negative control. Upon co-injection of miR-128 duplex RNA the luciferase luminescent activity relative to control renilla luminescence significantly dropped. (Fig. 4I n=3 experiments). From this we concluded that miR-128 can interact directly with the zebrafish *bmp4* 3'UTR.

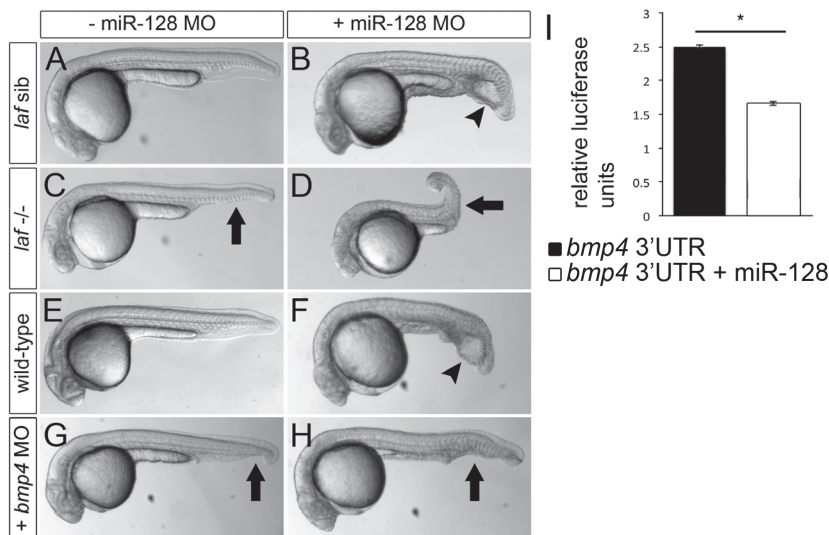


**Figure 4: MIR-128 requires *alk8* and *bmp4* for tail tissue expansion**

(A) Non-injected *laf/alk8* sibling (n=58/78) (B) Injection of miR-128 MO in *laf/alk8* sibling embryos result in an expansion of the ventral tail tissue (black arrowhead) at 1 dpf (n=47/74). *Laf/alk8* mutants injected with miR-128 MO develop a loss of ventral tail structures (black arrow) at 1 dpf (n=28/74), similar to non-injected *laf/alk8* mutants (C, black arrow) (n=20/78). (E) Wild-type non-injected embryo at 1 dpf (n=15). (F) Injection of miR-128 MO results in an expansion of the ventral tail tissue (n=18/20) (black arrowhead) while *bmp4* MO injection induces a partial loss of the ventral fin, indicated by a black arrow in G (n=20/24). (H) When miR-128 and *bmp4* MOs are injected simultaneously embryos develop a loss of ventral fin tissue (n=30/41) (black arrow). (I) Significant reduction in relative luciferase units when the *bmp4* 3'UTR interacts with miR-128 (n=3 experiments of  $p < 0.001$ ).

## MiR-128 MO knockdown phenotype is independent from miR-128

To test for the specificity of the miR-128 MO we hypothesized that miR-128 MO injection in mutants deficient for miR-128 should not induce any phenotype. To examine whether mature miR-128 is lost in maternal and zygotic *dicer* (*MZdicer*) mutants<sup>23</sup> we extracted and analysed mRNA from both *MZdicer* mutant and wild-type embryos. As expected, mature miR-128 was not detected in *MZdicer* mutant embryos (data not shown). Surprisingly we did observe a thickening of the ventral tail region in *MZdicer* mutant embryos at 1 dpf when injected with the miR-128 MO (Fig. 5A-F). From these results we conclude that the observed defects in tail morphogenesis upon injection of the miR-128 MO are not dependent on the presence of mature miR-128.

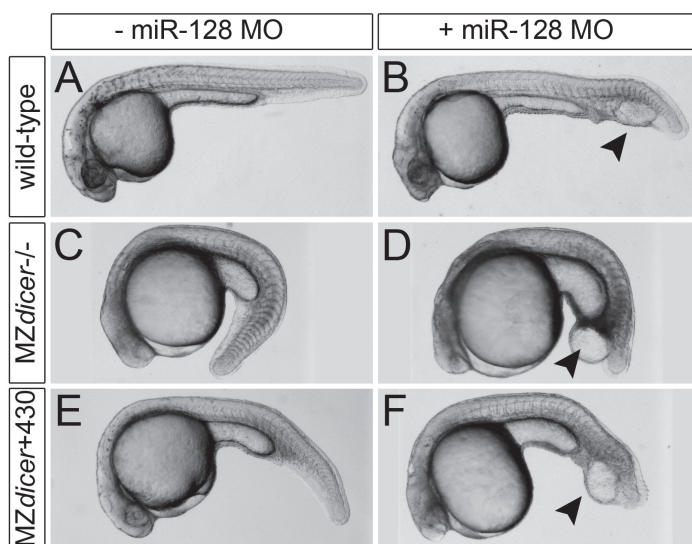


Figure 5: *miR-128* MO induced tail abnormalities are *miR-128* independent (C-F) Injection of miR-128 MO in *MZdicer*<sup>-/-</sup> (D, n=19/21) and *MZdicer*+430 embryos (F, n=24/24) results in a similar expansion of ventral tail tissue comparable to what is observed in wild-type injected embryos (B).

## CONCLUSIONS

In this manuscript we have reported that injection of a miR-128 MO resulting in efficient miR-128 knockdown induced an enrichment of ventral tail tissue. We concluded that the tail phenotype was the result of enhanced *bmp4* expression resulting in enhanced Bmp activity. In addition we demonstrated that miR-128 can interact in a direct manner with the zebrafish *bmp4* 3'UTR. Nevertheless, injection of miR-128 MOs in *MZdicer* mutants demonstrated that the MO induced a phenotype was miR-128 independent. We hypothesized that the MO sequence used to target miR-128 might be fully or partially complementary to a sequence prone for knockdown of an mRNA. Blasting the miR-128 MO sequence against the zebrafish genome however did not reveal any putative MO target genes. Although, we are not aware of any reports describing a function for miRNA hairpin precursors we do not rule out the possibility that this MO interferes with pre-miR-128 hairpins and this results in the phenotypes observed. Most likely the sequence of the MO used to target mature miR-

128 has an off target effect which results in this very specific phenotypic outcome making this study a very interesting lesson in the importance of controlled MO experiments.

MOs are the most common used tool for temporal knockdown experiments in zebrafish (reviewed in 24 and 25). MOs are synthetic oligonucleotides chains of about 25 subunits that are similar to DNA and RNA oligonucleotides. However, MOs have a morpholine ring rather than a ribose ring, making them more stable. In addition, MOs have a negatively charged backbone making them less likely to interact non-specifically with other components of the cell and therefore having less toxic capacities. Nevertheless, it is well appreciated in the field that MO based experiments need to be properly controlled due to off target effects. When using a splice blocking MO to target a messenger RNA (mRNA) of interest one can use reverse transcriptase PCRs (RT-PCRs) to confirm that the MO interfered with splicing of the target mRNA. Another class of commonly used MOs are the translational blocking MOs (ATG MOs) which inhibit ribosome recognition of the target mRNA. For these ATG MOs antibodies can be applied to prove reduced protein levels upon knockdown. A common off target effect reported from a high throughput screen using ATG MOs is induction of cell death, visible around the eyes, in the brain and in the somites at 22 hpf<sup>26</sup>. To control for MO toxicity it has been recommended to perform co-injections using a *p53* MO that does not induce any phenotypes<sup>27</sup>. To control for MO sequence specificity, a 4-base mismatch MO is frequently used.

Since the first miRNA MO knockdown screen, published in 2007<sup>13</sup>, loss of mature miRNA expression has been applied as a proof of miRNA knockdown efficiency. Regular control experiments, like RT-PCRs and antibody staining, are not feasible since miRNAs are non-coding and splicing is not taking place. The above described control does not address the specificity of the MO knock-down. As demonstrated in our experiments even though mature miR-128 expression was lost, this was accompanied by off target effects. We would therefore like to suggest some guidelines for controlled miRNA research in zebrafish. Firstly, to demonstrate that the observed phenotype is not caused by MO toxicity, *p53* MO co-injections should be performed. Secondly, to control for sequence specificity, a 4-base mismatch MO could be injected. Thirdly, injection of an additional MO targeting the same miRNA hairpin but with a non-overlapping sequence should inflict similar loss of function phenotypes<sup>13</sup>. However, due the occurrence of multi-copy miRNA precursors in the zebrafish genome this control is not always feasible. To target individual miRNA copies, specific MOs can be designed targeting only one copy. However, this does not always result in an efficient knockdown as we observed when we co-injected miR-128-1 and miR-128-2 MOs. Fourthly, a comparison of the miRNA knockdown phenotype with the *MZdicer* mutant phenotype can provide evidence for a specific effect of the miRNA knockdown<sup>28,29</sup>. Since *MZdicer* mutants represent a full loss of Dicer function one would expect a miRNA loss of function phenotype to be also represented in *dicer* mutants. However, recent studies have reported miRNAs that are processed Dicer independently<sup>30,31</sup>. Thus, to verify whether *MZdicer* mutants represent a true null for a miRNA of interest, total RNA should be isolated for subsequent northern blot expression analysis. When a miRNA of interest is indeed not processed in *MZdicer* mutants and the *dicer*<sup>-/-</sup> phenotype correlates to an observed miRNA MO phenotype, this suggests specificity the miRNA knockdown. For further evidence, rescue experiments reintroducing the miRNA of interest in *dicer* mutant embryos, can

be performed<sup>28</sup>. However, hypothetically different miRNAs can potentially have opposite effects. In this case the *dicer* mutant phenotype does not necessarily phenocopy a knockdown of a single miRNA.

Alternative methods for miRNA knockdown can also be applied. Locked Nucleic Acid (LNA) based AntagomiRs have been shown to specifically knockdown miRNAs when added into the embryo medium<sup>32</sup>. Nevertheless, LNAs are not often used as miRNA knockdown reagents in zebrafish, possibly due to toxicity effects<sup>13</sup>. Apart from chemical knockdown reagents, tissue specific knockdown can be achieved by so-called “miRNA sponges”. These miRNA inhibitors form a long transcript that contains multiple binding sites for a miRNA of interest<sup>33</sup>. RNA of these constructs can be expressed in all cells or tissue specifically when cloned behind a promoter of interest<sup>34</sup>.

In addition to miRNA knockdown experiments, miRNA overexpression analysis can complement loss of function studies. Injection of double stranded miRNA oligonucleotides should hypothetically induce a phenotype, which is opposite to what is observed when knocking down the same miRNA. However, since miRNA duplex injection induces expression of the miRNA in all cells, the phenotypic outcome can be unpredictable. Ectopic miRNA expression can inflict new miRNA:mRNA interactions with targets that will normally not be expressed in the same cell. Therefore, overexpression analysis can be more difficult to interpret compared to miRNA knockdown studies. A more specific method for overexpression would be to generate overexpression transcripts, encoding multiple pri-miRNA hairpins behind a tissue specific promoter element.

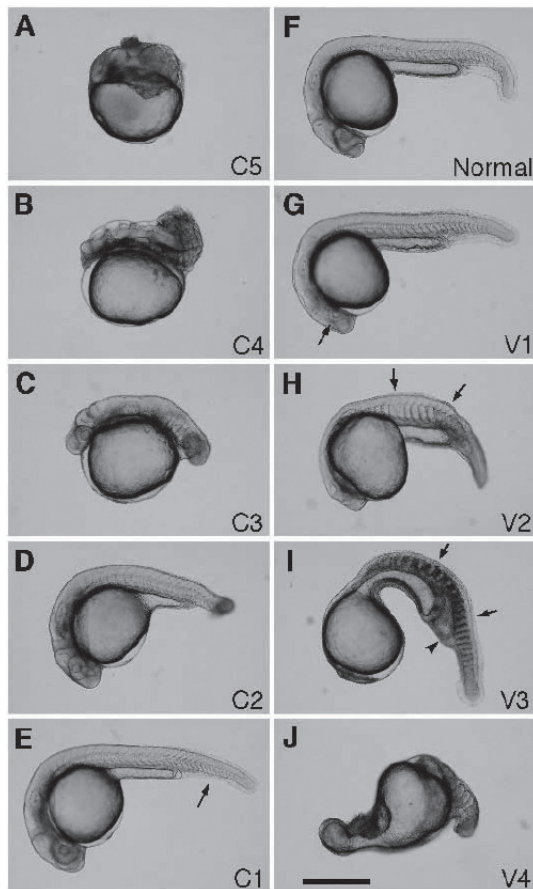
To conclude, we suggested multiple control experiments which can be considered when investigating phenotypic abnormalities upon chemical knockdown of miRNAs in zebrafish.

## REFERENCES

1. M. R. Urist, Bone: formation by autoinduction. *Science* **150**, 893 (Nov 12, 1965).
2. J. M. Wozney et al., Novel regulators of bone formation: molecular clones and activities. *Science* **242**, 1528 (Dec 16, 1988).
3. Y. Cui, F. Jean, G. Thomas, J. L. Christian, BMP-4 is proteolytically activated by furin and/or PC6 during vertebrate embryonic development. *EMBO J* **17**, 4735 (Aug 17, 1998).
4. D. B. Constam, E. J. Robertson, Regulation of bone morphogenetic protein activity by pro domains and proprotein convertases. *J Cell Biol* **144**, 139 (Jan 11, 1999).
5. X. H. Feng, R. Derynck, Specificity and versatility in tgf-beta signaling through Smads. *Annu Rev Cell Dev Biol* **21**, 659 (2005).
6. M. Kondo, Bone morphogenetic proteins in the early development of zebrafish. *FEBS J* **274**, 2960 (Jun, 2007).
7. S. C. Little, M. C. Mullins, Extracellular modulation of BMP activity in patterning the dorsoventral axis. *Birth Defects Res C Embryo Today* **78**, 224 (Sep, 2006).
8. W. Balemans, W. Van Hul, Extracellular regulation of BMP signaling in vertebrates: a cocktail of modulators. *Dev Biol* **250**, 231 (Oct 15, 2002).
9. M. Hammerschmidt, G. N. Serbedzija, A. P. McMahon, Genetic analysis of dorsoventral pattern formation in the zebrafish: requirement of a BMP-like ventralizing activity and its dorsal repressor. *Genes Dev* **10**, 2452 (Oct 1, 1996).
10. M. C. Mullins et al., Genes establishing dorsoventral pattern formation in the zebrafish embryo: the ventral specifying genes. *Development* **123**, 81 (Dec, 1996).
11. M. Hammerschmidt et al., *dino* and *mercedes*, two genes regulating dorsal development in the zebrafish embryo. *Development* **123**, 95 (Dec,

- 1996).
12. Y. Kishimoto, K. H. Lee, L. Zon, M. Hammerschmidt, S. Schulte-Merker, The molecular nature of zebrafish swirl: BMP2 function is essential during early dorsoventral patterning. *Development* **124**, 4457 (Nov, 1997).
  13. W. P. Kloosterman, A. K. Lagendijk, R. F. Ketting, J. D. Moulton, R. H. Plasterk, Targeted inhibition of miRNA maturation with morpholinos reveals a role for miR-375 in pancreatic islet development. *PLoS Biol* **5**, e203 (Aug, 2007).
  14. B. L. Roman et al., Disruption of *acvr11* increases endothelial cell number in zebrafish cranial vessels. *Development* **129**, 3009 (Jun, 2002).
  15. E. Wienholds, M. J. Koudijs, F. J. van Eeden, E. Cuppen, R. H. Plasterk, The microRNA-producing enzyme Dicer1 is essential for zebrafish development. *Nat Genet* **35**, 217 (Nov, 2003).
  16. C. Thisse, B. Thisse, T. F. Schilling, J. H. Postlethwait, Structure of the zebrafish *snail1* gene and its expression in wild-type, spadetail and no tail mutant embryos. *Development* **119**, 1203 (Dec, 1993).
  17. C. Thisse, B. Thisse, High-resolution in situ hybridization to whole-mount zebrafish embryos. *Nat Protoc* **3**, 59 (2008).
  18. W. P. Kloosterman, E. Wienholds, E. de Bruijn, S. Kauppinen, R. H. Plasterk, In situ detection of miRNAs in animal embryos using LNA-modified oligonucleotide probes. *Nat Methods* **3**, 27 (Jan, 2006).
  19. S. Chocron, M. C. Verhoeven, F. Rentzsch, M. Hammerschmidt, J. Bakkens, Zebrafish *Bmp4* regulates left-right asymmetry at two distinct developmental time points. *Dev Biol* **305**, 577 (May 15, 2007).
  20. H. Bauer et al., Follistatin and noggin are excluded from the zebrafish organizer. *Dev Biol* **204**, 488 (Dec 15, 1998).
  21. R. Postel, P. Vakeel, J. Topczewski, R. Knoll, J. Bakkens, Zebrafish integrin-linked kinase is required in skeletal muscles for strengthening the integrin-ECM adhesion complex. *Dev Biol* **318**, 92 (Jun 1, 2008).
  22. K. A. Mintzer et al., *Lost-a-fin* encodes a type I BMP receptor, *Alk8*, acting maternally and zygotically in dorsoventral pattern formation. *Development* **128**, 859 (Mar, 2001).
  23. A. J. Giraldez et al., MicroRNAs regulate brain morphogenesis in zebrafish. *Science* **308**, 833 (May 6, 2005).
  24. J. S. Eisen, J. C. Smith, Controlling morpholino experiments: don't stop making antisense. *Development* **135**, 1735 (May, 2008).
  25. B. R. Bill, A. M. Petzold, K. J. Clark, L. A. Schimmenti, S. C. Ekker, A primer for morpholino use in zebrafish. *Zebrafish* **6**, 69 (Mar, 2009).
  26. S. C. Ekker, J. D. Larson, Morphant technology in model developmental systems. *Genesis* **30**, 89 (Jul, 2001).
  27. M. E. Robu et al., p53 activation by knockdown technologies. *PLoS Genet* **3**, e78 (May 25, 2007).
  28. A. K. Lagendijk, M. J. Goumans, S. B. Burkhard, J. Bakkens, MicroRNA-23 Restricts Cardiac Valve Formation by Inhibiting Has2 and Extracellular Hyaluronic Acid Production. *Circ Res*, **109**, 649-657.
  29. S. Ghani et al., Macrophage development from hematopoietic stem cells requires PU.1 coordinated microRNA expression. *Blood*, (Jul 5, 2011).
  30. D. Cifuentes et al., A novel miRNA processing pathway independent of Dicer requires Argonaute2 catalytic activity. *Science* **328**, 1694 (Jun 25, 2010).
  31. S. Cheloufi, C. O. Dos Santos, M. M. Chong, G. J. Hannon, A dicer-independent miRNA biogenesis pathway that requires Ago catalysis. *Nature* **465**, 584 (Jun 3, 2010).
  32. S. U. Morton et al., microRNA-138 modulates cardiac patterning during embryonic development. *Proc Natl Acad Sci U S A* **105**, 17830 (Nov 18, 2008).
  33. M. S. Ebert, J. R. Neilson, P. A. Sharp, MicroRNA sponges: competitive inhibitors of small RNAs in mammalian cells. *Nat Methods* **4**, 721 (Sep, 2007).
  34. M. S. Ebert, P. A. Sharp, MicroRNA sponges: progress and possibilities. *RNA* **16**, 2043 (Nov, 2010).
  35. M. Westerfield, *The Zebrafish Book - A guide for laboratory use of zebrafish (Brachydanio rerio)*. (University of Oregon Press, Oregon, 1995).

## SUPPLEMENTAL FIGURE

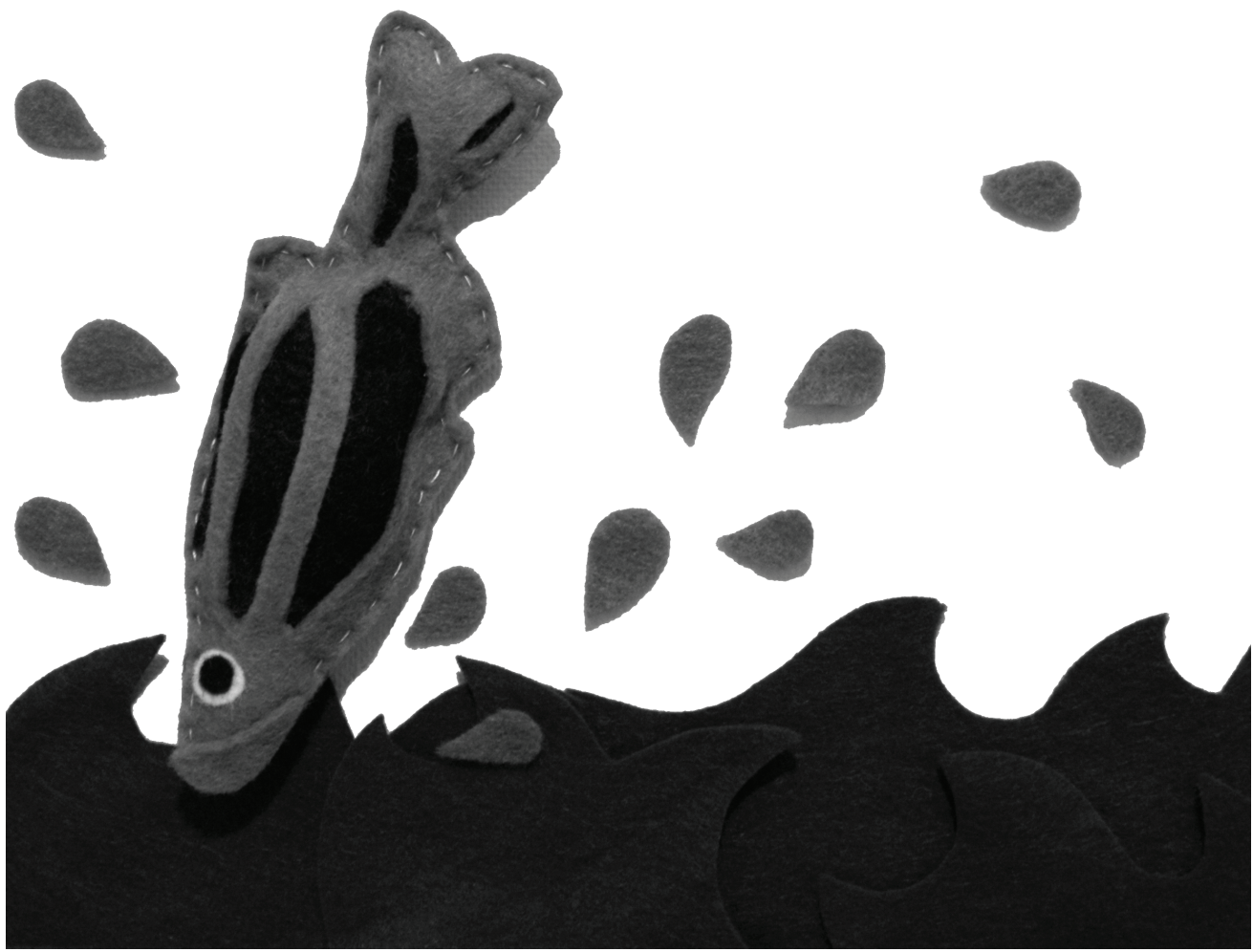


*Supplemental Figure 1: phenotypes of embryos from two heterozygous swrta72 parents injected with xbmp4 mRNA*  
 (A) Non-injected swrta72 homozygous embryo showing the dorsalized C5 phenotype. (B-J) Injected embryos. (B) Dorsalized C4. (C) Dorsalized C3. (D) Dorsalized C2. (E) Dorsalized C1 phenotype. Only the ventral tail fin (arrow) is affected, and most of these embryos survive.

(F) Normal embryo. (G) Ventralized V1 embryo with anterior neural defects (arrow points to reduced eyes), but with a notochord. (H) Ventralized V2 embryo with reduced or absent notochord, expanded posterior somites (arrows), but remaining head structures. (I) Ventralized V3 embryo with little or no head structures left, no notochord, and expanded posterior somites (arrows) as well as enlarged blood islands (arrowhead). (J) Ventralized V4 embryo which is grossly abnormal, lacks all anterior structures, but still shows somites.

*Adapted from Kishimoto et al.<sup>12</sup>*







## GENERAL DISCUSSION

### **MiR-23 function in the endocardial cushions: What about other target genes?**

A.K. Lagendijk<sup>1</sup> and J. Bakkers<sup>1,2</sup>.

1. Hubrecht Institute, KNAW & Iniversity Medical Center, Utrecht, The Netherlands.
2. Interuniversity Cardiology, Institute of the Netherlands, Utrecht, The Netherlands

7

## GENERAL DISCUSSION

### MiR-23 function in the endocardial cushions: What about other target genes?

In this thesis we made use of the zebrafish (*Danio Rerio*) as a model to investigate, endocardial cushion (EC) formation, the initial step of valve development. We introduced two novel players, microRNA-23 (miR-23) and Transmembrane protein 2 (Tmem2), that are both required to restrict the size of the ECs. Thus far, a role for microRNAs (miRNAs) during EC development had not been described. Our results demonstrated that miR-23 is required to restrict the size of the ECs by downregulation of *hyaluronic acid synthase 2 (has2)*. Tmem2 was initially identified as an essential factor during looping of the heart tube. In addition, loss of Tmem2 function resulted in hyperplastic ECs. Finally, we showed that miR-23 interacts with the *tmem2* 3'UTR although the function of this regulation is unknown thus far.

In Chapter 3 and 4 we demonstrated that both miR-23 and Tmem2 are required to restrict the number of endothelial cells that form the ECs<sup>1,10</sup>. The hyperplastic ECs of *tmem2* and *MZdicer* mutant embryos failed to develop into mature valve leaflets. Since congenital valve and septal defects together contribute to a vast percentage of congenital heart disease<sup>2-4</sup> understanding how cardiac valves are formed is of great importance.

We identified three novel miR-23 target genes; *has2*, *tmem2* and *icat* (also known as *ctnnbip1*). Expression of all three target genes in mouse endothelial cells is induced by TGF- $\beta$ <sup>1</sup>. Mechanistically, we showed that inhibition of EC differentiation by miR-23 is mediated by inhibiting Has2 activity, which produces extracellular hyaluronic acid (HA), an essential extracellular matrix (ECM) component. Has2 is crucial for valvulogenesis since *Has2*  $-/-$  mice do not form ECs<sup>5</sup>. In addition, we observed that *has2* is sufficient to induce differentiation of zebrafish endothelial cells. Our results demonstrate that *has2* induction in *MZdicer* mutants and miR-23 morphants is a crucial for ectopic EC formation. We proposed a model describing a non-cell autonomous role for miRNAs in suppressing the EC cell program by inhibition of HA production. Interaction of miR-23 with the *has2* 3'UTR alone however, is likely not sufficient to induce ectopic EC differentiation. We injected a *has2* target protector Morpholino that block miRNA-mRNA interactions<sup>6</sup>. However, we did not observe ectopic *has2* expression in the endocardium when miR-23:*has2* interaction was blocked suggesting the involvement of additional miR-23 target genes (A.K Lagendijk and J. Bakkers, personal communication). Since knockdown of *has2* did rescue endocardial patterning defects, additional miR-23 targets might function upstream of *has2* or in parallel making endocardial cells more susceptible to differentiate into an EC like cell when positioned in an HA rich environment. Although very little is known about upstream regulators of *has2* expression we observed that during TGF- $\beta$  induced EMT in vitro, *Has2* was strongly upregulated<sup>1</sup>. Also we showed that miR-23 can inhibit the TGF- $\beta$  induced EMT in mouse embryonic endothelial cells<sup>1</sup>. Since TGF- $\beta$  signaling is known to enhance mesenchymal transformation during valvulogenesis<sup>7,8</sup>, miR-23 might also regulate EC formation via inhibition of TGF- $\beta$  signaling components functioning upstream of Has2. The miR-23-24-27 cluster was shown to target *smad3*, *smad4* and *smad5*<sup>9</sup> thereby steering the impact of TGF- $\beta$  signaling at the transcriptional level. We identified a putative 6-mer

miR-23 binding site only in the zebrafish *smad3a* 3'UTR. Yet, we could not detect silencing of this sequence by miR-23 (A.K Lagendijk and J. Bakkers, personal communication). We did however identify two additional miR-23 target genes; *tmem2* and *icat/ctnnbip1*<sup>1</sup>. Interestingly, we described in Chapter 4 that Tmem2, like miR-23, functions as an antagonist of EC differentiation<sup>10</sup>. Thereby we have identified a functional interaction of miR-23 with a gene that promotes the EC cell state (*has2*) and a gene that inhibits EC differentiation (*tmem2*). It is noteworthy that a balancing agonist/ antagonist function for miRNAs has been described previously for miR-430 in Nodal signaling<sup>6</sup>.

We detected *tmem2* expression in both endocardial and myocardial cells in zebrafish while *Tmem2* in mouse appeared to be restricted to the endocardium<sup>10</sup>. Noteworthy, we have not observed *tmem2* expressing cells in zebrafish EC cells. Also, in mouse ECs *Tmem2* appears to be expressed only in the overlaying endothelial cell layer of the cushions while *Tmem2* is excluded from the mesenchymal cells of the cushions<sup>10</sup>. Thus, we did not identify any spatial overlap in *tmem2* and *miR-23* expression in the zebrafish ECs. We did observe enhanced *tmem2* expression in MZ*dicer* mutant hearts although we remain to distinguish endocardial from myocardial *tmem2* expression in these mutants (A.K. Lagendijk and J. Bakkers, personal communication). Mishima and colleagues described that mRNA targets are often expressed at very low levels in the cell types where they interact with miRNAs<sup>11</sup>. MiRNAs thereby function by preventing protein expression of genes that are not needed in certain cell types. Possibly, the interaction between miR-23 and *tmem2* is of this nature.

Mechanistically, we showed that *bmp4* functions downstream of Tmem2, regulating differentiation of *has2/Alcama* (Dm-grasp) expressing endocardial cells. *bmp4* in zebrafish is initially expressed by all myocardial cells. Shortly after fusion of the two bilateral heart fields, *bmp4* expression intensifies at the left side of the cardiac disc, which directs leftward displacement of the linear heart tube<sup>12</sup>. In the looped heart at 2dpf, *bmp4* has retracted from the chamber myocardium and is expressed restrictively in myocardial AVC cells. Work by our laboratory showed that Wnt/ $\beta$ -catenin is essential for patterning of *bmp4* in the myocardium<sup>13</sup>. When *bmp4* does not restrict to the AVC, downstream patterning defects of other AVC markers occur, including *tbx2b*<sup>13</sup>. Bmp4 signaling from the myocardium induces the differentiation of EC cells in the endocardium. However, *has2* expression analysis on *bmp4* morphants and *alk8/lost-a-fin* mutant embryos revealed that Bmp function is not fully required for induction EC cells (A.K Lagendijk and J. Bakkers, personal communication). On the contrary, Has2 function is both sufficient and required for EC formation<sup>1,5,14</sup>.

Though *tmem2* is initially expressed ubiquitously in zebrafish embryos, *tmem2* expression restricts at later stages<sup>10</sup>. We know that at 2 dpf Tmem2 is expressed by both myocardial and endocardial cells. RNA expression of *tmem2* suggests a rather punctate expression in both layers of the heart<sup>10</sup>.

Experiments performed by the Yelon lab showed that restoring myocardial Tmem2 function in mutants that lack both maternal and zygotic *tmem2*, rescued a failure of early heart field fusion in these mutants<sup>15</sup>. Interestingly, both fusion of endocardial and myocardial cells at the midline is restored<sup>15</sup>. In addition, the Yelon lab showed that recovering Tmem2 function in the endocardium of zygotic *tmem2* mutants could rescue ectopic expression of the EC marker Alcama/ Dm-grasp, indicating a cell-autonomous role for Tmem2 in endocardial cells<sup>15</sup>. Together, these data demonstrate that Tmem2 functions both in myocardial and

endocardial cells in zebrafish. Since we showed that *bmp4* functions downstream of *Tmem2* in EC patterning and we also described ectopic *bmp4* expression in *tmem2* (*wkm*) mutants, we propose that *Tmem2* might be necessary for restricting *Bmp4* function, and thus EC induction, to the AVC. At 30 hpf when restrictive AVC *has2* expression is first observed (Fig. 1A)<sup>1</sup>, EC cells start to differentiate, followed by expression of *Alcama/Dm-grasp*<sup>16</sup>. At this stage *bmp4* is still expressed throughout the myocardium (Fig. 1A) and *Tmem2* in both endocardial and myocardial cells, though we believe it might be excluded from the AVC (Fig. 1A).

Since, *Bmp4* supports EC differentiation of underlying endocardial cells, *Bmp4* function is not wanted permanently in the chamber myocardium. Therefore, during EC formation *bmp4* expression gradually restricts to the AVC (Fig. 1B). Noteworthy, in *wkm* mutants, this *bmp4* restriction does not occur<sup>10</sup>. Concomitantly to *bmp4* restriction, miR-23 starts to be expressed in EC cells (Fig. 1B)<sup>1</sup>. We believe *Tmem2* might play an important role in restricting *Bmp4* signaling to the AVC, supporting EC formation that has already been initiated earlier by *has2*-HA signaling in these cells (Fig. 1B). The interaction between miR-23 and *tmem2* in the developing ECs would be mostly a security policy, preventing *Tmem2* activity while EC are being formed (Fig. 1B). More importantly, increasing miR-23 levels in ECs subsequently shuts down the ongoing *has2*-HA positive feedback loop so that the cushions can transform into mature valve leaflets (Fig. 1B). Losing miR-23 function ultimately results in EC expansion due to continuation of *has2*-HA signaling. Potentially increased levels of *tmem2* in EC cells of miR-23 morphants appears to be insufficient to interfere with the effect of increased *Has2* activity.

To investigate a potential *Tmem2*-miR-23 feedback we performed miR-23 expression analysis in *wkm* mutants. We detected wild-type like miR-23 expression in the EC cells of *wkm* mutants. Interestingly, miR-23 was not expressed ectopically by cells outside the endocardial AVC (A.K. Lagendijk and J. Bakkers, personal communication), as reported for *has2* in *wkm* mutants<sup>10</sup>. Since we have shown that miR-23 is a relatively late marker for EC cells, expressed from 53 hpf, approximately 20 hours after the onset of EC induction, this observation is in line with previous findings that *has2* expressing endocardial cells in *wkm* mutants remain in a premature state<sup>10</sup>.

Finally, apart from miR-23 expression in ECs we have also detected miR-23 in various other tissues during embryonic development. Intriguingly, we found that miR-23 was expressed in the pharyngeal arches, the pectoral fin buds and the lateral line, all tissues containing mesenchymal cells. *tmem2* is also expressed in the pectoral fin buds leaving the possibility that the miR-23-*tmem2* interaction happens outside the heart in other tissues.

We have also introduced *icat/ctnnbip1* as a functional target of miR-23. Thus far *icat* has not been functionally related to cardiac development. *In vitro* studies have shown though that ICAT competes with TCF in the cytoplasm for binding  $\beta$ -catenin, subsequently inhibiting activation of downstream target genes<sup>17</sup>. Wnt/ $\beta$ -catenin signaling components are expressed in both mesenchymal and endothelial cells that together make up the ECs. Furthermore, canonical Wnt/ $\beta$ -catenin signaling is required for the induction of EC cells as well as for later valve remodelling<sup>8,18-20</sup>. We have conducted several *icat in situ* hybridization experiments. Due to low level of *icat* expression, these studies remain rather inconclusive. Nevertheless, we did observe low levels of *icat* in the atrial outer curvature cells and in the ventricle (A.K. Lagendijk and J. Bakkers, personal communication). Hypothetically speaking

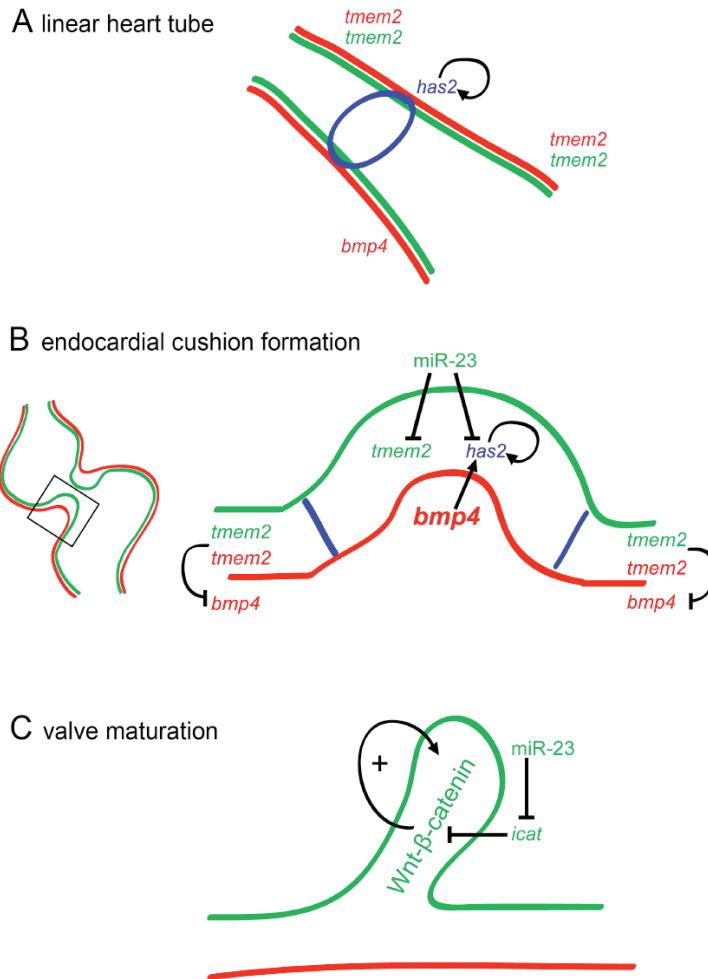


Figure 1: Schematic representation of putative miR-23 regulated processes

(A) Drawing of zebrafish embryonic heart at the linear heart tube stage around 30 hpf. *has2* expression starts to restrict to endocardial cells at the AV boundary (blue ring of expression), initiating EC differentiation. In this linear heart tube *bmp4* is expressed in all myocardial cells and *tmem2* possibly endocardial and myocardial cells. Red = myocardium, Green = endocardium. The black arrow indicates the autoregulatory loop of *has2*-HA signaling at the AV boundary.

(B) Left: Drawing of the looped zebrafish heart. Right: EC area boxed in left panel. From 53hpf miR-23 starts to be expressed in EC cells. MiR-23 targets *has2*, thereby reducing the effect of ongoing *has2*:HA signaling. Also, miR-23 might prevent expression of EC differentiation antagonists, like *tmem2*. The function of *Tmem2* outside the AVC might be to reduce *Bmp4* activity in the chambers. Since *Tmem2* is not present at the AV boundary, *bmp4* expression can restrict to this area and support EC formation by inducing *has2* expression. Red = myocardium, Green = endocardium. Blue lines indicate the borders of the AVC.

(C) Proliferation of endocardial cells during valve leaflet maturation requires Wnt- $\beta$ -catenin signaling (indicated by +). MiR-23 targets an inhibitor of Wnt- $\beta$ -catenin, *icat*. Potentially inhibition of *icat* function by miR-23 is essential for valve maturation to occur.

when miR-23 and *icat* would be expressed in EC cells simultaneously then knockdown of miR-23 would result in increased *icat* levels. As a consequence, Wnt/ $\beta$ -catenin signaling would be downregulated, suggesting again an antagonistic effect on the induction of EC formation. However, miR-23 expression in EC cells was first detected at 53 hpf, while the first EC cells differentiate already at 30 hpf<sup>1,16</sup>. Therefore, enhanced *Icat* function from 53 hpf onwards might be insufficient to interfere with early cushion formation since the stage of induction has been passed at this stage. Also, similarly to what we described previously for *Tmem2*, we do not know what the result of diminished Wnt/ $\beta$ -catenin signaling accompanied by enhanced *has2*-HA signaling would be in EC cells. Interestingly, Wnt/ $\beta$ -catenin signaling has also been proven to function during valve leaflets maturation<sup>21</sup>. In miR-23 morphants we observed a continuation of *has2* expression at 3 dpf suggesting EC cells maintain a premature state<sup>1</sup>. In addition, mature valve leaflets were not observed in miR-23 morphants and *MZdicer* mutant hearts. Possibly, miR-23 is required to inhibit *icat* function during the process of valve maturation by releasing active  $\beta$ -catenin (Fig. 1C). Taken together, in a wild-type situation, miR-23 could function as a backup to prevent expression of genes that would interfere with EC formation, including hypothetical *tmem2* expression in EC cells (Fig. 1B). Subsequently, increasing miR-23 expression levels in the EC cells attenuate differentiation of endocardial cells into immature EC cells by restricting a non-cell autonomous process of *has2*-HA signaling that is originated at an earlier time point from within the EC cells (Fig. 1A and B). In addition, miR-23 could further promote valve maturation by inhibiting *Icat* function and thereby increasing the impact of Wnt/ $\beta$ -catenin signaling (Fig. 1C).

We encountered several limitations during our screen for miR-23 target genes, including poor annotation of zebrafish 3'UTR sequences. Potentially miR-23 candidate genes that were dropped during this screen could still turn out to be bona fide miR-23 targets. We believe that future experiments should be more directed towards tissue specific identification of miRNA targets. Also, new techniques are emerging in the field that can be applied to show miRNA:mRNA target interactions *in vivo* (reviewed by Thomas et al.<sup>22</sup>). Making use of zebrafish transgenic lines, FACS sorting can be conducted for example to collect myocardial or endocardial cells. Thus far microarray profiling of cells exposed to either miRNA loss of function or miRNA overexpression have been applied frequently to profile putative miRNA targets (reviewed by Thomas et al.<sup>22</sup>). Microarray based analysis however cannot distinguish direct miRNA targets from mRNAs indirectly affected by miRNA function. Recently, simultaneous protein and RNA isolation procedures are emerging<sup>23-27</sup>. Using these techniques, miRNAs still bound to their target mRNAs can be isolated, while still residing in the RISC complex. Next, a RT-PCR based method<sup>27</sup> can be conducted to generate a library of mRNA sequences that were bound to a specific miRNA of interest. Further cloning and sequencing of these mRNAs will reveal novel target that were bound *in vivo* in a specified group of cells. To date, these RISC bound target identification techniques have not been applied for miRNA studies in zebrafish. Future applications of continuously improving methodology in the miRNA field will reveal many more miRNA target genes, possibly providing more insights in the actual *in vivo* mechanism of action for individual miRNAs in specific cell types. Results obtained from these *in vivo* target identification in a wild-type environment will prove whether a vast amount of targets identified to date using miRNA loss of function or miRNA overexpression scenarios are valid.

## REFERENCES

1. A. K. Lagendijk, M. J. Goumans, S. B. Burkhard, J. Bakkers, MicroRNA-23 Restricts Cardiac Valve Formation by Inhibiting Has2 and Extracellular Hyaluronic Acid Production. *Circ Res*, **109**, 649-657.
2. J. I. Hoffman, S. Kaplan, The incidence of congenital heart disease. *J Am Coll Cardiol* **39**, 1890 (Jun 19, 2002).
3. L. D. Botto, A. Correa, J. D. Erickson, Racial and temporal variations in the prevalence of heart defects. *Pediatrics* **107**, E32 (Mar, 2001).
4. P. J. Gruber, J. A. Epstein, Development gone awry: congenital heart disease. *Circ Res* **94**, 273 (Feb 20, 2004).
5. T. D. Camenisch et al., Disruption of hyaluronan synthase-2 abrogates normal cardiac morphogenesis and hyaluronan-mediated transformation of epithelium to mesenchyme. *J Clin Invest* **106**, 349 (Aug, 2000).
6. W. Y. Choi, A. J. Giraldez, A. F. Schier, Target protectors reveal dampening and balancing of Nodal agonist and antagonist by miR-430. *Science* **318**, 271 (Oct 12, 2007).
7. E. J. Armstrong, J. Bischoff, Heart valve development: endothelial cell signaling and differentiation. *Circ Res* **95**, 459 (Sep 3, 2004).
8. A. D. Person, S. E. Klewer, R. B. Runyan, Cell biology of cardiac cushion development. *Int Rev Cytol* **243**, 287 (2005).
9. C. E. Rogler et al., MicroRNA-23b cluster microRNAs regulate transforming growth factor-beta/bone morphogenetic protein signaling and liver stem cell differentiation by targeting Smads. *Hepatology* **50**, 575 (Aug, 2009).
10. K. A. Smith et al., Transmembrane protein 2 (Tmem2) is required to regionally restrict atrioventricular canal boundary and endocardial cushion development. *Development* **138**, 4193 (Oct, 2011).
11. Y. Mishima et al., Zebrafish miR-1 and miR-133 shape muscle gene expression and regulate sarcomeric actin organization. *Genes Dev* **23**, 619 (Mar 1, 2009).
12. S. Chocron, M. C. Verhoeven, F. Rentzsch, M. Hammerschmidt, J. Bakkers, Zebrafish Bmp4 regulates left-right asymmetry at two distinct developmental time points. *Dev Biol* **305**, 577 (May 15, 2007).
13. M. C. Verhoeven, C. Haase, V. M. Christoffels, G. Weidinger, J. Bakkers, Wnt signaling regulates atrioventricular canal formation upstream of BMP and Tbx2. *Birth Defects Res A Clin Mol Teratol* **91**, 435 (Jun, 2011).
14. T. D. Camenisch, J. A. Schroeder, J. Bradley, S. E. Klewer, J. A. McDonald, Heart-valve mesenchyme formation is dependent on hyaluronan-augmented activation of ErbB2-ErbB3 receptors. *Nat Med* **8**, 850 (Aug, 2002).
15. R. Totong et al., The novel transmembrane protein Tmem2 is essential for coordination of myocardial and endocardial morphogenesis. *Development* **138**, 4199 (Oct, 2011).
16. D. Beis et al., Genetic and cellular analyses of zebrafish atrioventricular cushion and valve development. *Development* **132**, 4193 (Sep, 2005).
17. C. J. Gottardi, B. M. Gumbiner, Role for ICAT in beta-catenin-dependent nuclear signaling and cadherin functions. *Am J Physiol Cell Physiol* **286**, C747 (Apr, 2004).
18. A. F. Hurlstone et al., The Wnt/beta-catenin pathway regulates cardiac valve formation. *Nature* **425**, 633 (Oct 9, 2003).
19. S. Liebner et al., Beta-catenin is required for endothelial-mesenchymal transformation during heart cushion development in the mouse. *J Cell Biol* **166**, 359 (Aug 2, 2004).
20. A. D. Gitler, M. M. Lu, Y. Q. Jiang, J. A. Epstein, P. J. Gruber, Molecular markers of cardiac endocardial cushion development. *Dev Dyn* **228**, 643 (Dec, 2003).
21. C. M. Alfieri, J. Cheek, S. Chakraborty, K. E. Yutzey, Wnt signaling in heart valve development and osteogenic gene induction. *Dev Biol* **338**, 127 (Feb 15, 2010).
22. M. Thomas, J. Lieberman, A. Lal, Desperately seeking microRNA targets. *Nat Struct Mol Biol* **17**, 1169 (Oct, 2010).
23. M. Beitzinger, L. Peters, J. Y. Zhu, E. Kremmer, G. Meister, Identification of human microRNA targets from isolated argonaute protein complexes. *RNA Biol* **4**, 76 (Jun, 2007).
24. G. Easow, A. A. Teleman, S. M. Cohen, Isolation of microRNA targets by miRNP immunopurification. *RNA* **13**, 1198 (Aug, 2007).
25. X. Hong, M. Hammell, V. Ambros, S. M. Cohen, Immunopurification of Ago1 miRNPs selects for a distinct class of microRNA targets. *Proc Natl Acad Sci U S A* **106**, 15085 (Sep 1, 2009).
26. F. V. Karginov et al., A biochemical approach to identifying microRNA targets. *Proc Natl Acad Sci U S A* **104**, 19291 (Dec 4, 2007).
27. Y. Andachi, A novel biochemical method to identify target genes of individual microRNAs: identification of a new *Caenorhabditis elegans* let-7 target. *RNA* **14**, 2440 (Nov, 2008).





**SAMENVATTING IN HET NEDERLANDS**

**DANKWOORD/ ACKNOWLEDGEMENTS**

**CURRICULUM VITAE**

**LIST OF PUBLICATIONS**

## SAMENVATTING IN HET NEDERLANDS

Tijdens mijn promotieonderzoek in de groep van Dr. Jeroen Bakkers in het Hubrecht Instituut voor Ontwikkelingsbiologie en Stam Cel Onderzoek, heb ik mij met name bezig gehouden met het identificeren van genetische factoren die van invloed zijn op het correct ontwikkelen van hartkleppen. De resultaten van dit onderzoek staan beschreven in dit proefschrift.

In het Bakkers lab maken we gebruik van de zebravis (*Danio rerio*) als modelorganisme. Net zoals de mens en de muis is ook de zebravis een zogenaamd gewerveld organisme. Het voordeel van het zebravis model voor embryologische studies is het feit dat bij de zebravis de bevruchting extern (in het water) plaatsvindt. Daarnaast kunnen we vaak zeer grote aantallen embryo's tegelijk verzamelen. Tot slot zijn zebravis embryo's transparant. We kunnen hierdoor het hart, dat ongeveer 1 dag na de bevruchting al functioneel is, live bestuderen.

Het belang van het correct ontwikkelen van hartkleppen tijdens de embryologie blijkt reeds uit het feit dat ongeveer 6 op de 1000 levend geboren baby's een aangeboren afwijking aan hart kleppen of septa (de muren die de hart kamers van elkaar scheiden) heeft ontwikkeld. In Hoofdstuk 1 beschrijf ik een eerder uitgevoerde studie waarbij in een groep van patiënten met een aangeboren hartklep/septum afwijkingen genetische variaties gevonden zijn in gene die belangrijk zijn voor normale hartontwikkeling. Ik geef hier een overzicht van de functie van deze individuele genen (waarin de variaties gevonden zijn) en hoe deze genen functioneel met elkaar zijn verbonden tijdens de ontwikkeling van de kleppen. De resultaten van deze genetische studie suggereren dat genetische variaties in verschillende genen die wel betrokken zijn bij hetzelfde proces kunnen resulteren in een vergelijkbare aangeboren hartafwijking.

In dit proefschrift worden twee nieuwe genen beschreven die van belang zijn voor het sturen van de hartklepontwikkeling. Het eerste gen is een microRNA, te weten microRNA-23. Normaliter vormen RNA moleculen als het ware een afschrift van een gen zoals deze staat beschreven in ons DNA. De code van dit afschrift wordt vervolgens nogmaals gelezen tijdens de productie van het eiwit dat door het gen in het DNA werd gecodeerd. De eiwitten vormen uiteindelijk de echte spelers van ons lichaam. MicroRNAs zijn uitzonderlijke RNA moleculen, aangezien ze niet functioneren als een afschrift waar eiwitten van worden gemaakt. MicroRNAs zijn echter kleine "regelneef" RNA moleculen, die het aflezen van normale RNA moleculen tijdens de productie van eiwitten kunnen remmen. MicroRNAs doen dit door te binden aan specifieke regio's in de RNA moleculen, waardoor eiwit productie niet kan plaatsvinden.

In de jaren negentig werd de eerste microRNAs beschreven in de worm (*Caenorhabditis elegans*). Initieel werden microRNAs functioneel gelinkt aan processen tijdens de ontwikkeling. Op dit moment zijn er duizenden microRNAs geïdentificeerd in veel verschillende organismen, waaronder ook de mens, de muis en de zebravis. Daarnaast is aangetoond dat microRNAs niet alleen belangrijk zijn tijdens de embryonale ontwikkeling, maar ook tijdens ziekte processen zoals tumor metastasering.

Voor de productie van de microRNAs zijn meerdere enzymen nodig. Een van deze enzymen is het eiwit Dicer. Wanneer de functie van Dicer wordt uitgeschakeld in muizen embryo's zijn deze niet levensvatbaar. Hieruit blijkt dat de microRNAs van cruciaal belang zijn voor de embryonale ontwikkeling. Zebavis embryo's waarbij *dicer* is uitgeschakeld (*dicer* mutanten) leven echter nog wel enkele dagen. We kunnen het zebavis model daarom goed gebruiken om te bestuderen wat het gevolg is van het verlies van microRNA functie tijdens de embryonale ontwikkeling.

Wij hebben ons toegespitst op het effect van het verlies van Dicer, en dus alle microRNAs, op de ontwikkeling van het embryonale hart. In Hoofdstuk 3 wordt beschreven dat er voornamelijk een sterk defect ontstaat in de cellen van het hart die later de hartkleppen gaan vormen. Door het verlies van Dicer ontwikkelen er als het ware te veel hartklepcellen waardoor het hart "verstopt" raakt met deze cellen. Vervolgens hebben wij aangetoond dat microRNA-23 een cruciale microRNA is tijdens dit proces van hartklepontwikkeling. Wanneer de functie van microRNA-23 in de zebavis wegvalt, wordt er wederom te veel klepweefsel aangemaakt, vergelijkbaar met het effect na het verlies van Dicer. Wanneer we microRNA-23 herintroduceren in de *dicer* mutanten kunnen we het teveel aan klepcellen terug dringen. We hebben ontdekt dat microRNA-23 dit remmende effect op hartklep vorming heeft door onder andere te binden aan RNA moleculen van het gen *has2* (*hyaluronic acid synthase 2*). Doordat microRNA-23 aan *has2* RNA moleculen bindt wordt er minder Has2 eiwit geproduceerd en daardoor neemt de functie van Has2 in de hartklepcellen af. Has2 eiwitten stimuleren normaliter de ontwikkeling van klepachtige cellen. Doordat microRNA-23 echter het niveau van Has2 activiteit kan verlagen wordt de hoeveelheid cellen die de kleppen gaan vormen in als het ware toom gehouden.

Tijdens het bestuderen van de functie van microRNA-23 waren wij genoodzaakt om een bestaande methode die we gebruiken om microRNAs aan te kleuren, te optimaliseren. Deze methode noemt men *in situ* hybridisatie, en wordt op grote schaal toegepast om RNA moleculen aan te tonen in gefixeerd weefsel. Omdat microRNAs zo klein zijn en soms maar in lage aantallen voorkomen is het aantonen van microRNAs een uitdagendere opgave. Met behulp van onze vernieuwde *in situ* methode konden we zeer exact laten zien in welke cellen van het hart microRNA-23 voorkomt. We hebben deze geoptimaliseerde methode verder uitgewerkt om de toepasbaarheid hiervan in het microRNA veld te vergroten. In Hoofdstuk 2 wordt deze methode in meer detail beschreven.

In Hoofdstuk 4 wordt er een nieuw gen, *tmem2* (*transmembrane protein 2*), beschreven dat tot voor kort niet eerder in verband werd gebracht met embryonale hartontwikkeling. In het Bakkers lab zijn enkele "forward genetic screens" (genetische screens) uitgevoerd met als doel het vinden van zebavis mutanten waarbij de kamers van hart niet correct positioneren ten opzichte van elkander. Tijdens de embryologie van zowel mens als zebavis ontstaat het hart initieel als een simpele, lineaire buis. Vervolgens worden de kamers van het hart gevormd en zal de buis zodanig buigen ("loopen") dat deze kamers correct worden georiënteerd. In de zebavis resulteert dit in een transformatie van de simpele lineaire hartbuis naar een S-vormig hart met twee kamers, een atrium en een ventrikel. Wanneer er defecten ontstaan tijdens deze transformatie in de vorm van het hart kan dit leiden tot ernstige aangeboren aandoeningen. Gevolgen kunnen zijn dat zuurstofrijk bloed niet goed

wordt gescheiden van zuurstofarm bloed of dat het bloed het hart verlaat via de verkeerde vaten. Dr. Kelly Smith identificeerde tijdens een van deze screens een zebrafish mutant, genaamd *wickham*, waarbij het hart niet buigt. De mutatie verantwoordelijk voor het defect in de *wickham* mutant werd gevonden in het gen *tmem2*. Na gedetailleerd onderzoek naar de defecten aan het hart van *wickham* mutanten bleek er naast het uitblijven van buiging van de hartbuis ook een defect te zijn in de vorming van hartklepcellen. We hebben tijdens onze studie laten zien dat *Tmem2* de vorming van hartklepcellen remt. *Tmem2* heeft hiervoor het eiwit *Bmp4* (Bone morphogenetic protein 4) nodig. In *wickham* mutanten wordt te veel klepweefsel gevormd, echter als *Bmp4* is uitgeschakeld heeft het verlies van *Tmem2* in de mutanten dit effect niet meer op de klepcellen. De invloed van *Tmem2* op de buiging van de hartbuis verloopt waarschijnlijk niet via *Bmp4*, maar via een reeds onbekend mechanisme.

Naast de in Hoofdstuk 4 beschreven *wickham* mutant zijn er in het lab meerdere van deze zogenaamde "looping" mutanten geïdentificeerd tijdens genetische screens. Al deze mutanten ontwikkelen een defect tijdens het buigen van de hartbuis. In Hoofdstuk 5 worden de resultaten beschreven die wij hebben verkregen na het karakteriseren van deze mutanten. In een van deze mutanten klopt (contracteert) het hart niet. Door het gebrek aan contractie is er ook geen bloedcirculatie in deze mutant. Onze resultaten, verkregen na het bestuderen van deze contractie-loze mutant bevestigen dat het kloppen van het hart niet noodzakelijk is voor de transformatie van een lineaire naar een S-vormige hartbuis. Met andere woorden, het is mogelijk om een hart te vormen dat er morfologisch normaal uitziet ook al klopt deze niet. In de overige looping mutanten, waarbij het hart overigens wel klopt, vonden we veelvuldig afwijkingen in de regio waar de kleppen van het hart zullen gaan vormen. De intensiteit van de afwijkingen die we beschreven hebben verschilt echter tussen de verschillende looping mutanten. Een causaal verband tussen de hoeveelheid klep cellen en de buiging (looping) van het hart is dan ook voorlopig niet te stellen.

Tot slot is er in Hoofdstuk 6 een project uiteengezet naar de functie van een andere microRNA, namelijk microRNA-128. We beschrijven dat in zebrafish embryo's waarbij microRNA-128 wordt uitgeschakeld, een zeer karakteristiek fenotype ontstaat waarbij er te veel weefsel wordt gevormd aan de onderzijde van de staartpunt. Tijdens de embryologische ontwikkeling van de mens, maar ook bij de zebrafish, worden de assen van het lichaam vastgelegd. Cellen van het embryo weten vervolgens of ze behoren tot de voorkant (anterior), achterkant (posterior), onderzijde (ventraal) of bovenzijde (dorsaal). Voor het vaststellen van deze assen is onder andere de dosis *Bmp* eiwitten waarmee cellen in aanraking komen van belang. Het overschot aan weefsel aan de onderkant (ventrale kant) van de staartpunt is eerder in verband gebracht met een te hoge dosis *Bmp* eiwitten in de cellen die deze regio gaan vormen. Het verlies van microRNA-128 leek dan ook te leiden tot een over-activatie van *Bmp* eiwitten met als gevolg meer weefsel aan de onderzijde van de staartpunt. Enkele kandidaat RNA moleculen waaraan microRNA-128 mogelijk bindt, werden bestudeerd. Als voornaamste kandidaat werd *bmp4* in meer detail onderzocht waarbij we hebben aangetoond dat microRNA-128 kan binden aan zebrafish *bmp4* RNA. Voor het tijdelijk uitschakelen van microRNA-128 tijdens zebrafish ontwikkeling hebben we gebruik gemaakt van zogenaamde morpholinos. Morpholinos lijken op DNA moleculen, maar zijn chemisch gemodificeerd waardoor ze zeer sterk kunnen binden aan

RNA moleculen. Deze morpholinos kunnen direct na de bevruchting in de zebrafischeieren worden geïnjecteerd. Uiteindelijk hebben we de morpholinos die we hebben gebruikt om de microRNA-128 functie weg te nemen in wild-type embryo's, ook geïnjecteerd in dicer mutanten embryo's. Aangezien er in deze embryo's geen microRNAs worden geproduceerd zou de morpholino injectie in theorie geen effect op de ontwikkeling van het embryo moeten hebben. Echter, ook in dicer mutanten konden wij duidelijk een verdikking van de staartpunt onderscheiden. Hieruit hebben wij geconcludeerd dat de morpholino die wij gebruikt hebben om aan microRNA-128 te binden ("targeten") waarschijnlijk een "off-target" effect heeft. Dit heeft ons doen besluiten om dit project te gebruiken als voorbeeld hoe microRNA morpholino studies dienen te worden gecontroleerd.

Samengevat verschaft dit proefschrift nieuwe inzichten op het gebied van microRNAs, hartklepontwikkeling en de buiging (looping) van het hart.

## DANKWOORD/ ACKNOWLEDGEMENTS

Zo'n boekje is er natuurlijk niet zomaar. Er zijn dan ook veel mensen die hier een plekje verdienen.

Als eerste een hele dikke DANKJEWEL voor Jeroen. Ik ben altijd erg blij geweest dat jij ergens aan het einde van de regenboog een potje goud vond voor mij. Het was wel eens vallen en opstaan tijdens mijn projecten. Samen hielden we echter altijd een positieve instelling. We zaten vaak op een lijn en waren het snel eens. Dit alles maakt onze samenwerking erg prettig. Je mag met recht trots zijn op de groep die je hebt opgezet in de afgelopen jaren. Heel veel succes met al die mooie projecten die er nog aan zitten te komen.

CHOCRON!, Sonja. De koningin van het lab. Met raad en daad sta je voor iedereen klaar, op ieder moment en altijd met een lach op je gezicht. Respect! Zonder jouw hulp met transplanteren hadden we nooit zo veel MZ*dicer* vissen gehad. We hebben geknald toen samen. Hilarisch ook onze wetenschappelijk zeer verantwoorde manier om de gulden middenweg te bepalen voor hoeveelheden reagentia etc. Wie gaat er nu lachen om mijn domme grapjes?

Kleine Kerst, Emily Noël. I am very happy you joined the Bakkers lab. We got along immediately. Always the person to turn to for some "fun fun fun"! Not only that, also great scientific advice or some mental support. You rock kleine! Thanks for proofreading my whole thesis. That must have been the Sunday of your dreams. See you in OZ, I will play you some Cathy May!

Federico Tessadori "Pizza", the dude. You have always been a great help in the lab, in for a discussion but also in for a beer, a cocktail (Tokio Ice Tea I think it was) or a cup of real coffee. Prego Fedele!

Ina "Bradwurst" Strate. When you came for your interview we went for some good cocktails at Zussen. What a good profile for a Bakkers chick! Go Ina, nail that knypek stuff!

Door de jaren heen had ik ook nog wat studenten onder mijn hoede; Evelyn, Johnathan en Silja. Thanks for all the great work you guys did, I could have never done that it all myself. Silja, your contribution made the miR-23 story simply better. Thanks for doing all those PCRs, the cloning and injections. I am very glad you decided to join the Bakkers team and I am sure you will do great.

De oud-Bakkertjes; Manon, Emma, Ruben, Marah en alle oud-Bakkers studenten. Bedankt voor alle gezelligheid, goede discussies en hulp. Ruben, Mobro! Herder! Thanks.

Naast de Bakkers groep is daar natuurlijk ook nog de van Rheenen groep. Allemaal samen in het kantoor. Erg leuk, omdat ik jullie allemaal zo ook snel leerde kennen.

Evelyne, Anoeek en Laila; gelukkig wisten we ook vaak onze weg uit het kantoor naar de kantine te vinden voor een biertje.

Mijn stage begeleiders; Paul, Annemiek en Wigard. Ik heb van jullie allemaal veel geleerd en jullie enthousiasme in het werk was erg aanstekelijk.

Alle ACT-ers. Bedankt voor de goede verzorging van de vissen en af en toe een lekker praatje.

My friends from the very beginning at the Hubrecht; Erik, Robert, Ben, Kelly and Saskia. We had so many good times both in and outside the lab. Because of all of you my move to Utrecht went very smoothly. Always someone to hang out with, whatever day of the week. Drinking, eating (dim sum!), dancing, BBQ, movies, holiday in Spain. Thanks for all, you guys are the best!

Robert, bedankt voor de in-design assistentie.

Shouwing, Saskia. Een vriendin waar je altijd op kan rekenen. Ik denk dat wij elkaars gekke fratsen snel door hadden en dat we daarom altijd zo goed met elkaar door een deur kunnen. Er kan er maar één zo knetter hard lachen als jij! Nu wij NY, jij ook snel OZ?

K-B, Kelly. A special friend you don't come across so often. You know what I mean, no more words necessary.

Drie keer op Movember weekend; Londen, Barcelona en toen nogmaals Londen. Alle drie de keren te gek! Iedereen die mee was, bedankt voor die super weekenden met fantastische verkleedpartijen en natuurlijk de uitmuntende snorren.

Op de valreep waren daar Tamara en Britta. Met name onder het genot van een biertje altijd veel lol met jullie. Dansen aan de gracht, wat een geweldige avond was dat! Graag hoor ik in de toekomst nog een keer het nieuws dat jullie in de Cambridge bar met z'n allen een pitcher sticky blue shots hebben gekild.

Lieve Lexies! Femke, Zairah en Lianne. Tijdens de studie leerde ik jullie allemaal afzonderlijk van elkaar kennen en nu vormen we een mooi stel samen. Jullie staan altijd garant voor een flinke dosis Nijmeegse gekheid. Sommige dingen kan ik hier maar beter niet herhalen. Ik kijk al uit naar ons volgende weekend weg.....Waar op de wereld zal dat zijn??

Lianne, bedankt dat je met zo veel enthousiasme mijn paranimf wilde zijn.

Alle meiden uit Eindhoven en omstreken. Ook al zie ik de meesten van jullie niet zo vaak meer, wanneer we elkaar zien is het altijd gezellig. Jammer dat ik ons jaarlijkse uitje nu even moet gaan overslaan. Gelukkig is er altijd de CD met Volendamse kneiters nog.

Lieve Wendy, al zo lang dikke vrienden en dat zal nooit veranderen. Even niet die heerlijke frietjes uit Eindhoven. Ik zal je missen, maar we zien jullie daar en dan maken we er een te gekke tijd van.

Chris en Janneke, via Wanda leerde ook ik jullie kennen. Is het niet super dat er uit zo'n tijd zulke goede vriendschappen zijn ontstaan? Heel dankbaar ben ik voor jullie steun in die tijd. Janneke, bedankt voor je fantastische artistieke bijdrage aan dit boekje.

Toen ik dit proefschrift ging schrijven heb ik me dagen schuil gehouden in de Centrale bibliotheek. Gelukkig waren daar Hanil en Janneke de mij vaak gezelschap hielden. Lekker lunchen en kopjes thee bij de Zaak. Super thanks hiervoor.

Tot slot natuurlijk verdient de familie hier een belangrijke plaats. De familie Portier, erg blij ben ik dat ik er ook bij hoor. Bruno, Angeline en de kids bedankt dat we altijd bij jullie in Naarden terecht konden.

Oma's en Opa. Jullie hebben altijd interesse in hoe het gaat in het lab, ook al is het vaak maar een raar wereldje denk ik voor jullie.

Ard Jan, Angelie en Jort. Met veel plezier rijden we richting de Kempen om bij jullie te "hengen". Beetje praten met een hapje en een drankje, altijd gezellig. Australië? Australië? Australië?  
Ard Jan. Ik ben heel blij dat jij mijn "big brother paranimf" wilde zijn.

Lieve Pap en Mam, zonder jullie was dit boekje er natuurlijk nooit geweest. Altijd kan ik op jullie rekenen. Bijvoorbeeld toen mijn computer ontplofte tijdens het schrijven van mijn Master thesis. Bij jullie in Zeewolde is er altijd plek voor mij en Wanda om een beetje tot rust te komen, heerlijk te eten en bij te praten. Ik ben erg blij met zulke geweldige ouders. Ik ga jullie missen. Gelukkig komen jullie ons daar opzoeken.

Lieve Wannie, stel dat je bij dat eerste biertje in Hemmingway had geweten dat het betekende dat je uiteindelijk naar Australië zou gaan? Wat een avontuur, een leven samen met jou. Bedankt voor al je liefde, geduld, gekkigheid en gezelligheid.

Iedereen alle goeds!

Tot op een meeting, een feestje of misschien wel op een mooi wit strand.....

A handwritten signature in black ink that reads "Anne". The signature is written in a cursive style and is underlined with a single horizontal stroke.



## CURRICULUM VITAE

The author of this thesis, Anne Karine Lagendijk, was born on the 14th of December 1980 in Someren (the Netherlands). After moving from Someren to Warri (Nigeria) and Brielle, the Lagendijk family lived for about 14 years in Luykgestel. In Luykgestel she finished primary school at “de Klepper” and continued her High School education at “Were Di College” (formerly known as “Hertog Jan College”) in Valkenswaard.

After finishing High School she shortly endeavored to become a physiotherapist but soon decided to move to Nijmegen to study Biomedical Sciences at the Radboud University. She performed a research project as part of her Bachelor degree in the group of Prof. Dr. Peter Deen at the Nijmegen Center for Molecular Life Sciences (NCMLS). Here, she studied localization of both wild-type and mutant forms of the AQP2 protein in various cell types.

As a part of her Master degree “Pathobiology” she moved to Brisbane (Australia) for an internship in the laboratory of Prof. Dr. Peter Koopman at the Institute for Molecular Bioscience (IMB, University of Queensland). Here, she searched for female-specific morphological events during ovary development in mice.

Upon her return in the Netherlands she continued to work in Developmental Biology and commenced another internship in the group of Prof. Dr. Ronald Plasterk at the Hubrecht Institute for Developmental biology and Stem Cell Research in Utrecht.

There, she studied the function of microRNAs in early zebrafish development using a morpholino knock-down approach.

After her graduation in 2006, Anne decided to stay at the Hubrecht Institute as a PhD student in the group of Dr. Jeroen Bakkens. She initially focused on the role microRNAs play specifically during embryonic heart development in zebrafish. During her PhD work she identified a single microRNA and also described other factors involved in cardiac valve formation. These projects are presented together in this thesis.

From February 2012 she will return to the IMB in Brisbane to work as a post-doc in the laboratories of Prof. Dr. Alpha Yap and Dr. Ben Hogan. She will use the zebrafish model to study intercellular forces between endothelial cells during the formation of both blood and lymphatic vasculature.

## LIST OF PUBLICATIONS

Smith KA, **Lagendijk AK**, Courtney A, Chen H, Paterson S, Hogan BM, Wicking C & Bakkers J.

Transmembrane protein 2 (tmem2) is required to regionally restrict atrio-ventricular canal boundary and endocardial cushion development.

*Development*, 2011 Oct;138(19):4193-8.

**Lagendijk AK**, Goumans MJ, Burkhard S, Bakkers J.

MicroRNA-23 restricts cardiac valve formation by inhibiting Has2 and extracellular hyaluronic acid production.

*Circ Res.*, Sep 2;109(6):649-57.

Ghani S, Lenze D, Stumm J, Hoogenkamp M, **Lagendijk AK**, Heinz S, Bonifer C, Bakkers J, Seyfried SA, Hummel M, Rosenbauer F.

Macrophage development from hematopoietic stem cells requires PU.1 coordinated microRNA expression.

*Blood*, 2011 Aug 25;118(8):2275-84.

**Lagendijk AK**, Smith KA, Bakkers J.

Genetics of congenital heart defects: a candidate gene approach.

*Trends Cardiovasc Med*. 2010 May;20(4):124-8.

Marques IJ, Weiss FU, Vlecken DH, Nitsche C, Bakkers J, **Lagendijk AK**, Partecke LI, Heidecke CD, Lerch MM, Bagowski CP. Metastatic behaviour of primary human tumours in a zebrafish xenotransplantation model.

*BMC Cancer*. 2009 Apr 28;9:128.

Kamsteeg EJ, Savelkoul PJ, Hendriks G, Konings IB, Nivillac NM, **Lagendijk AK**, van der Sluijs P, Deen PM.

Missorting of the Aquaporin-2 mutant E258K to multivesicular bodies/lysosomes in dominant NDI is associated with its monoubiquitination and increased phosphorylation by PKC but is due to the loss of E258.

*Pflugers Arch*. 2008 Mar;455(6):1041-54.

Kloosterman WP, **Lagendijk AK**, Ketting RF, Moulton JD, Plasterk RH.

Targeted inhibition of miRNA maturation with morpholinos reveals a role for miR-375 in pancreatic islet development.

*PLoS Biology* 2007 Aug;5(8):e203.

van Beest M, Robben JH, Savelkoul PJ, Hendriks G, Devonald MA, Konings IB, **Lagendijk AK**, Karet F, Deen PM.

Polarisation, key to good localisation.

*Biochim Biophys Acta*. 2006 Aug;1758(8):1126-33.



